

POLITECNICO DI TORINO

College of Chemical and Materials Engineering

**Master's degree course
in Chemical Engineering and Sustainable Processes**

Master's Degree Thesis

Advanced Oxidation Processes for water disinfection



Supervisor:

prof. Alessandro Hugo Antonio Monteverde

Candidate:

Vincenzo Alfieri

July 2021

Contents

I. Riassunto in italiano	iii
1. Introduction.....	1
2. Drinking water treatment technologies	5
2.1 Water potabilization	5
2.2 Drinking water sources.....	6
2.2.1 Drinking water sources in Italy	6
2.2.2 Wastewaters as drinking water sources.....	7
2.3 Water treatment process	8
2.4 Water disinfection	9
2.5 Water disinfection methods.....	11
2.5.1 Conventional methods.....	11
2.5.2 Disinfection by-products	13
2.6 Advanced oxidation processes for water disinfection.....	14
3. Electrochemical advanced oxidation processes.....	17
3.1 Anodic oxidation	17
3.1.1 Model for Organic Oxidation by Heterogeneous Hydroxyl Radicals.....	18
3.2 Effect of the anode material	20
3.2.1 Lead dioxide anodes.....	21
3.2.2 Tin dioxide anodes	21
3.2.3 Ti based oxide anodes	22
3.2.4 BDD anodes	23
3.3 Effect of main operating parameters	25
3.3.1 Effect of current density and fluid-dynamics.....	25
3.3.2 Effect of supporting electrolyte nature and concentration	28
3.3.3 Effect of the nature and concentration of the organic pollutant.....	29
3.3.4 Effect of the pH.....	29
3.3.5 Effect of the temperature.....	30
4. Reactor design for EAOP	33
4.1 Principles of electrochemical reactors design	33
4.1.1 Cell potential difference	34
4.1.2 Rate control of an electrode process	35
4.2 Principles of reactor design in EAOP for water disinfection	37

4.2.1	Cell configurations: divided and undivided reactors.....	37
4.2.2	Electrode configurations: monopolar or bipolar connections	38
4.2.3	Flow pattern: mixed-tank and flow cells.....	39
4.2.4	Continuous and discontinuous mode.....	40
4.2.5	Interelectrode gap	41
4.2.6	Heat transfer	41
4.2.7	Scale-up.....	42
4.3	Examples of EAO reactor for water disinfection	44
4.3.1	The planar electrode in a flow cells: commercial alternatives	44
4.3.2	Three-dimensional EAO cell.....	46
4.3.3	Microfluidic reactors	48
5.	Mathematical modelling of EAO reactors.....	51
5.1	EAO reactors studied in CFD simulations	51
5.2	Mathematical modeling of EAO reactors.....	53
5.2.1	Hydrodynamics modeling	53
5.2.2	Mass transport modeling	57
5.2.3	Current and potential distribution modeling	60
6.	Design of an electrochemical advanced oxidation reactor	63
6.1	COMSOL Multiphysics	63
6.2	Case study	64
6.3	Mathematical model and simulation	65
6.3.1	Geometry	66
6.3.2	Simulation	68
6.3.3	Hydrodynamic.....	68
6.3.4	Mass transport	70
6.3.5	Current and potential distribution	71
7.	Results and discussion	75
7.1	Hydrodynamics and mass transport results.....	75
7.2	Current and potential distribution results	84
8.	Conclusions and future developments	93
9.	Bibliography	95
10.	Appendix	101
10.1	Grid independence analysis for hydrodynamics simulations.....	101
10.2	Grid independence analysis for current distribution simulations.....	104

I. Riassunto in italiano

L'acqua è il requisito principale per la sopravvivenza di tutti gli organismi, compreso l'uomo. Pertanto, garantire un approvvigionamento idrico adeguato è un problema importante per tutti gli esseri umani. Tuttavia, il difficile accesso all'acqua potabile è ancora uno dei principali problemi che il mondo sta affrontando nel 21° secolo. A partire secolo scorso sono state sviluppate e sfruttate una grande varietà di tecnologie per rispondere alla necessità di approvvigionamento acqua potabile sicura. Questi metodi di trattamento sono ampiamente descritti in letteratura. Le tecnologie di disinfezione convenzionali, se da un lato possono assicurare l'inattivazione dei patogeni, dall'altro possono portare alla possibile formazione di sottoprodotti nocivi, che possono essere anche più tossici dei composti originali. Gli svantaggi di tali metodi di disinfezione hanno portato i ricercatori a sviluppare tecnologie più sicure per rimuovere i contaminanti dall'acqua, compresi i processi di ossidazione avanzata (AOP). Gli AOP si basano sulla produzione in loco di radicali idrossilici altamente reattivi ($\bullet\text{OH}$), specie estremamente reattive che reagiscono in modo non selettivo con la maggior parte dei composti organici e sono in grado di degradare gli inquinanti. Esistono diversi AOP emergenti, ma questo lavoro si concentra sull'eAOP, i processi di ossidazione elettrochimica avanzata, in particolare sull'ossidazione anodica, AO o EO, l'applicazione elettrochimica più popolare tra gli eAOP. I principali aspetti positivi dei metodi elettrochimici per la disinfezione dell'acqua sono l'elevata efficienza, le condizioni operative moderate, la possibilità di automazione, la versatilità e il basso costo, in particolare quando sono alimentati da energia rinnovabile. In questo contesto, la progettazione di un reattore elettrochimico per la disinfezione dell'acqua tramite tecniche CFD è lo scopo principale di questa tesi.

L'ossidazione anodica consiste nell'ossidazione degli inquinanti in una cella elettrochimica attraverso due differenti meccanismi, come riportato in Figure 3.1.

Figure 3.1

- Ossidazione anodica diretta: trasferimento diretto di elettroni all'anodo. Questo tipo di processo porta a una decontaminazione molto scarsa.
- Ossidazione indiretta o mediata: ossidazione per reazione chimica con specie generate dallo scarico dell'acqua sulla superficie dell'anodo, come l'ossigeno attivo fisisorbito (noto anche come radicale idrossile fisisorbito, $\bullet\text{OH}$) o l'ossigeno attivo chemisorbito, ad esempio l'ossigeno nel reticolo di un anodo di ossido metallico (MO). L'azione di queste specie ossidanti dipende dall'attività elettrocatalitica dell'anodo e porta rispettivamente alla decontaminazione totale o parziale.

I materiali anodici possono essere classificati come attivi o non attivi, a seconda dei meccanismi coinvolti nel processo di ossidazione, ma la suddivisione non è molto chiara, in quanto anodi diversi possono esibire comportamenti intermedi. Generalmente, gli elettrodi attivi sono costituiti da un supporto metallico rivestito da uno strato di ossido conduttivo inorganico. Gli elettrodi non attivi sono tipicamente ossidi metallici completamente ossidati, come Ti/PbO_2 , o anodi di diamante drogato con boro (BDD). In questo caso l'ossidazione è mediata da radicali $\bullet\text{OH}$ fisisorbiti generati sulla superficie dell'anodo durante lo scarico dell'acqua. Diversi studi hanno mostrato l'efficienza molto più elevata degli elettrodi non attivi come PbO_2 e BDD. In realtà, gli anodi di biossido di piombo, Nonostante le effettive prestazioni mostrate, presentano un grave problema negativo che ne limita fortemente l'applicazione. Il PbO_2 può subire lisciviazione e rilasciare ioni Pb^{2+} in soluzione, causando la contaminazione dell'acqua. Quindi, recentemente l'interesse per il PbO_2 per il trattamento delle acque si è ridotto. Risultati

promettenti si sono ottenuti invece con anodi di ossido a base di titanio. Il titanio (Ti) è economico e diffuso in natura, ma è facile da ossidare per formare uno strato di TiO_2 , che porta a una bassa conduttività ($10^{-9} \Omega^{-1}\text{cm}^{-1}$) non adatta all'ossidazione anodica. La riduzione delle fasi di TiO_2 a Magnéli ($\text{Ti}_n\text{O}_{2n-1}$, $n =$ da 4 a 10) è il principale metodo di drogaggio che è stato utilizzato per produrre elettrodi ad alta conduttività elettrica anche estremamente resistenti alla corrosione. La fase Magnéli ideale è Ti_4O_7 , che ha la più alta conduttività elettrica a temperatura ambiente; è la fase target per la preparazione degli elettrodi. Gli studi sui materiali a base di Ti sono ancora oggi in corso. Il film sottile di diamante drogato con boro (BDD) è un nuovo materiale per elettrodi sintetici che ha recentemente ricevuto grande attenzione, grazie allo sviluppo di tecnologie per la sintesi di film di diamante conduttivo di alta qualità. Tuttavia, i materiali e i metodi per la costruzione di questi elettrodi sono costosi e non adatti alla realizzazione di scale-up per impianti di grandi dimensioni. Pertanto, sono necessari ulteriori studi per ridurre i costi di fabbricazione degli elettrodi BDD.

Tra i parametri controllati nei processi di ossidazione elettrochimica, la densità di corrente (intensità per unità di superficie dell'elettrodo) è uno dei termini più frequentemente citati perché regola la velocità di reazione. Una cella può funzionare in modalità galvanostatica o potenziostatica, a seconda di quale sia il parametro costante tra la corrente e il potenziale. Di solito, gli eAOP funzionano in modalità galvanostatica; quindi, la densità di corrente è un parametro chiave negli EAOP poiché regola la quantità di specie ossidanti prodotte. A seconda del valore della densità di corrente, è possibile distinguere tra diversi regimi. Quando è bassa, l'ossidazione non è cineticamente limitata dal trasporto di massa di sostanze organiche alla superficie dell'anodo. Ad alti valori di densità di corrente il processo è controllato dal trasporto di massa, mentre a valori intermedi di densità di corrente il processo è in regime cinetico misto. In generale, nella fascia di densità di corrente bassa, un aumento della densità di corrente porta ad una maggiore rimozione degli inquinanti. Al contrario, nella fascia alta, l'aumento porta all'evoluzione dell' O_2 , portando così ad una diminuzione dell'efficienza e ad un aumento dei costi energetici. Questo scenario apparentemente semplice è in realtà complicato dalla formazione aggiuntiva di altri ossidanti. Pertanto, un aumento della densità di corrente non produce automaticamente un aumento dell'efficienza di degradazione.

Gli elettroliti di supporto vengono utilizzati negli eAOP per la degradazione dei composti per consentire il flusso di corrente elettrica. Inoltre, l'efficienza degli eAOP può essere migliorata con l'aggiunta di ioni, non solo per migliorare il flusso di corrente elettrica, ma anche per produrre agenti ossidanti forti come le specie di cloro attivo. Tipicamente, diversi studi su scala di laboratorio riportati in letteratura impiegano soluzioni sintetiche di un dato inquinante (puro o in miscela) e alte concentrazioni di sali, aggiunti come elettrolita di supporto per aumentare la conducibilità ionica. Tuttavia, il trattamento dell'acqua destinata alla potabilizzazione è molto più difficile. Le modifiche della composizione dell'acqua dovrebbero essere attentamente regolate. L'aggiunta di grandi concentrazioni di sali a una fonte d'acqua non è una buona pratica e dovrebbe essere evitata perché produce anche inquinamento secondario.

Il pH è un parametro importante nei processi elettrochimici perché nella maggior parte dei casi esiste un valore di pH ottimale per l'efficienza di rimozione degli inquinanti. Questo comportamento è dovuto alla struttura chimica dell'inquinante. Tuttavia, la variazione di pH può avere effetti contrastanti sull'efficienza di degradazione, quindi il valore di pH ottimale dipende dal caso specifico per i processi di ossidazione diretta.

Contrariamente ad altri parametri, l'effetto della temperatura sull'efficienza complessiva del processo EO non è stato ampiamente valutato.

Per quanto riguarda la configurazione reattoristica, ove possibile, per la semplicità e per i bassi costi, è preferibile una geometria di reattore indivisa con un unico compartimento elettrolitico. Questa disposizione riduce anche cadute di potenziale e problemi di trasporto di massa tipicamente presenti nei reattori con membrane a scambio ionico e separatori microporosi. Si deve inoltre considerare il degrado delle membrane ed il loro costo, associato anche alle guarnizioni necessarie per il fissaggio del separatore. D'altra parte, la suddivisione del reattore in due compartimenti con due circuiti elettrolitici separati offre diversi vantaggi. Il vantaggio principale è dovuto alla ridotta perdita di reagenti o prodotti sugli elettrodi; non ci sono reazioni collaterali indesiderate agli elettrodi opposti dovute alla miscelazione di elettroliti anodici e catodici. Inoltre, viene controllata la migrazione degli ioni, si possono separare miscele pericolose e viene assicurata la protezione degli elettrodi dalla corrosione causata da agenti chimici aggressivi. Pertanto, considerando le leggere differenze tra le due configurazioni su piccola scala, nonché la quantità trascurabile di idrogeno prodotto, la configurazione prevalente presente nella maggior parte degli studi di letteratura è quella indivisa, per via della semplicità e dei bassi costi.

La cella a piastre parallele, indivisa o divisa, è la classica geometria delle celle elettrochimiche industriali. Tali celle a piastre parallele possono costituire una singola unità ed operare in modo monopolare. Generalmente, gli elettrodi bipolari si sono dimostrati i più efficienti, ma la configurazione monopolare implica costi operativi inferiori a causa del potenziale di cella inferiore risultante.

Il flusso all'interno del reattore è un aspetto cruciale da considerare per aumentare l'efficienza dei processi elettrochimici. La scelta corretta del modello di flusso, determinata dal design della cella, può risolvere le limitazioni legate a uno scarso trasporto di massa. Le celle a flusso sono l'alternativa più interessante trovata in letteratura, rispetto alle celle a serbatoio miscelato. Il principale vantaggio delle celle a flusso è il coefficiente di trasporto di massa più elevato rispetto alle celle miscelate, che permette di effettuare trattamenti a concentrazioni molto più basse rispetto alle celle miste (Tabella 4.1).

Table 4.1

In letteratura, la maggior parte degli studi sono condotti in modalità di funzionamento discontinuo. In questa modalità, le celle a passaggio singolo sono collegate a un serbatoio tramite una pompa di ricircolo in modo da aumentare il numero di passaggi dell'acqua attraverso la cella e quindi la portata (Figura 4.4).

Figure 4.4

In ogni caso, sono state trovate pochissime ricerche sullo studio del processo continuo. La modalità continua dovrebbe essere impiegata solo in applicazioni di grandi dimensioni, ma la tecnologia non è ancora sufficientemente matura per tali applicazioni.

Un altro parametro di fondamentale importanza è il distanziamento tra gli elettrodi. È necessaria una distanza ottimale tra gli elettrodi per l'efficacia dei trattamenti dell'acqua. La maggior parte dei lavori su scala di laboratorio riporta l'uso di una distanza tra gli elettrodi tra 0,5 e 3,0 cm.

Per quanto riguarda il tipo di celle utilizzate, la cella di flusso a elettrodi piani e paralleli è la configurazione più utilizzata nei processi di elettrochimici. Essa, infatti, fornisce un profilo di flusso riproducibile, con lo stesso design, per reattori da laboratorio e su larga scala. Come accennato in precedenza, le rapide velocità di trasporto di massa consentono alle celle di flusso di superare le celle a serbatoio agitate per la loro efficacia nei processi di degradazione. Ulteriori miglioramenti si ottengono attraverso promotori di turbolenza per aumentare la miscelazione della soluzione, incorporando elettrodi porosi per aumentare l'area elettroattiva o combinando

più celle impilate in serie o in parallelo. Quest'ultima opzione viene applicata quando si desidera una scala più ampia rispetto alla classica cella a flusso singola impiegata su scala di laboratorio. Tra la varietà dei diversi tipi di celle, la FM01-LC è una delle più diffuse. Il reattore FM01-LC è una cella filtropressa elettrochimica su scala di laboratorio con un'area dell'elettrodo proiettata di 64 cm² nella sua configurazione di base (Figura 4.7).

Figure 4.7

Ha un canale di flusso dell'elettrolita rettangolare, vuoto o dotato di un promotore di turbolenza. Le esigenze richieste per una buona progettazione elettrochimica sono ben soddisfatte da questo tipo di celle a flusso controllato, che possono essere facilmente assemblate in modo modulare. Inoltre, il reattore FM01-LC può essere estremamente versatile nella scelta della forma dell'elettrodo, del materiale e della morfologia superficiale, il che rende questo reattore uno dei più studiati.

I reattori a elettrodo tridimensionale (3D) o garantiscono un'ottima soluzione agli inconvenienti che limitano l'applicazione dell'elettrodo bidimensionale (2D). La tecnologia elettrochimica 3D si basa su un processo elettrochimico 2D con diverse analogie come i materiali degli elettrodi e i processi di trattamento. L'unica differenza è il terzo elettrodo. Viene anche chiamato elettrodo a particelle o elettrodo a letto, ed è sostanzialmente costituito da materiali granulari che vengono riempiti tra due controelettrodi, come si può vedere nella Figura 4.11.

Figure 4.11

Quando c'è un sistema convenzionale ma gli elettrodi sono tridimensionali, possono anche essere considerati come un tipo di reattore 3D. L'aggiunta di carbone attivo granulare (GAC) o particelle metalliche può anche aumentare la conduttività e il trasporto di massa o l'assorbimento di inquinanti rispetto al processo 2D (Tabella 4.2).

Table 4.2

Tra le varie tipologie di reattori, negli ultimi anni sono state impiegate con successo le celle microfluidiche per il trattamento di acque reflue contaminate da inquinanti organici. Le celle elettrochimiche microfluidiche presentano distanze tra gli elettrodi molto piccole di decine o poche centinaia di micrometri, e quindi presentano numerosi vantaggi per il trattamento delle acque reflue rispetto alle tradizionali celle a flusso o a serbatoio. In primo luogo, è difficile garantire tensioni di cella sufficienti quando il mezzo non ha una grande conduttività, quindi gli elettroliti di supporto si aggiungono al sistema quando si utilizzano i trattamenti convenzionali. Questo può essere un ostacolo per un'ampia applicazione dell'elettrochimica convenzionale. Infatti, l'aggiunta di sostanze chimiche può essere la causa della formazione di inquinanti secondari.

La caratterizzazione dei reattori EAO può essere eseguita sperimentalmente, ma questi esperimenti sono troppo costosi e lunghi. In questo contesto, il recente sviluppo delle tecniche di fluidodinamica computazionale (CFD) ha permesso la progettazione, la caratterizzazione e lo scale-up preliminare di questi tipi di reattori. Diversi ricercatori hanno utilizzato tecniche CFD per modellare l'idrodinamica, il trasferimento di massa, le distribuzioni di potenziale e corrente in molti reattori EAO, ma principalmente per i tipi di filtropressa.

La tecnica CFD permette di risolvere le equazioni fondamentali del trasporto all'interno del reattore elettrochimico, utilizzando metodi come il metodo del volume finito o degli elementi finiti. Entrambe le procedure numeriche danno risultati simili. In questo lavoro è stato utilizzato un software multidisciplinare per la simulazione multifisica che utilizza il metodo degli elementi finiti (FEM).

Le equazioni di governo in condizioni di flusso laminare per fluidi incomprimibili, considerando gli elettroliti come fluidi newtoniani, sono le note equazioni di Navier-Stokes (NS). Sono un insieme di equazioni differenziali alle derivate parziali che includono le equazioni della velocità del fluido per ciascuna coordinata. Le equazioni di trasporto sono accoppiate con l'equazione di continuità. In regime transitorio, una semplice forma vettoriale di queste equazioni può essere espressa dalle seguenti equazioni.

Equazione 5.1

Equazione 5.2

In condizioni turbolente, è presente una grande quantità di fluttuazioni di velocità e il flusso non è più in condizioni laminari. Pertanto, le equazioni del moto e della continuità devono essere corrette per studiare tali fluttuazioni. La modellazione della turbolenza è ancora una sfida importante poiché i fenomeni di turbolenza dovrebbero essere descritti su diverse scale spaziali e temporali. Pertanto, esistono diversi approcci per correlare le fluttuazioni di velocità e pressione in condizioni turbolente. L'approccio matematico più diffuso per rappresentare le equazioni turbolente è la media temporale delle variabili di velocità e pressione. Secondo questo approccio, le equazioni NS diventano equazioni di Reynolds Average Navier-Stokes (RANS). Le equazioni RANS e di continuità sono rappresentate come segue.

Equazione 5.3

Equazione 5.4

Tutte le equazioni riportate, in regime di flusso laminare o turbolento, in genere, non hanno soluzione analitica. Quindi, è necessaria l'applicazione di metodi numerici per risolvere tali equazioni. In questo lavoro COMSOL Multiphysics è stato lo strumento utilizzato per risolvere le equazioni di governo.

Nel caso del reattore FM01-LC, le particolari forme dei collettori di ingresso e uscita creano disomogeneità di flusso con formazione di vortici. Inoltre, come già accennato, il flusso del fluido nell'FM01-LC solitamente non raggiunge un regime di flusso completamente sviluppato prima di lasciare il reattore, determinando effetti di ingresso e uscita. Quindi è presente un alto livello di turbolenza indipendentemente dall'intervallo del numero Re studiato. Queste osservazioni sembrano essere valide anche per altre celle riportate in letteratura, nonostante l'assenza di distributori di flusso. In effetti, il modello turbolento è stato applicato con successo per simulare flussi, anche a bassi numeri di Re , come si evince dalla tabella 5.1.

Table 5.1 - Different reactors using RANS **equations**; $k-\epsilon$ model

Un altro aspetto importante da valutare nei reattori EAO è il trasporto di massa. Il trasporto di massa è legato al campo di concentrazione delle specie ioniche dalla massa alla superficie dell'elettrodo in presenza di un campo elettrico. I radicali formati all'elettrodo viaggiano dall'interfaccia alla massa e poi reagiscono con gli inquinanti. In questo contesto, un'analisi dell'evoluzione della concentrazione attraverso la simulazione matematica è un potente strumento per valutare l'efficacia dei trattamenti. Le equazioni guida che descrivono il trasporto di massa all'interno delle celle sono il bilancio di massa (Eq. 5.13) e l'equazione di Nernst-Planck (Eq. 5.14).

Equazione 5.13

Equazione 5.14

Diversi studi sul trasporto di massa sono stati effettuati assumendo il termine di migrazione dell'Eq. (5.14) trascurabile. Questa ipotesi è valida in caso di presenza di elettrolita di supporto e se le specie elettroattive desiderate sono presenti in forma diluita, condizioni comunemente impiegate in diversi studi di degradazione su scala di laboratorio. Inoltre, spesso si considera il regime stazionario e si ipotizza l'assenza delle reazioni omogenee nel bulk, dovute ad un

istantaneo abbattimento dell'inquinante sulla superficie dell'elettrodo, determinando così una concentrazione zero della specie sull'elettrodo. In questo modo si deve risolvere solo la risoluzione del campo idrodinamico e l'equazione convezione-diffusione per tutte le specie.

A causa della mancanza di lavori, una via alternativa per valutare il trasporto di massa all'interno della cellula è l'uso di correlazioni empiriche. Altre correlazioni utilizzabili derivano dal calcolo della corrente limite. Infatti, la caratterizzazione sperimentale del trasporto di massa rappresenta un punto di partenza per valutare le prestazioni dei reattori elettrochimici poiché fornisce equazioni empiriche che collegano la densità di corrente limite e il coefficiente di trasporto di massa. La dipendenza dal trasporto di massa rispetto alla convezione è espressa da una correlazione di gruppo adimensionale, come segue (Eq. 5.20).

Equazione 5.20

La distribuzione di corrente e potenziale nella cella e sugli elettrodi sono tra i principali aspetti ingegneristici e progettuali. La non uniformità di corrente e potenziale può causare scarse prestazioni in termini di efficienza di corrente a causa del verificarsi di reazioni parassite. Questo è associato alla forma e al materiale dell'elettrodo, alla geometria della cella, alle fasi della reazione elettrochimica e agli aspetti del trasporto di massa. Per valutare le distribuzioni di potenziale e corrente negli elettrodi 2D, si può tener conto che la densità di corrente, in qualsiasi punto all'interno della cella, può essere determinata dal gradiente di potenziale locale, secondo la legge di Ohm.

Equazione 5.23

Allo stato stazionario, il potenziale elettrico può essere descritto dall'equazione di Laplace, come riportato nell'equazione 5.24.

Equazione 5.24

Nell'elettrolita, che è un conduttore di ioni, la densità di corrente netta può essere valutata come somma dei flussi di tutti gli ioni, come espresso nell'equazione 5.25.

Equazione 5.25

Quindi, nelle celle elettrochimiche possono verificarsi tre diversi casi di distribuzione del potenziale e della corrente. La distribuzione della corrente primaria considera solo le perdite dovute alla resistenza della soluzione, trascurando gli effetti cinetici degli elettrodi e gli effetti dipendenti dalla concentrazione. La distribuzione della corrente secondaria tiene conto della cinetica dell'elettrodo, nonché della resistenza della soluzione. La distribuzione terziaria della corrente considera l'effetto dei cambiamenti di composizione elettrolitica e forza ionica, nonché la resistenza della soluzione e la cinetica degli elettrodi. Sebbene il numero di lavori riportati per altre applicazioni elettrochimiche, come celle a combustibile e batterie, sia ampio, i riferimenti che utilizzano CFD per valutare la distribuzione di corrente e potenziale negli elettrolizzatori sono limitati.

Modellazione del reattore

La letteratura scientifica è ricca di studi sperimentali che dimostrano l'efficacia dei trattamenti elettrochimici di ossidazione avanzata per la disinfezione dell'acqua, mentre sono pochi gli studi CFD sulla modellazione dei reattori. Inoltre, la maggior parte dei lavori è incentrata sullo studio degli inquinanti presenti nelle acque reflue, mentre sono presenti pochissimi studi sulle acque destinate alla depurazione. In questo contesto, lo scopo di questo lavoro è studiare l'ambiente di reazione di un reattore filtropressa utilizzando CFD.

A tal fine, uno studio di Gharibian et al. ^[80] è stato preso come punto di partenza per una prima caratterizzazione. Nel paper di riferimento è stata studiata l'idrodinamica e il trasferimento di massa all'interno di un reattore filtropressa, utilizzando la degradazione del blu di metilene

come sistema di prova. Il blu di metilene è una molecola organica refrattaria utilizzata come colorante e largamente impiegata come colorante in batteriologia, come indicatore nelle reazioni di ossidazione e come antidoto al cianuro. Il dominio geometrico oggetto della simulazione è costituito dall'area vuota all'interno del distanziatore (figura 6.2) che divide i due elettrodi e rappresenta lo spazio in cui scorre il fluido, quindi il corpo del reattore. Le misure geometriche del reattore sono elencate nella tabella (6.2).

Figure 6.2

Table 6.2

Le equazioni del trasporto di quantità di moto accoppiate con le equazioni del modello di turbolenza sono state risolte numericamente con il metodo degli elementi finiti, utilizzando COMSOL Multiphysics® 5.5. Sono state valutate diverse configurazioni di mesh al fine di ottenere il miglior compromesso tra il costo computazionale e l'accuratezza dei risultati, ottenendo infine variazioni di velocità locale trascurabili con il cambiamento della dimensione della cella della mesh. La mesh finale per il dominio computazionale (Fig. 6.7) era costituita da 404269 elementi, di cui 276266 elementi di mesh tetraedrici.

Figure 6.7

Sono state utilizzate le opzioni di risoluzione predefinite del software. Il materiale utilizzato per la simulazione è acqua liquida, scelta dalla libreria dei materiali. La temperatura è stata fissata a 298 K. Sono state impiegate funzioni di parete, assumendo il flusso nella regione vicino alla parete basata su una distribuzione di velocità universale, evitando così la risoluzione delle equazioni di trasporto in questa regione. Supponendo una variazione trascurabile della viscosità, della densità e della temperatura dell'elettrolita, sono state utilizzate le equazioni di continuità e le equazioni RANS per il flusso di un fluido newtoniano incomprimibile in condizioni turbolente allo stato stazionario. Le espressioni utilizzate sono le stesse presentate nel capitolo precedente (Eq. 5.3 - 5.7).

Come già discusso, a causa della mancanza di studi in questo contesto, piuttosto che calcolare direttamente il coefficiente di trasporto di massa globale, è stata effettuata una caratterizzazione della cella per valutare i profili del coefficiente di trasporto di massa locale, prendendo come riferimento un lavoro di Vázquez et al. [89]. Il flusso adimensionale, espresso da Sh , è una funzione della velocità del fluido adimensionale (Re) moltiplicata per le proprietà del fluido adimensionali (Sc). Nei reattori a convezione forzata, questa correlazione è riportata nella forma dell'equazione 5.20. Le correlazioni impiegate in questo lavoro sono riportate nella tabella (6.4).

Table 6.4

La prima correlazione è stata ottenuta dall'adattamento lineare dei k_m risultanti dal lavoro di Gharibian et al., mentre le altre due sono stati utilizzate per avere un confronto diretto con il più diffuso FM01-LC, prendendo come riferimento lavori con spaziatura S diversa tra gli elettrodi (entrambe valide nel range Re osservato). Le correlazioni scelte sono state accoppiate con il campo di flusso ottenuto. È stato quindi possibile stimare i gruppi adimensionali Re , Sh e k_m in diverse posizioni nel canale della cella di flusso considerando che il processo fosse controllato dal trasporto di massa. Questo è stato confermato anche dallo studio di Gharibian et al., poiché il decadimento sperimentale della concentrazione di MB nel tempo è risultato adattarsi a una cinetica del primo ordine (da un bilancio di massa sull'intero sistema elettrochimico), che è caratteristica di una reazione elettrochimica controllata dal trasferimento di massa. I coefficienti di trasporto di massa locale sono stati valutati considerando tre diverse sezioni, a $z = 5$ cm; $z = 8$ cm; $z = 11$ cm. Ad ogni valore di z selezionato, sono state tracciate 20 diverse linee parallele partendo da un'estremità del canale fino a raggiungere quella opposta, come mostrato in figura 6.8.

Figure 6.8

Per ogni linea è stato ottenuto un profilo di velocità teorico con 20 velocità di flusso medie locali lungo la larghezza del canale (dimensione y). Ciascun profilo di velocità media è stato ottenuto utilizzando il comando “Line Average” ed è stata considerata la velocità media locale del flusso (v) rappresentativa della linea. È stato calcolato un numero di Reynolds medio locale, per ciascuna corrispondente velocità di flusso media locale (v), secondo l'equazione 5.10.

È stato calcolato un numero di Sherwood locale, attraverso l'equazione 5.20, per ciascuna velocità di flusso media locale (v) e Re medio locale. Per ogni corrispondente Sh medio locale ottenuto, è stato valutato un valore di k_m medio dall'Equazione (6.9) ed è stato considerato come la media dei k_m per ogni linea.

Equazione 6.9

Per lo studio della distribuzione di corrente e potenziale, è stato preso come riferimento il lavoro di Perez et al. ^[90]. In un primo momento, il loro modello è stato validato, prendendo come oggetto di studio solo la parte centrale del canale di un FM01-LC. Nel caso del loro lavoro, il canale aveva una distanza tra gli elettrodi di 0,55 cm, mentre nel caso studio analizzato è di 1,1 cm. Quindi è stato utilizzato un nuovo dominio, considerando solo la parte centrale del canale, che è il luogo in cui si generano i radicali durante lo scarico dell'acqua. Il dominio è mostrato in figura 6.9.

Figure 6.9 - 3D domain of the channel

Sono state calcolate le distribuzioni di corrente primaria e secondaria. Come sistema di prova è stata utilizzata l'ossidazione dell'acqua in presenza di H_2SO_4 come elettrolita di supporto. Gli input per le simulazioni sono stati tratti dagli studi di microelettrolisi dell'ossidazione dell'acqua eseguiti dagli stessi autori (Tabella 6.6).

Table 6.6

La densità di corrente in qualsiasi punto all'interno del canale è stata determinata dal gradiente del potenziale locale, utilizzando l'equazione 5.23. La distribuzione del potenziale nell'elettrolita è stata descritta dall'equazione di Laplace (5.24).

Per la distribuzione di corrente primaria, sono state considerate le seguenti condizioni al contorno lungo l'anodo e il catodo (6.10, 6.11).

Equazione 6.10

Equazione 6.11

Per le pareti isolanti è stata utilizzata l'equazione 5.29.

Equazione 5.29

Per il modello di distribuzione della corrente secondaria, le condizioni al contorno sono espresse come segue.

Nessun flusso di corrente su tutte le superfici isolanti, Eq. (5.29). Sia all'elettrodo di lavoro che al contro elettrodo è stata applicata una cinetica di Tafel.

Equazione 5.27

La cinetica applicata al contro elettrodo è stata scelta tra varie cinetiche per la reazione di evoluzione dell'idrogeno, al fine di validare il modello e avere una curva I-E simile rispetto al lavoro considerato. Una volta validato il modello, è stato valutato l'andamento delle curve I-E al variare della conduttività elettrica e della spaziatura tra gli elettrodi. In questo modo è stato calcolato il consumo energetico specifico ed è stato effettuato un confronto tra acque ad alta conduttività e acque destinate alla potabilizzazione, quindi a bassa conduttività.

Tuttavia, in questo lavoro il processo elettrochimico corrisponde all'ossidazione dell'acqua, quindi non viene studiata la distribuzione della corrente terziaria. È importante ricordare che durante la degradazione elettrochimica di sostanze organiche, dovrebbe essere considerata la

distribuzione di corrente terziaria. Questa analisi dovrebbe essere utile per avere un punto di partenza in cui aggiungere la distribuzione di corrente terziaria.

Risultati e discussione

I risultati idrodinamici sono riassunti nelle figure riportate di seguito. È chiaramente visibile la corrispondenza tra i due risultati in figura 7.1. Gli effetti di ingresso e uscita all'ingresso e all'uscita sono dovuti alla formazione di zone a velocità più elevata, denominati zone di flusso preferenziale.

Figure 7.1

Figure 7.2

Figure 7.3

Figure 7.4

Per quanto riguarda l'andamento del flusso, le alte velocità dovute all'ingresso e il flusso quasi sviluppato vicino all'uscita sono chiaramente visibili. Inoltre, la velocità è pressoché uniforme nel profilo a $z = 8$ cm, mentre a $z = 11$ cm il fluido è influenzato dall'uscita. Ciò suggerisce che nella zona di $6 < z < 9$ cm la velocità è pressoché uniforme.

Per quanto riguarda il trasporto di massa, la simulazione numerica del flusso fornisce uno strumento molto utile per prevedere i k_m in un canale del reattore quando viene selezionata un'appropriata correlazione di trasporto di massa.

Nelle figure 7.5-7.7 è riportato l'andamento dei coefficienti di trasporto di massa locale, calcolati utilizzando le correlazioni indicate nella tabella 6.4.

Figure 7.5

Figure 7.6

Figure 7.7

Come si può osservare, la correlazione ottenuta dal caso studio è stata quella che ha fornito i più alti coefficienti di trasporto di massa locale. Le correlazioni sono variabili con la geometria, quindi la correlazione sperimentale ottenuta per il reattore studiato è quella che meglio prevede i coefficienti di trasporto di massa locale. Tuttavia, il confronto tra le diverse correlazioni può essere utile per comprendere meglio i risultati ottenuti. Valori di k_m locali molto più alti sono probabilmente dovuti alla minore larghezza (3 cm) e lunghezza (16 cm) della cella di flusso considerata rispetto ai reattori FM01-LC come si vede chiaramente nella tabella 7.1, e quindi alle maggiori velocità raggiunte su media.

Table 7.1

Nel caso di una reazione controllata dal trasporto di massa, queste velocità portano a k_m locali più grandi. Ciò potrebbe suggerire che questo tipo di cella, senza distributori di ingresso e uscita, possa avere prestazioni migliori rispetto a un reattore FM01-LC. Tuttavia, si deve considerare che un canale più stretto e più corto determina una minore area dell'elettrodo e quindi una minore superficie disponibile per la degradazione.

Per meglio comprendere il comportamento idrodinamico di questo reattore, atipico negli studi CFD riportati in letteratura, è stato effettuato un confronto con il reattore molto più utilizzato, l'FM01-LC. Il reattore utilizzato in questo lavoro, come già accennato, è tra i pochi senza distributori di ingresso, a differenza del più utilizzato FM01-LC. Per questi motivi si è deciso di ottimizzare la configurazione del reattore aggiungendo distributori di fluido in ingresso e in uscita. I distributori utilizzati sono costituiti da 5 condotti rettangolari, posti subito dopo l'ingresso del reattore. Per avere un confronto diretto tra le due configurazioni si è deciso di mantenere la stessa area di elettrodo e larghezza di canale, raggiungendo quindi le caratteristiche geometriche del reattore e dei distributori riportate nella tabella 7.3.

Table 7.3

I profili di velocità sono stati studiati sulle stesse linee studiate per il reattore senza distributori (Figure 7.11-7.13).

Figure 7.11

Figure 7.12

Figure 7.13

I risultati sono molto simili allo studio di Rivero et al. [86]. Tuttavia, probabilmente a causa di una diversa configurazione geometrica della zona di ingresso, il flusso è leggermente asimmetrico. In generale è possibile osservare un profilo di velocità media superiore a quello ottenuto senza la presenza di collettori. In nessun punto della larghezza del canale si hanno valori di velocità inferiori ai profili ottenuti senza distributori.

Come previsto, a parità di velocità in ingresso, i profili di velocità sono mediamente più elevati quando si utilizzano distributori. Ciò influisce sicuramente sul trasporto di materia nel reattore, come già riportato in un confronto nel lavoro di Rivero et al., che hanno ottenuto un migliore trasporto di massa nel reattore in presenza di distributori di ingresso, e nei dati di letteratura sui k_m , come mostrato nella Tabella 7.2.

Table 7.2

Tuttavia, a causa della mancanza di lavori in questo ambito e dell'assenza di dati sperimentali da questa nuova configurazione, purtroppo non è stato possibile quantificare le variazioni dei valori di k_m .

Per quanto riguarda la distribuzione di corrente e potenziale, la figura 7.14 mostra un grafico in sezione trasversale della distribuzione del potenziale, nello studio di distribuzione primario, all'interno della cella, perfettamente coincidente con la distribuzione del potenziale nel lavoro di Perez et al. [90].

Figure 7.14

L'analisi della distribuzione di corrente primaria ha dimostrato che la distribuzione della corrente adimensionale j_x/j_{ave} è influenzata dagli angoli curvi, come si può vedere in figura 7.15.

Figure 7.15

Il valore minimo di j_x/j_{ave} ottenuto dalle simulazioni differisce dal valore ottenuto nel lavoro di riferimento; tuttavia, il comportamento osservato è lo stesso. In questo lavoro, questo valore è pari a 0.98, quindi al massimo la corrente devia dello 0.2% da j_{ave} , e ciò si verifica solo agli angoli. Pertanto, la distribuzione della corrente primaria all'anodo BDD (a $z = 0$) nel canale può essere considerata uniforme, poiché possono essere trascurati gli effetti di bordo originati dagli angoli curvi.

La simulazione della distribuzione di corrente secondaria è stata eseguita a diversi potenziali di cella, da 0.6 V a 3 V, al fine di raggiungere un intervallo di potenziale compreso di $2.3 < E < 2.75$ V, in cui avviene la formazione dei radicali idrossilici. La distribuzione della corrente secondaria è mostrata in Fig. 7.17 e 7.18 con un valore di sovratensione di 1,7 V.

Figure 7.17

Figure 7.18

I risultati ottenuti sono stati in totale accordo con quello del lavoro di Perez et al.. Inoltre, si osserva chiaramente che alle altezze considerate la distribuzione di corrente non presenta effetti di bordo agli angoli, contrariamente alla distribuzione di corrente primaria.

Dopo aver verificato l'uniformità della distribuzione di corrente, è stata studiata la relazione tra tensione e corrente, nell'intervallo di potenziali applicato durante il test di microelettrolisi dal

lavoro di Perez et al. e considerando la stessa conducibilità elettrica di 35 S m^{-1} . La somiglianza tra le curve I-E è stata accertata, come si vede dalla figura 7.19.

Figure 7.19

Successivamente, sono state effettuate diverse simulazioni nel reattore del caso studio. È stato simulato solo il canale (esclusi i distributori), come si può vedere in figura 7.20.

Figure 7.20

L'intervallo in cui hanno operato vari studi in letteratura per il reattore FM01-LC corrisponde all'intervallo di densità di corrente tra 5 e 20 mA cm^{-2} . In quelle condizioni, sono stati raggiunti potenziali tra $2,3$ e $2,75 \text{ V}$. A questi valori di potenziale avviene la formazione di radicali idrossili, mentre a tensioni più elevate avviene la reazione di evoluzione dell'ossigeno. Considerando il reattore studiato, si può notare (Fig. 7.22) che a parità di conducibilità del lavoro di Perez et al. ($k = 35 \text{ S m}^{-1}$), i potenziali raggiunti sono in tale intervallo, il che indica che il reattore è efficace nella formazione di radicali a quelle densità di corrente.

Figure 7.22

Tuttavia, lo scopo di questo lavoro è lo studio della disinfezione dell'acqua destinata alla potabilizzazione, pertanto sono state studiate conduttività inferiori. In un primo momento, è stato studiato l'andamento della curva I-E per conduttività decrescenti. I valori utilizzati sono stati 10 , 20 e 35 S m^{-1} . I risultati sono visibili nella figura seguente (7.23).

Figure 7.23

Al diminuire della conduttività, aumentano le perdite ohmiche nella soluzione, portando a aumenti di voltaggio che potrebbero portare all'evoluzione dell'ossigeno. Inoltre, ciò aggiungerebbe ulteriori costi energetici. Per risolvere questi problemi la distanza tra gli elettrodi può essere ridotta per diminuire le perdite ohmiche. Sono state quindi considerate tre diverse configurazioni. La distanza tra gli elettrodi del reattore fin qui considerata è di 1.1 cm . Sono state aggiunte due ulteriori configurazioni, $S = 0.55 \text{ cm}$ e $S = 0.4 \text{ cm}$, (Tabella 7.5) in accordo con i valori trovati in letteratura per questo tipo di celle.

Table 7.5

A questo punto è stato studiato l'andamento della relazione I-E con la massima conduttività ammissibile nel caso di trattamenti di acqua potabile, considerando le specifiche delle aziende che vorrebbero realizzare questi impianti. La conduttività massima consentita, $S = 0.1 \text{ S m}^{-1}$, corrisponde ad un valore molto inferiore a quelli riscontrati in letteratura per il trattamento delle acque reflue. È stato studiato l'andamento della tensione al variare della corrente. I risultati sono visibili nella figura 7.24.

Figure 7.24

Come previsto, in questo caso i valori del potenziale sono molto più alti dei valori precedentemente considerati in presenza di un elettrolita di supporto. I valori del potenziale raggiunto sono al di là dei potenziali di evoluzione dell'ossigeno. Inoltre, la maggiore quantità di perdite ohmiche dovute alla bassa conduttività aumenta il consumo energetico. Per avere una misura diretta delle differenze tra i casi, è stato considerato il consumo energetico specifico relativo al trattamento di 0.5 L di acqua in 5 h , facendo riferimento al caso studio inizialmente considerato. Inizialmente lo studio è stato condotto sulla configurazione di base ($S = 1.1 \text{ cm}$ e $k = 35 \text{ S m}^{-1}$), quindi sono state studiate altre configurazioni. Sono stati considerati tre diversi tipi di reattori con spaziatura decrescente tra gli elettrodi (Tabella 7.5). La spaziatura minima richiesta per questo tipo di celle è stata scelta in accordo con i valori di letteratura. Per valori inferiori a 0.4 cm i costi di pompaggio sarebbero troppo elevati. Per ogni configurazione sono stati valutati diversi valori di conduttività. I primi tre valori, $k = 35 \text{ S m}^{-1}$, $k = 20 \text{ S m}^{-1}$, $k = 10 \text{ S m}^{-1}$, sono compatibili con i valori presenti in letteratura per il trattamento delle acque reflue.

Questi valori si ottengono aggiungendo un elettrolita di supporto, che nel caso del trattamento delle acque reflue, se opportunamente scelto, può essere utilizzato. Si è quindi considerato il valore di conduttività di $0,1 \text{ S m}^{-1}$, il valore massimo ammissibile nell'acqua da trattare, indicato dalle aziende coinvolte nella progettazione di questi impianti. È stato considerato un singolo valore di densità di corrente, 10 mA cm^{-2} , in accordo con articoli scientifici in cui sono stati utilizzati elettrodi BDD. A questo valore dovrebbe avvenire la formazione dei radicali ossidrilici coinvolti nei processi di degradazione. Per ogni caso sono state valutate la tensione corrispondente e infine il consumo di energia. I risultati sono elencati nella tabella 7.6.

Table 7.6

Per alti valori di conduttività, al diminuire della spaziatura, si hanno leggere variazioni nei consumi energetici. Si verifica una diminuzione della tensione che porta a minori consumi, ma le variazioni sono scarse. Ciò suggerisce che, quando si utilizzano elettroliti di supporto, la distanza tra gli elettrodi non ha una grande influenza nel processo. Nel caso a $k = 0.1 \text{ S m}^{-1}$ e $S = 1.1 \text{ cm}$, il consumo di energia è più che il quadruplo dei casi con conduttività più elevate. Diminuendo la spaziatura si ha un decremento notevole, tuttavia il consumo rimane su valori molto superiori al doppio rispetto al caso ideale. Le variazioni percentuali del consumo energetico sono riassunte nella tabella seguente (7.7), passando da 1.1 cm a 0.4 cm .

Table 7.7

Si può notare che maggiore è la conduttività, minore è il consumo di energia influenzato dalla diminuzione della distanza tra gli elettrodi. Nonostante la maggiore diminuzione percentuale (51.8 %), è chiaro che il consumo di energia a $k = 0.1 \text{ S m}^{-1}$ rimane molto più elevato, rispetto ai casi in cui si utilizzano elettroliti di supporto. Poiché nel caso delle celle di flusso la spaziatura non può essere ulteriormente ridotta, si dovrebbero trovare alternative per ridurre i costi troppo elevati che l'uso di queste tecnologie richiederebbe quando si utilizza acqua a conduttività molto basse.

Conclusioni

L'obiettivo principale di questo lavoro è stato quello di fornire un primo approccio alla progettazione di un reattore elettrochimico per la disinfezione dell'acqua utilizzando tecniche CFD. Sono state mostrate le varie configurazioni di reattore utilizzate in questo contesto. La configurazione della cella a flusso è risultata essere la più utilizzata, a causa del miglior trasporto di massa rispetto ai classici serbatoi misti. Sono stati presentati altri reattori innovativi, che potrebbero contribuire in futuro a risolvere i problemi legati a queste tecnologie. Uno dei principali svantaggi di questa tecnologia è l'uso di elettroliti di supporto, che porta a un minor consumo di energia ma potrebbe produrre inquinamento secondario nell'acqua destinata alla potabilizzazione. La maggior parte dei lavori trovati in letteratura ha utilizzato reattori su scala di laboratorio, a causa del fatto che questa tecnologia è ancora relativamente immatura. Di conseguenza, si è deciso di studiare gli aspetti fisici di una singola cellula su scala di laboratorio, che potrebbero fornire una base per un futuro scale-up. Sono stati descritti i diversi modelli CFD presenti in letteratura. In questo contesto è evidente la mancanza di studi riguardanti la modellizzazione di reattori elettrochimici progettati appositamente per la disinfezione dell'acqua. Tuttavia, è stata effettuata una prima caratterizzazione di un reattore. L'idrodinamica, studiata mediante le equazioni RANS, accoppiate ai modelli di turbolenza $k-\epsilon$, ha dato risultati in accordo con i dati ottenuti in letteratura. Se il processo è controllato dal trasferimento di massa, i miglioramenti idrodinamici possono portare a profili di velocità media più elevati all'interno della singola cella e quindi a un migliore trasporto di massa. Pertanto, i

distributori di ingresso e uscita si sono rivelati utili per fornire un migliore profilo idrodinamico e trasporto di massa. Per quanto riguarda gli aspetti elettrochimici, è stata eseguita una simulazione numerica della distribuzione di corrente primaria e secondaria lungo l'elettrodo di lavoro. L'analisi della distribuzione della corrente primaria ha dimostrato che la distribuzione della corrente è più uniforme lontano dagli angoli curvi originati dal distanziatore tra gli elettrodi; tuttavia, il valore di j_x/j_{ave} minimo è risultato 0.98, agli angoli. Pertanto, la distribuzione della corrente primaria all'anodo nel reattore studiato può essere considerata uniforme, poiché si possono trascurare gli effetti di bordo agli angoli curvi della cella. La distribuzione della corrente secondaria a diversi valori di sovratensione non ha mostrato effetti di bordo in nessuna punto, confermando quindi la convenienza di utilizzare questo tipo di cella grazie alla sua distribuzione uniforme della corrente sulla superficie dell'anodo, evitando la possibilità di avere reazioni parassite. Tuttavia, è importante ricordare che durante la degradazione elettrochimica di sostanze organiche, dovrebbe essere studiata la distribuzione di corrente terziaria. La presente analisi dovrebbe essere utile come punto di partenza per incorporare in futuro la distribuzione della corrente terziaria. Dall'andamento delle curve I-E valutate a diverse conduttività elettriche e distanze tra gli elettrodi, è stato calcolato il consumo di energia. Per alti valori di conduttività, quando la distanza diminuisce da $S = 1.1$ cm a $S = 0.4$ cm, sono state osservate variazioni limitate nel consumo di energia, quindi la distanza tra gli elettrodi non ha influenzato molto il processo (al massimo 2.7% a $k = 10$ S m⁻¹). Nel caso a $k = 0,1$ S m⁻¹ e $S = 1,1$ cm, considerando quindi la conduttività massima consentita nel trattamento dell'acqua destinata alla potabilizzazione, il consumo di energia è più che quadruplo rispetto a tutti i casi con conducibilità superiori. Diminuendo la spaziatura si ha un decremento notevole, tuttavia il consumo rimane su valori molto superiori al doppio rispetto al caso ideale. Poiché nel caso delle celle di flusso la spaziatura non può essere ulteriormente ridotta, si dovrebbero trovare alternative per ridurre i costi troppo elevati che l'uso di queste tecnologie richiederebbe quando si utilizza acqua a conduttività molto bassa. L'utilizzo di questi reattori sembra essere molto efficace nella disinfezione delle acque reflue, in quanto vi è la possibilità di utilizzare adeguati elettroliti di supporto e costi energetici drasticamente inferiori rispetto ai trattamenti delle acque destinate alla potabilizzazione. Ulteriori tecnologie, come l'utilizzo di reattori microfluidici, potrebbero essere studiate più approfonditamente, poiché consentono di operare senza elettroliti di supporto, evitando di utilizzare un possibile fonte di inquinamento secondario. Tuttavia, questa tecnologia è ancora immatura. In conclusione, questo lavoro è il punto di partenza per la progettazione tramite CFD di un reattore elettrochimico per la disinfezione dell'acqua, poiché include i principali aspetti fisici coinvolti nella modellazione di tali reattori. I modelli per il calcolo del coefficiente di trasporto di massa, così come i moduli di distribuzione della corrente terziaria, che tengono conto anche delle variazioni di concentrazione legate alla degradazione delle sostanze organiche, sono altri aspetti da aggiungere nella modellazione, al fine di fornire previsioni più precise.

1. Introduction

Water is the main requirement for the survival of all organisms, including humans. Hence, assuring adequate water supply is a major issue for all human beings. Nevertheless, the difficult access to safe drinking water is still one of the main problems that the world is facing in the 21st century ^[1].

This problem could begin terribly challenging to solve and could be worsened in the future because of the climate change, which directly influences the hydrological cycle, the amount and quality of water resources.

Moreover, other aspects such as demographic increase, economic growth, social changes and new technologies advancements also have a serious effect on water resources. Growing human population and industry development have favoured the spread of several new contaminants and pathogens within the water sources.

Therefore, the alteration of water bodies is a threat to human health, which is negatively affected by unsafe water, and make difficult an adequate sanitation and hygiene, which in turn enhances the risk of contracting and spreading diseases. Hence, the consumption of water contaminated with faeces, scarce faecal disposal and wrong hygienic practices favour the diffusion of pathogenic microorganisms, including viruses, bacteria, and parasites.

On July 28, 2010, the United Nations General Assembly formally recognised the right to safe and clean drinking and sanitary water as an essential human right ^[2]. In accordance with this statement, everybody has the right to sufficient, secure, clean, accessible, and economical water for personal domestic and sanitation use.

To achieve universal access, there is urgency to assure adequate water supply, sanitation, and hygiene due to the huge implications of these issues for public health, food security and equality. Nevertheless, nowadays, access to a safe source of drinking water is far to be possible in many countries around the world.

In high-income countries, full access to drinking water and sanitation has been nearly reached, and thus, the major goals are the maintenance and replacement of water supply infrastructures and the improvement of existing wastewater treatment processes. On the contrary, in developing countries, the drinking and sanitation water supplies do not cover all the population, and hence, the main challenge continues to be assuring a global access.

Furthermore, differences also exist in developing countries between urban and rural areas. One out of every three people living in rural areas is still without safe drinking water sources, and two out of every five of these people are without improved sanitation structures ^[3]. Moreover, due to the rapid demographic increase in the slums in developing countries in the world, it is estimated that the urban areas in these areas will be more vulnerable in a short time.

The countries with the poorest levels of progress are concentrated in sub-Saharan Africa (Fig. 1.1), where nearly half of the people use unsafe drinking water sources, and most of the population uses rivers, lakes, ponds, and irrigations canals as their main water source ^[3]. These sources are probably faecally contaminated since 80% of wastewater resulting from industries and rural activities in these zones is discharged into surface waters in absence of treatment, thus increasing the risk of waterborne diseases.

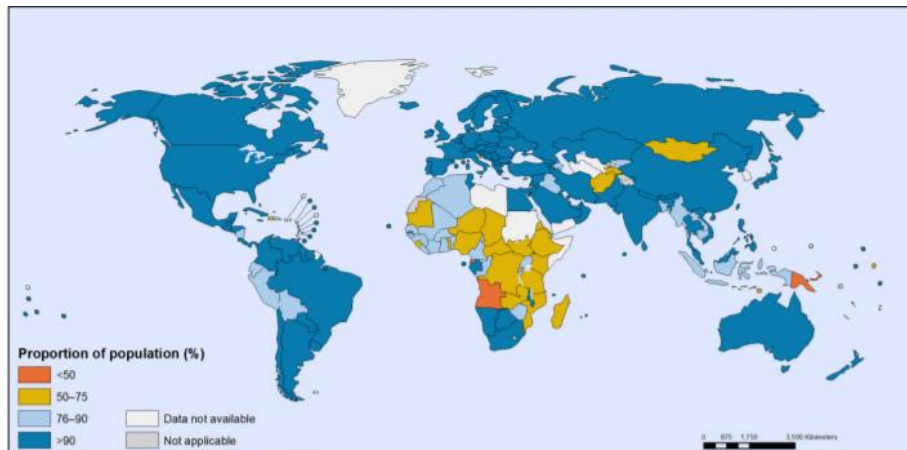


Figure 1.1 - Proportion of county populations using an improved drinking water source in 2015 ^[3]

A variety of technologies have been developed and exploited since the 19th century to respond to the need for safe drinking water. These treatment methods are widely described in the literature.

One of the first objective of this work is to provide a summary of conventional drinking water treatment technologies, highlights their possible drawbacks, thus the need to find alternative routes. On one hand they may assure pathogens inactivation, on the other hand a second issue has to be taken into account carefully: the possible formation of harmful by-products, which can be even more toxic than the original compounds.

The disadvantages of such disinfection methods have led the researchers to develop safer technologies to remove contaminants from water, including advanced oxidation processes (AOPs).

AOPs are based on the production on site of highly reactive hydroxyl radicals ($\bullet\text{OH}$), extremely reactive species that non-selectively react with most organics and are able to degrade pollutants. There are different emerging AOPs, but this work is focused on the eAOP, the electrochemical advanced oxidation processes, particularly on the anodic oxidation, AO, or EO, the most popular electrochemical application among the eAOP.

The main positive aspects of electrochemical methods for water disinfection are their high efficiency, moderate operating conditions, possibility of automation, versatility, and low cost, particularly when they are powered by renewable energy.

In this context, the design of an electrochemical reactor for water disinfection through CFD techniques is the main purpose of this thesis. The first part of the work is a review on traditional technologies and anodic oxidation methods used in literature, whereas in succession reactor design principles and mathematical modeling are presented. It is then reported a case study of a CFD reactor design for water disinfection.

Going even more in detail, the second chapter illustrates the main traditional technologies used in water purification, highlighting the resulting negative aspects entailing such methods, and present the advantages of advanced oxidation process technologies.

The third chapter presents the technology object of the study, anodic oxidation. The different electrode materials employed in literature are presented and the main parameters influencing these processes have been studied. It is worth highlighting that a large amount of lab-scale studies used these technologies in wastewaters treatment, whereas few research were found on the application of such methods on water intended for potabilization.

The fourth chapter shows the various reactor configurations used in this context, explaining why the flowcell configuration is the most employed, and the various aspects to consider while constructing a cell for this purpose. Then, some examples of lab-scale reactors, as well as commercial cells and new emerging configurations are described.

The fifth chapter illustrates the main aspects of CFD modeling, introducing the different models found in literature. Also in this context it is evident the lack of studies regarding the modeling of electrochemical reactors designed for water disinfection, whereas a lot of CFD works on a first hydrodynamic characterization of such reactors have been found.

In the sixth chapter the case study object of this study is presented. The numerical methods used in reactor design simulations, as well as the geometry, are explained.

In the seventh chapter there are the results and the discussion of the simulations, eventually followed by the conclusions and the possible future developments.

2. Drinking water treatment technologies

2.1 Water potabilization

Potabilization is a physical-chemical process consisting in the removal of contaminants from raw water in order to obtain a water suitable for normal domestic consumption, for fields irrigation or for industrial uses.

In Italy, to be defined as drinkable, a water must respect the limits set by EU Directive 98/83/EC implemented in Legislative Decree 2/02/2001, n.31 [4].

Water intended for human consumption must be healthy, clean, and must meet the minimum requirements set out in the following tables (Table 2.1 and Table 2.2).

Table 2.1 - Microbiological parameters set by EU directive 98/83/EC implemented in Legislative Decree 2/02/2001, n.31, from [4]

Microorganism	Number/100mL
Escherichia coli (E. coli)	0
Enterococcus	0

Table 2.2 - Chemical parameters set by EU directive 98/83/EC implemented in Legislative Decree 2/02/2001, n.31, from [4]

Substance	Permitted value	Unit measure
Acrylamide	0,1	µg/l
Antimony	5	µg/l
Arsenic	10	µg/l
Benzene	1	µg/l
Benzo (a) pyrene	0,01	µg/l
Boron	1	mg/l
Bromate	10	µg/l
Cadmium	5	µg/l
Chromium	50	µg/l
Copper	1	mg/l
Cyanide	50	µg/l
1.2 dichloroethane	3	µg/l
Epicirohydrin	0,1	µg/l
Fluoride	1,5	mg/l
Lead	10	µg/l
Mercury	1	µg/l
Nickel	20	µg/l
Nitrate (as NO ₃)	50	mg/l
Nitrite (as NO ₂)	0,5	mg/l
Pesticides	0,1	µg/l

Pesticides - total	0,5	µg/l
Polycyclic hydrocarbons aromatic	0,1	µg/l
Selenium	10	µg/l
Tetrachlorethylene	10	µg/l
Trihalomethanes-Total	30	µg/l
Vinyl chloride	0,5	µg/l

The quality standards defined by the law are reached through disinfection technologies. To ensure the effectiveness of disinfection throughout the water distribution chain, the legislation defines a minimum recommended concentration of disinfectant residue, which is absolutely safe from a health point of view.

However, in the practice of disinfection, multiple measures are taken into account to minimize the formation of by-products (DBPs - Disinfection by Products) as some of them, as in the case of trihalomethanes, can be toxic at certain levels of concentration.

Italian legislation has adopted a parametric value for the main by-products from treatment with hypochlorite (trihalomethanes) far more stringent than the value of the European directive [5]. In consideration of the widespread disinfection with chlorine dioxide, also chlorite has been included at national level, as an additional parameter respect to the EU directive, adopting as a limit the guide value established by the World Health Organization.

Nevertheless, on January 12, 2021, the new EU Directive for drinking water came into force, introducing a series of changes including the updating of water quality standards [6]. Member States have two years to transpose the changes into their national rules. Twenty years after the entry into force of the first directive on drinking water (98/83/EC implemented in Italy by Legislative Decree 31/2001), it was decided to update and tighten the threshold for some "old" contaminants, such as lead, in order to make drinking water even safer.

The chemical parameters have undergone a large revision, such as the modification of the values for some parameters and the introduction in the list of new substances. Chlorate and chlorite, by-products of the chemical disinfection with chlorine and its compounds, are now present among these substances. Haematological effects and disorders on the thyroid gland are ascribed to chlorate. Haloacetic acids (HAAs), potential carcinogens compounds, are other by-products of the traditional drinking water disinfection process considered into the EU Directive. This underlines how Member States have been focusing on the potential risks associated with traditional disinfection methods as chlorination, responsible for the possible formation of harmful by-products.

In this context, advanced oxidation processes (AOP) are seen as alternative technologies to replace the traditional methods of disinfection.

2.2 *Drinking water sources*

2.2.1 Drinking water sources in Italy

Rivers, streams, lakes, and aquifers are all potential sources of potable water. In Italy, the water resources used for drinking water supply are mostly of underground origin, from wells and springs, and, to a lesser extent, they originate from surface waters, with a minimum share of marine or brackish water (Figure 2.1) [7].

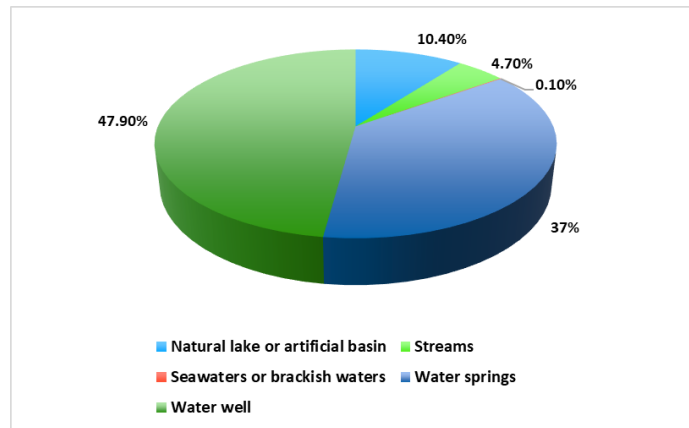


Figure 2.1 - Sources of water supply for potable use, from [7]

Internal waters, from surface or underground, are enriched with minerals which have essential biological functions in the human organism human [8].

In the presence of particular rocks, soils or sediments, in the waters can be found a significant concentration of toxic elements such as arsenic, fluorine, boron or uranium. This is relevant in Italy, given the geological history of our country, very long and complex, and characterized by the presence of numerous active volcanic areas.

Surface and underground water bodies are exposed to anthropogenic contamination, which can be particularly significant in areas with high agricultural and industrial activities, increased by the lack of adequate wastewater treatment.

2.2.2 Wastewaters as drinking water sources

In some contexts, also wastewaters may be used as drinking water sources. Water scarcity and low water quality in several regions of the world have determined an increasing water request and are becoming serious problems [9].

In many regions, long periods of dryness occur frequently. Moreover, usually in the same regions, the infrastructures for water treatment and distribution are not sufficient or available. In many parts of the world it may not be possible to provide sewage facilities for all residents, now or in the future Errore. L'origine riferimento non è stata trovata.. In those cases, decentralized wastewater treatments are used in managing the WWs.

Hence water recycling and reuse seem to be necessary. In the last decades the development of new technologies in WW treatment have allowed recycled water applications to be widespread also to indirect and direct potable reuses [11].

However, the spread of the application is limited as many constraints still exist. Lack of infrastructures, high costs of transport and overall public objection still restrict the use of the use of WWs as drinking water sources [12].

In this context, electrochemical technologies may be very useful, for example, in the disinfection process where a high concentration of oxidant can be generated in situ. The treatment only needs the application of an electric current and allow a simple process management and remote control Errore. L'origine riferimento non è stata trovata..

2.3 Water treatment process

Water treatment processes provide barriers and protections from waterborne diseases. These barriers, when used in succession of treatment processes, are known jointly as a *treatment process train* ^[13] (Figure 2.2). However, the water treatment process may vary slightly at different locations, depending on the technology of the plant and the water it needs to process, but the basic principles are largely the same.

The most common *treatment process train* for water supplies, known as *conventional treatment*, consists of *coagulation*, *flocculation*, *sedimentation*, *filtration*, and *disinfection*. Usually, a disinfectant as chlorine, or an alternative one, such as chlorine dioxide or ozone, is added at both the beginning and end of the process train to enhance the disinfection power.

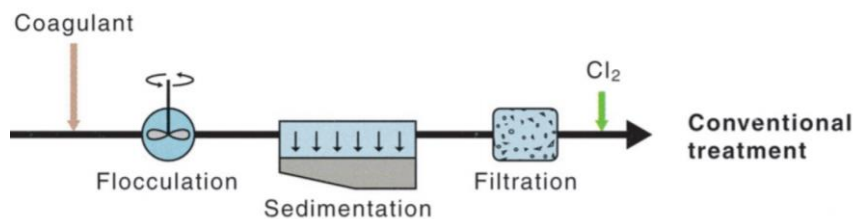


Figure 2.2 - Typical water treatment process train, from [13]

Coagulation change the physical and chemical state of dissolved and suspended solids and facilitates their removal by sedimentation and filtration. The most common primary coagulants are hydrolyzing metal salts, for instance alum $[\text{Al}_2(\text{SO}_4)_3 \cdot 14\text{H}_2\text{O}]$, ferric sulfate $[\text{Fe}_2(\text{SO}_4)_3]$, and ferric chloride (FeCl_3). Further chemicals that may be added to improve the coagulation process are charged organic molecules, polyelectrolytes. These chemicals ensure the aggregation of the suspended solids during the next treatment step, flocculation.

Flocculation is a physical process in which the treated water is shuffled to increase interparticle collisions, thus promoting the contact and the formation of larger particles. After adequate flocculation, most of the aggregates settle out during the 1–2 h of sedimentation. Microorganisms are entrapped or adsorbed to the suspended particles and removed during sedimentation.

Sedimentation is another physical process, involving the gravitational settling of suspended particles heavier than water which fall down and can be separated from water.

Filtration is the following process, consisting in the passage of the water through a filter medium in order to remove particulate matter from the water and reduces turbidity. There are different systems of filtration. In Europe, slow sand filtration is employed, operating at low filtration rates. Rapid filtration is commonly used in the United States. Rapid filters typically consist of 50–75 cm of sand and/or anthracite having a diameter between 0.5 and 1.0 mm.

Coagulation, flocculation, sedimentation, and filtration collectively remove many contaminants as presented in Table 2.3.

Table 2.3 - Coagulation, Sedimentation, Filtration: typical removal efficiencies and effluent quality, from [13]

Organisms (% Removal)	Coagulation and Sedimentation (% Removal)	Rapid Filtration (% Removal)	Slow sand Filtration (% Removal)
Total coliforms	74–97	50–98	>99.999
Fecal coliforms	76–83	50–98	>99.999
Enteric viruses	88–95	10–99	>99.999
<i>Giardia</i>	58–99	97–99.9	>99
<i>Cryptosporidium</i>	90	99	99

These treatments also reduce turbidity, giving clear water and also enhance disinfection efficiency. If not removed by such methods, particles may entrap microorganisms and make final disinfection more difficult. Filtration is an important barrier in the removal of the protozoan parasites *Giardia lamblia* and *Cryptosporidium*, because of their larger size. These microorganisms are very resistant to inactivation by disinfectants, so disinfection alone cannot assure complete prevention from waterborne illness.

On the other hand, viruses and bacteria, because of their smaller size, can pass through the filtration process. Hence disinfection remains the ultimate barrier to these microorganisms.

2.4 Water disinfection

Disinfection is employed as method for the removal of pathogenic microorganisms from drinking water. It is a crucial process in water treatments, as it has to ensure the disactivation of pathogenic organisms.

Generally, disinfection is done through the addition of a chemical, more specifically an oxidant. Chlorine is by far the most used disinfectant to treat drinking water, but also other oxidants are utilized, such as chloramines, chlorine dioxide, and ozone.

Inactivation of microorganisms proceeds through a series of physicochemical and biochemical steps. Various models have been employed in order to predict the result of disinfection, basing on experimental data. *Chick–Watson Model* is the main disinfection theory used to express the rate of inactivation of microorganisms, described as a first-order chemical reaction as it can be seen in the following equations (2.1, 2.2).

$$\frac{N_t}{N_0} = e^{-kt} \quad (2.1)$$

Or equivalently:

$$\ln \frac{N_t}{N_0} = -kt \quad (2.2)$$

Where N_0 is the number of microorganisms at time 0, N_t is the number of microorganisms at time t , k is the decay constant (1/time) and t is the time. The logarithm of the survival rate N_t/N_0 is plotted as a straight line over the time (Figure 2.3).

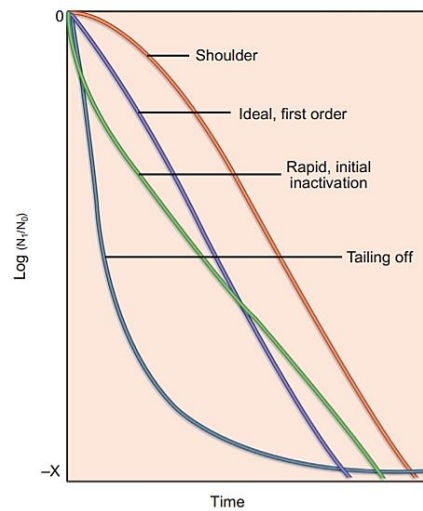


Figure 2.3 - Types of inactivation curves observed for microorganisms, from [13]

As it can be seen from the graph, laboratory data often deviate from first-order kinetics.

Shoulder curves may result from clumps of organisms or different hits of critical sites before inactivation. This kind of curves are easy to find in disinfection by chloramines.

The tailing-off curve is obtained with many types of disinfectants and may be explained by the survival of a resistant subpopulation, aggregation or genetical resistance.

Disinfection efficiency is determined by different factors, such as temperature and pH. Temperature controls the rate of chemical reactions and modify the value of the constant k . The rate of kill increases as the temperature increases.

The pH can affect the ionization of the disinfectant and the activity of the organism. Most waterborne organisms are negatively affected by pH levels below 3 and above 10. In the case of halogens such as chlorine, pH variations determine the amount of $HOCl$ (hypochlorous acid) and OCl^- (hypochlorite) in solution. The former is more effective than the latter in the

disinfection of microorganisms. Hence, as hypochlorous acid is prevailing at low pH, working at low pH favour the efficiency of the disinfection.

2.5 Water disinfection methods

Conventional disinfection methods may be divided among chemical and physical processes.

The chemical processes include the use of disinfecting substances such as chlorine, chloramines, chlorine dioxide or ozone which are added to the water. These processes have proven their efficiency over many decades. In addition to the inactivation of the microorganisms, they also provide a disinfection reservoir which provide a barrier for the recontamination for time.

On the other hand, unwanted side reactions of the disinfectants with substances present in the water may be a frequent drawback of the chemical processes. These reactions cause the formation of disinfection byproducts (DPBs), some of which are considered risky. There are also dangers in producing, transporting and managing big amounts of such substances as chlorine and ozone.

In physical disinfection processes the removal or death of microorganisms occurs by means of irradiation with ultraviolet, heating to elevated temperatures, ultrasound, or separation through membrane filtration.

Contrary to chemical processes, physical technologies are only effective in the immediate surroundings of their operating devices and do not assure the absence of recontamination for time.

A brief explanation of some of these methods is given below.

2.5.1 Conventional methods

The most used conventional method is the *Chlorination*. Chlorine and its compounds are the most employed disinfectants for treating drinking and wastewater. Chlorine is a strong oxidant which form a mixture of hypochlorous acid ($HOCl$) and hydrochloric acids (HCl) when added as a gas to water (Equation 2.3).



Hypochlorous acid can dissociate according to the following equation (2.4).



The dissociation of hypochlorous acid in H^+ and OCl^- (hypochlorite ion) depends on the pH of the water.

The amount of $HOCl$ is greater at neutral and low pH levels, hence a greater disinfection ability of chlorine occurs at these pH levels. Chlorine as $HOCl$ or OCl^- is defined as *free chlorine*.

$HOCl$ combines with ammonia and organic compounds to form what is known as *combined chlorine*.

The reactions of chlorine with ammonia and nitrogen-containing organics result in the formation of *chloramines*. These products preserve some of the disinfecting power of hypochlorous acid but are much less effective than chlorine.

Free chlorine is quite efficient in inactivating pathogenic microorganisms and bacteria, whereas enteric viruses and protozoan parasites are more resistant to it.

Chloramination is the process involving inorganic chloramines, oxidant agents produced by combining chlorine and ammonia (NH₄). The species of chloramines formed depend on different aspects, including the ratio of chlorine to ammonia-nitrogen, chlorine concentration, temperature, and pH. The predominant product formed is monochloramine when the chlorine-to-ammonia mass ratio is lower than 5. This species shows greater disinfection efficiency than the other forms, dichloramine and trichloramine.

Chloramines are slow acting, thus they have mainly been used as secondary disinfectants when a residual in the distribution system is required. As instance, when ozone is used to treat potable water, no residual disinfectant remains. Due to the possible bacteria growth after ozonation of tap water, chloramines are used subsequently in the distribution system to prevent these phenomena.

Chlorine dioxide (ClO₂) is a further disinfectant widely used. It is extremely soluble in water and, contrarily to chlorine, does not react with ammonia or organic to form trihalomethane, which is potentially carcinogenic. As it cannot be stored, chlorine dioxide must be generated on site.

It is formed from the reaction of chlorine gas with sodium chlorite as it follows (Equation 2.5)



Chlorine dioxide does not dissociate in water but exists as a dissolved gas. Chlorine dioxide is more efficient in inactivating bacteria and viruses in water than chlorine.

Ozone (O₃), a powerful oxidant, can be produced by using an electric discharge through a stream of air or oxygen. As ozone does not produce trihalomethanes or other chlorinated by-products, suspected carcinogens, it has increased in popularity as a disinfectant.

On the other hand, ozone is more expensive than chlorination to apply to drinking water and during ozonation aldehydes and bromates may be formed, bringing to adverse health effects.

As mentioned previously, ozone does not leave any residual in water and the process is usually followed by chlorination or addition of chloramines to prevent regrowth of bacteria.

The efficiency of ozone as a disinfectant is not affected by pH and ammonia. Ozone is a more effective oxidant than chlorine.

Ultraviolet light method is a physical process to disinfect water and wastewater using ultraviolet light at the UV-C wavelength, in order to modify the DNA of microorganisms and thus prevent their reproduction.

It has become widely spread because it does not produce carcinogenic or toxic by-products, or taste and odor problems. Moreover, it is not necessary to handle or store toxic chemicals. A wavelength from 240 to 280 nm directly attacks the vital DNA of bacteria, viruses and other microorganisms. The radiation induces a photochemical reaction which breaks the DNA. The bacteria lose their ability to reproduce and are destroyed.

On the other hand, it has several disadvantages, including high costs, no disinfectant residual, difficulty in determining the UV dose needed, maintenance and cleaning of UV lamps, and possible photoreactivation of some enteric bacteria.

However, some improvements in UV technology are providing lower cost, more efficient lamps, and more dependable equipment.

The efficiency of UV light is decreased in wastewater effluents by substances that influence UV transmission in water. Suspended matter may protect microorganisms from the activity of UV light; hence, filtration of wastewater is commonly needed for efficient UV light disinfection.

2.5.2 Disinfection by-products

Such conventional disinfection treatments as chlorination, chloramination, chlorine dioxide, ozonation, ultraviolet (UV) are mostly applied to the water to guarantee the absence of pathogens. Nevertheless, while they may assure pathogens inactivation, a second issue has to be taken into account carefully: the possible formation of harmful by-products, which can be even more toxic than the original compounds.

All chemical disinfectants cause the formation of organic and/or inorganic disinfection by-products (DBPs), which may be carcinogenic or harmful. A summary of the types of disinfectant by-products is showed in Table 2.4.

The most diffused chlorination by-products comprise chloroform, bromodichloromethane, dibromochloromethane, and bromoform. These compounds are collectively known as the *trihalomethanes* (THM), and the term total trihalomethane (TTHM) refers to their united concentrations. These compounds are formed by the reaction of chlorine with organic matter, mostly humic acids, normally in the water in nature.

Haloacetic acids are a group of by-products produced with chlorine. Also monochloramine produce THM, but in lower concentrations than chlorine. It also produces other DBPs, including cyanogen chloride. The five haloacetic acid most diffused are monochloroacetic acid, dichloroacetic acid, trichloroacetic acid, monobromoacetic acid, and dibromoacetic acid, and they are known as HAA5.

Ozone oxidizes bromide to produce bromate, which is mutagenic and is carcinogenic in animals.

Many of these by-products are classified as probable carcinogens. However, the data of numerous epidemiological studies of populations consuming chlorinated drinking water in the United States demonstrate that the risks of cancer seem to be low^[11].

A maximum contaminant level (MCL) has been established for alle these harmful substances, as already mentioned in paragraph 2.1. Meanwhile, it is fair to underline that the risks related to the waterborne microorganisms overcome the risk from low levels of DBPs produced during water treatment^[14].

However, there are some precautions to avoid, or lower, the formation of DBPs. For instance, the formation of THMs during chlorination can be reduced by removing precursors before the contact with chlorine, by improving coagulation, or reducing the amount of organic matter.

As it has been seen, UV is also an alternative to chemical disinfection, but does not provide any residual disinfection, thus the addition of low doses of chemical disinfectants may be required, causing the formation of some DBPs.

Table 2.4 - Primary disinfectant byproducts

Disinfectant	Byproduct
Chlorine	Thrialomethanes, haloacetic acids
Chloramine	Nitrite
Chloride dioxide	Chlorite, chlorate
Ozone	Bromate

2.6 Advanced oxidation processes for water disinfection

The disadvantages of such disinfection methods have led to research efforts in order to develop more effective technologies to remove contaminants from water, including advanced oxidation processes (AOPs).

There are different established and emerging AOPs, as the ozone-based or the UV-based, electrochemical (eAOP), catalytic (cAOP), and physical (pAOP) ^[15].

AOPs are based on the production on site of highly reactive hydroxyl radicals ($\bullet\text{OH}$), extremely reactive species that non-selectively react with most organics and able to degrade even highly recalcitrant compounds. Hydroxyl radical is the second strongest oxidant known after fluorine. Moreover, $\bullet\text{OH}$ radicals have a short lifetime, estimated as only a few nanoseconds in water, and so they can cleanse itself from the treatment system. Mechanisms of radical formation depend on the specific technology, on process parameters and can be affected by system design and water quality.

On the other hand, AOPs are very expensive technologies both from a capital and operational point of view. They can present problems of radical uptake by unwanted species and therefore a reduction in efficiency. Oxidation by-product generation during the application of AOPs is another critical factor for process viability.

Nonetheless, advanced oxidation processes are widely used since the production of hydroxyl radicals as a disinfectant means guarantees a high removal of contaminants resistant to traditional treatments.

In this framework, if compared with other chemical disinfection methods, the advantages of eAOP, a specific AOP, need to be underlined. Electrochemical processes produce oxidizing species through electrochemical systems. Water disinfection benefits by means of eAOP are evident: no transport, storage and dosage of disinfectants are necessary. The disinfecting effect can be controlled according to the on-site requirements ^[16].

Moreover, electrochemical water disinfection shows a reservoir effect and needs less maintenance than other disinfection methods. In addition to this, some studies have shown how photovoltaic power supplies make it possible to use electrochemical water disinfection far from

the electrical supply grid ^{[17],[18]}. This may be important for its use to produce drinking water in developing countries. Electrochemical water disinfection can also be coupled with other disinfection methods ^[19].

Given the potential positive aspects deriving from the use of electrochemical advanced oxidation processes, several studies have been carried out on this technology in recent years.

However, the industrial applications of this technology in water treatment, especially in water purification, are still very few.

A further explanation of the eAOP, as well as its basic operational principles, is given in the next chapter.

3. Electrochemical advanced oxidation processes

The development of new environmentally friendly technologies able to degrade organic matter and eliminate pathogens has become an extremely urgent challenge, due to the drawbacks related to the conventional technologies.

As already mentioned, great progress has been made regarding the electrochemical technologies, especially for the abatement of biorefractory substances. As a matter of fact, the application of these technologies in the effort against environmental pollution has been the theme of several books and authoritative reviews.

The most important advantages of electrochemical methods for water disinfection are their high efficiency, moderate operating conditions, possibility of automation, versatility, and low cost, particularly when they are powered by renewable energy.

The feasibility of electrochemical technologies has been tested with a wide variety of synthetic wastewater or water types containing a diversity of target compounds, thus achieving a huge amount of results that have allowed proper conditions to be set for the quick and complete elimination of organics from real effluents.

Nevertheless, some disadvantages still persist, hence limiting their industrial application. Examples include the short lifetime, the high cost of some electrode materials, low current efficiency or potential maldistribution under some conditions.

In addition, some intrinsic drawbacks, such as mass transport limitations, low space-time yield and surface area to volume ratio and temperature increase have not yet been satisfactorily resolved.

Moreover, the effect of pH, pollutant type and concentration, effluent conductivity, electrochemical reactor design, and electrode arrangement, potential or current density distribution and the formation of byproducts have not been fully explored in all the studies.

In conclusion, further studies are necessary to develop these processes on an applicable scale.

The simplest and most popular eAOP is anodic oxidation (AO), where organics can be directly oxidized at the anode surface by electron transfer and/or indirectly oxidized by $\bullet\text{OH}$ weakly physisorbed at the anode surface.

3.1 *Anodic oxidation*

Anodic oxidation, AO, or EO, is the most popular electrochemical application among the advanced electrochemical oxidation processes (EAOP) for the removal of organic pollutants from water.

Anodic oxidation consists in the oxidation of pollutants in an electrochemical cell through two different mechanisms, as reported in figure 3.1.

- Direct anodic oxidation: direct transfer of electrons to the anode. This type of process leads to very scarce decontamination.

- Indirect or mediated oxidation: oxidation by chemical reaction with species generated by the water discharge on the surface of the anode, such as physisorbed active oxygen (also known as physisorbed hydroxyl radical, $\bullet\text{OH}$) or chemisorbed active oxygen, for instance oxygen in the lattice of a metal oxide anode (MO). The action of these oxidizing species depends on the electrocatalytic activity of the anode, and leads to total or partial decontamination, respectively.

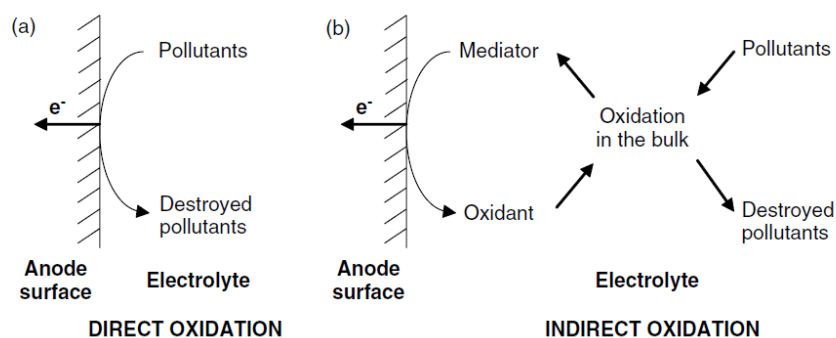


Figure 3.1 Schemes for (a) direct and (b) indirect electrolytic treatment of pollutants, figure taken from [20]

Given the existence of different heterogeneous species formed by the discharge of water, two approaches are possible for the abatement of pollutants:

- Electrochemical conversion, in which the organic refractories are selectively transformed into biodegradable and harmless compounds under the action of chemisorbed active oxygen.
- Electrochemical combustion, or electrochemical incineration, whereby organic substances are completely mineralized by physisorbed active oxygen to H_2O , CO_2 , and inorganic ions.

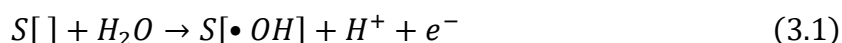
Both approaches require the application of high anode potentials, thus causing competition with the oxygen evolution reaction (OER) [21].

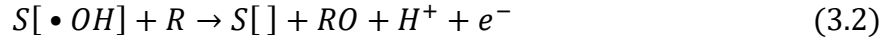
Direct oxidation is possible at low potential values, lower than the OER potential, but the reaction rate is usually slow and strongly depends on the electrocatalytic activity of the anode. The main problem with this approach is the progressive decrease in catalytic activity, due to the formation of a polymer layer on the anode surface [22].

The region of the oxidation potential of the pollutants, compared with OER potential, is therefore a key parameter to understand both the selectivity and the efficiency of the treatment, and it strongly depends on the specific characteristics of the anodic material, which determines its ability to produce $\bullet\text{OH}$ of different nature and concentration.

3.1.1 Model for Organic Oxidation by Heterogeneous Hydroxyl Radicals

The reaction mechanism leading to the oxidation of organics involves oxygen transfer reactions with a high anodic potential, through the production of adsorbed hydroxyl radicals $\bullet\text{OH}$ generated by the water discharge reactions (equations 3.1 and 3.2), where $S[]$ represents the surface site where $\bullet\text{OH}$ species can be adsorbed:





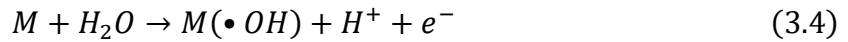
The unwanted oxygen evolution reaction occurs simultaneously as showed in the following equation (3.3).



There are two limit cases, the *active* electrodes and the *non-active* electrodes.

There is a simplified model for the selective oxidation or combustion of organics with simultaneous O₂ evolution proposed by Comninellis ^[23].

The model assumes that the starting reaction in both types of anodes *M* corresponds to the oxidation of water leading to the formation of the physisorbed hydroxyl radical (equation 3.4).



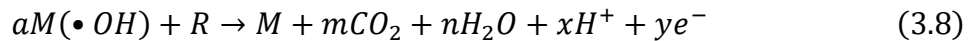
At the *active* anodes, the surface strongly interacts with •OH and therefore a superior oxide or superoxide *MO* can be formed, according to the following reaction (equation 3.5).



This can occur when the metal oxide constituting the anode provides oxidation states above the standard potential for the OER reaction. The *MO/M* redox couple acts as a mediator in the oxidation of organic substances and competes with the OER through the chemical decomposition of the higher oxides (respectively showed in equations 3.6 and 3.7).

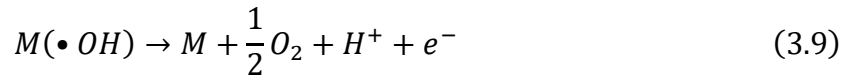


At the *non-active* anodes, where higher oxides formation does not occur, the hydroxyl radicals, commonly known as physisorbed active oxygen *M(•OH)*, allow the non-selective oxidation of organic substances, which can cause complete combustion to CO₂



Where *R* is an organic compound with *m* carbon atoms and needs a oxygen atoms to be totally mineralized to CO₂.

In both types of anodes, •OH can also be simultaneously oxidized (equation 3.9) or can undergo dimerization with the formation of hydrogen peroxide (equation 3.10) and a consequent decrease in the efficiency of the process.



The electrochemical activity of the physisorbed active oxygen *M(•OH)* is related to the overpotential for the oxygen evolution and its chemical reactivity is related to the oxidation rate of organic substances. They are both highly dependent on the strength of the *M – (•OH)* interaction.

Thus, while anodes with a low oxygen evolution potential (i.e. anodes which are good catalysts for OERs) lead to the partial oxidation of organic substances, anodes with a high oxygen evolution potential (i.e., anodes which are bad catalysts for OERs) favor the complete oxidation

of organic substances to CO_2 , thus becoming ideal electrodes for water treatment as in the case of PbO_2 and BDD.

Their behavior is a consequence of the weaker $M - (\bullet OH)$ interaction, which favors higher anodic reactivity for the oxidation of organic substances. A classification of the most common anodes for EO with their properties can be found in the table 3.1.

Table 3.1 - Classification of anode materials based on their oxidation power and potential for O_2 evolution in acidic media; (a)Standard potential for OER is 1.23 V versus normal hydrogen electrode

Anode type	Composition	Electrocatalytic ability for the OER	Oxidation potential (V) ^a	Overpotential for OER (V)
Active	RuO_2-TiO_2	Good	1.4-1.7	0.18
	$IrO_2-Ta_2O_5$	Good	1.5-1.8	0.25
	Ti/Pt	Good	1.7-1.9	0.30
Non-active	Ti/ PbO_2	Poor	1.8-2.0	0.50
	Ti/ $SnO_2-Sb_2O_5$	Poor	1.9-2.2	0.70
	p-Si/BDD	Poor	2.2-2.6	1.3

3.2 Effect of the anode material

The percentage of abatement and the efficiency of the electrochemical oxidation depend mostly on the nature of the anode material, and thus, the proper choice of the electrocatalytic material is crucial.

As stated by Walsh^[24] and Urriaga^[20], the electrode must have the following characteristics:

- high physical and chemical stability, being resistant to erosion, corrosion, and formation of passive layers;
- high electrical conductivity;
- high catalytic activity and selectivity;
- low cost and high durability (i.e., long service life).

The technologies are still far from produce materials which meet all the requirements, but significant steps have been made toward the production of better electrode materials.

As already mentioned, the anodic materials can be classified as *active* or *non-active*, depending on the mechanisms involved in the oxidation process, but the subdivision is not strongly clear, as different anodes can exhibit intermediate behaviors.

Generally, *active* electrodes are constituted by a metal support coated by a layer of inorganic conductive oxide. Originally, the most used oxides were RuO_2 and IrO_2 . The addition of catalytically active components and oxides such as TiO_2 , SnO_2 , and Ta_2O_5 has also been used to improve the performances of these materials while maintaining their main catalytic characteristics.

As previously reported, with *active* electrodes such as Ti/RuO_2 , Ti/Pt and Ti/IrO_2 , the electrochemical oxidation is supposed to occur through higher metal oxides that can catalyze the transformation of organic substances to more oxidized compounds by several chemical and

electrochemical steps. However, in this case, low faradic efficiencies have generally been observed.

Non-active electrodes are typically fully oxidized metal oxides, such as Ti/PbO₂, or boron doped diamond (BDD) anodes. In this case the oxidation is mediated by physi-adsorbed •OH radicals generated at the anode surface during the water discharge.

Several studies have showed the much higher efficiency of the *non-active* electrodes like PbO₂ [25], [26] and BDD [27] [28], [29]. Therefore, this kind of electrodes are the most used for electrochemical processes of advanced oxidation.

3.2.1 Lead dioxide anodes

Lead dioxide anodes are cheap and easy to prepare, with good conductivity, chemical stability, and a large surface area. Hence, they are suitable for industrial applications. Moreover, there is a great concern in the development of PbO₂ anodes for the oxidation of organics, because of their large overpotential for oxygen evolution, which enables the production of hydroxyl radicals during water discharge.

Thanks to the production of •OH radicals, PbO₂ performs quite well organics mineralization and it has been used for the oxidation of several compounds.

The effectiveness of PbO₂ is strongly affected by the crystal structure and the incorporation of doping species such as Fe, Co, Bi, F. The addition of doping species diminishes the size of the crystal particles, increases the specific surface area and leads to crystal cell expansion and structure defects. These two aspects increase the active sites on the surface of the PbO₂ electrode, making it more conducive to the generation of hydroxyl radicals. Therefore, the electrocatalytic activity is enhanced.

For almost all pollutants, PbO₂ anodes assure faster mineralization than other anode materials, but they are less efficient than BDD anodes under the same operating conditions [30], [31], [32], [33], [34]. This is due to the hydrated surface of PbO₂, which make the adsorption of hydroxyl radicals stronger. Consequently, PbO₂ is less reactive than BDD, which has an inert surface with weak adsorption properties, thus allowing a more likely action towards the oxidation of organic compounds.

Despite the effective performance shown by lead dioxide anodes during electro-oxidation, this material has a serious negative issue that strongly limits its application. PbO₂ can undergo leaching and release Pb²⁺ ions in solution, causing water contamination.

Hence, recently the interest in PbO₂ for water treatment is reduced.

3.2.2 Tin dioxide anodes

Pure SnO₂ is a semiconductor with a low conductivity at ambient temperature; thus, it cannot be used as electrode material. However, its conductivity can be enhanced by doping with Ar, B, Bi, F, Cl, P, and, particularly, Sb, which is frequently used in electrochemical applications.

Antimony-doped SnO₂ electrodes have a good conductivity and an overpotential for oxygen evolution of about 1.9 V vs SHE, which makes it effective electrode material for degradation of organics.

Stucki et al. [35] first reported the use of antimony-doped tin oxide deposited on a titanium base metal (Ti/SnO₂-Sb₂O₅) for electrochemical wastewater treatment and many other papers demonstrated the great potential of SnO₂ for wastewater treatment [[36], [37], [38], [39]].

Unfortunately, these electrodes are not currently commercially available, because of their short service life. Therefore, these anodes are subjected to many laboratory investigations for further improvement.

Aside from the addition of doping species, other various methods had been attempted to overcome the defects of SnO₂ electrodes, involving intermediate layers and nano-architecture [40].

The intermediate layer can reinforce the bonding between the electrode active layer and the matrix, avoiding the shedding of the active layer, improving the electrocatalytic activity and increasing the electrode service life. At present among the commonly used intermediate coatings there are Pt [40] and IrO₂ [41].

Nano-structure construction is also an effective way to enhance the electrocatalytic activity, basically including two approaches, one is to build a nano-structured matrix to improve the active catalyst loading, and the other is to fabricate nano-sized or nanocrystalline SnO₂.

3.2.3 Ti based oxide anodes

Titanium (Ti) is cheap and widespread in nature, but it is easy to be oxidized to form a TiO₂ layer, which leads to low conductivity ($10^{-9} \Omega^{-1}\text{cm}^{-1}$) not suitable for anodic oxidation.

The reduction of TiO₂ to Magnéli phases (Ti_nO_{2n-1}, n = 4 to 10) is the main doping method that has been used to produce highly electrically conductive electrodes that are also extremely resistant to corrosion. The ideal Magnéli phase is Ti₄O₇, which has the highest room temperature electrical conductivity (up to $416 \Omega^{-1}\text{cm}^{-1}$); thus it is the target phase for electrode preparation. Due to these properties, Ti_nO_{2n-1} electrodes have recently been used as anodes for electrochemical oxidation of water contaminants.

As a matter of fact, several studies have shown that Ti₄O₇ electrode, known by the trade name of Ebonex®, is a good non-active anode as it has a large O₂ evolution overvoltage and can generate weakly adsorbed hydroxyl radicals from water oxidation. It has exhibited a better effectiveness than the classical anodes Pt and can constitute an alternative to BDD anode, as it is cheaper, but slightly less efficient in organics degradation [[43], [44], [45], [46]]. Moreover, recent work compared Ebonex® electrodes with BDD, showing that the former produces lower amounts of radicals than the latter but with higher reactivity [44].

The Magnéli phase titanium oxides can be prepared either by heating TiO₂ with metallic titanium under an inert atmosphere or by reducing TiO₂ at high temperatures using a reducing agent such a hydrogen gas. Typically, TiO₂ is used as the main feedstock due to its abundance and relatively low cost. Reduction requires high temperatures (>1000 °C) and a reducing atmosphere (usually hydrogen) [47].

Due to the oxygen deficient nature of substoichiometric TiO₂, oxygen incorporation into the lattice structure can occur during anodic polarization and thus the formation of a passivating TiO₂ coating.

Recent work with Ti₄O₇ electrodes has demonstrated that periodic polarity inversions during the oxidation of sulfide were able to prevent electrode passivation [48]. These studies show that

Ti₄O₇ electrode behave both as inactive and active anode. As inactive anode it forms •OH during water oxidation, and as active anodes it forms a higher oxide during water oxidation. However, the higher oxide formed (TiO₂) is not able to participate in oxygen transfer reactions and thus substrate oxidation^[48]. More detailed studies of the passivation of Ti₄O₇ are necessary.

Some other studies attempted to modify Ti to be an efficient anode for contaminants degradation by forming TiO₂ nanotubes (TNT) which was acted as non-active anode. However, TNT had a poor conductivity.

Lately, the electrochemical reduction method was used to obtain Blue-TNT, achieving a good conductivity. The Blue-TNT has a large window of potential and it is highly electrocatalytic active. However, it was revealed that the Blue-TNT has a short lifetime and narrow current density. Nevertheless, the short lifetime can be enhanced by elements doping, such as Co and B^[49].

As it is reported, Ti-based material studies are still today in progress. Future research should focus on a better understanding of these electrodes and further effectiveness perspectives.

3.2.4 BDD anodes

Boron-doped diamond (BDD) thin film is a new synthetic electrode material that has recently received great attention, due to the development of technologies for the synthesis of high-quality conducting diamond films at a commercially suitable deposition rate.

Diamond films are constructed on different materials, such as silicon, tungsten, molybdenum, titanium, niobium, tantalum, or glassy carbon, by chemical vapor deposition (CVD). The CVD method is relatively cheap and has resulted in a diffuse interest in polycrystalline diamond layers for industrial applications.

High-quality BDD electrodes possess several technologically important characteristics that make them the most promising and widely studied electrode for EAOPs^[50]:

- An extremely large potential window in aqueous and nonaqueous electrolytes
- Corrosion stability also in very aggressive media
- Inert surface with low adsorption properties and strong resistance to deactivation
- Very low double-layer capacitance and background current

To make diamond films conducting, they are doped with boron atoms. The doping level of boron in the diamond layer is expressed as B/C ratio and is in the range of 1000-10000 ppm. The boron atoms replace carbon atoms in the diamond lattice making a p-type semiconductor, where the dopant depletes an extra electron for chemical bonding hence creating excess holes in the semiconductor.

BDD electrodes are extremely stable under anodic polarization, due to the C atoms being in sp³ hybridization. Nevertheless, BDD film electrodes are still subject to failure, due to film delamination from the substrate, or wear at grain boundaries at high applied current densities^[51].

The traditional substrate for diamond electrodes is p-silicon, as it forms a compact self-limiting oxide and has a quite low electrochemical activity, which prevents film delamination^[51]. However, the fragility of Si makes it not suitable for industrial applications, thus various studies have investigated different substrates for the BDD films, including Ta, Nb, W, Ti, and various

interlayers on metal substrates. Chaplin et al. [51] demonstrated that the substrate stability of nanocrystalline BDD electrodes followed the order of: Ta > Si > Nb > W >> Ti.

However, the most important aspect to prevent film delamination is matching the thermal expansion coefficients of the diamond and that of the substrate. A large difference between the coefficients value of diamond and the substrate can lead to irregularities in the film that permit electrolyte permeation through the BDD film and cause substrate corrosion. Metals whose thermal expansion coefficient value decrease from the metal substrate to its corresponding oxide are the most resistant substrates to film delamination. For such metals the oxide is denser than the pure metal and thus will not result in delamination of the BDD film when the substrate becomes oxidized. This is the case for Si and Ta, and both have been demonstrated to be very stable electrode substrates. On the other hand, a thermal expansion coefficient increase from the metal to the oxide corresponds to a physical expansion of the oxide that causes BDD delamination. This is the case for Nb, W, and Ti, leading to BDD film delamination.

However, different strategies have been used to improve the adhesion of BDD films to a Ti substrate and overcome the difference in the thermal coefficient values. The use of Ti is advisable because it is cheap, highly conductive, and much more robust than Si. Increasing the stability of BDD/Ti electrodes is an interesting area of research, with the further objective of decreasing the cost of BDD electrodes.

It has been demonstrated that the surface functional groups of BDD electrodes have a significant effect on charge transfer at the electrode surface. As shown in Fig. 3.2, freshly prepared electrodes are H-terminated, but anodic polarization forms various oxygenated-functional groups (i.e., hydroxyl ($\equiv\text{C}-\text{OH}$), carbonyl ($=\text{C}=\text{O}$), carboxyl ($-\text{COOH}$)) that have been observed by X-ray photoelectron spectroscopy (XPS) measurements [52].

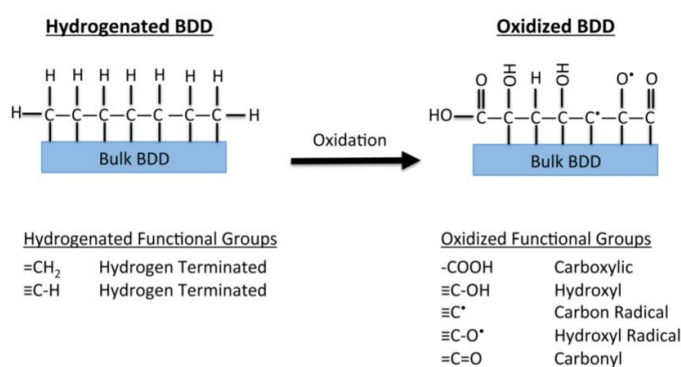


Figure 3.2 - Prevalent functional groups present on the hydrogenated and oxidized BDD surface - taken from [53]

A recent study has been focused on the formation of these various oxygenated functional groups using density functional theory (DFT) calculations [52], finding that these oxygenated functional groups are subject to further oxidation, that results in the formation of carbon radical ($\equiv\text{C}^\bullet$) and deprotonated hydroxyl radical sites ($\equiv\text{C}-\text{O}^\bullet$). These radical sites are hypothesized to be active for compound oxidation.

Hence, BDD has been found to be the most effective anode material for degradation of pollutants during electrolysis in the region of water discharge. The BDD anode induces the formation of a large quantity of weakly adsorbed $\bullet\text{OH}$. Therefore, it has high reactivity for

organics oxidation, inducing to efficient water treatment. Many papers have demonstrated that BDD anodes lead to complete mineralization of several pollutants.

However, the materials and methods for the construction of these electrodes are expensive and not suitable for the realization of scale-up for large-scale plants. Thus, further studies are needed to reduce the fabrication costs of BDD electrodes.

3.3 *Effect of main operating parameters*

3.3.1 Effect of current density and fluid-dynamics

Among the parameters controlled in electrochemical oxidation processes, the current density (intensity per unit area of electrode) is one of the term most frequently referred to because it regulates the reaction rate.

A cell can operate in galvanostatic or potentiostatic mode, depending on which is the constant parameter between the current and the potential. In galvanostatic mode, a constant value of J (in Am^{-2} or mAcm^{-2}) or I (in A or mA) is supplied to the cell. In potentiostatic mode a constant E (in V) is provided to the anode or the cathode of the cell vs. an electrode reference. A constant potential can also be provided to the cell (E_{cell}), but this does not correspond to the potentiostatic mode.

Usually, EAOPs are operated in galvanostatic mode; thus, the current density is a key parameter in EAOPs since it regulates the amount of oxidizing species produced.

Depending on the value of the current density, it is possible to distinguish among different regimes. When J is low, the EO is not kinetically limited by the mass transport of organics to the anode surface. At high J range the process is mass transport controlled, whereas at intermediate values of J the process is under a mixed kinetic regime.

Generally speaking, in the low J range an increase in current density leads to greater pollutant removal. Contrarily, in the high J range, the increase of J enhances the O_2 evolution, thus leading to a decrease in current efficiency and an increase in energy costs. For intermediate J values, higher J values should cause an increase in the pollutant removal but also a decay in current efficiency.

This apparently simple scenario is actually complicated by the additional formation of other oxidants. Therefore, an increase in current density does not automatically produces an increase in the oxidation efficiency or oxidation rate. Thus, for a given anode material, the effect of current density on the efficiency of the process depends on the characteristics of the stream to be treated. However, the use of higher current densities usually leads to higher operating costs due to the increased energy consumption.

Hence, it seems necessary to provide some examples to show some possible consequences between the increase of the current density and the effectiveness of the degradation.

In the study of Martínez-Huitle et al. [54], when the applied current density was increased from 20 to 60 mA cm^{-2} , COD removal velocity was increased, as shown in figure #. This increase in COD removal rate was due to the production of strong oxidizing species and the minimization of mass transport limitations and the parasitic OER.

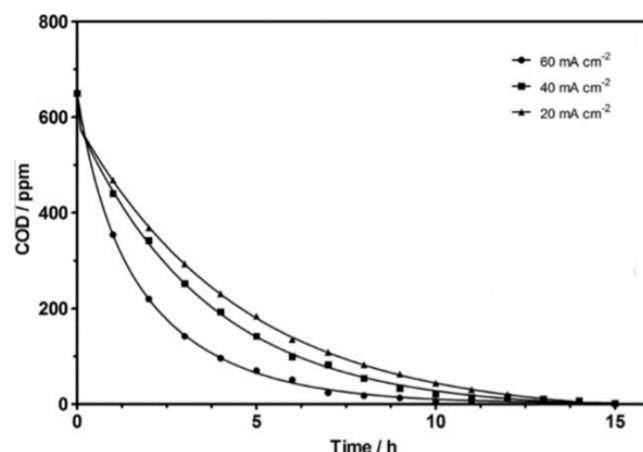


Figure 3.3 - Influence of current density on the evolution of COD as a function of time, during the electrochemical treatment of actual textile water using BDD anode. Conditions: 25 °C, 5 g dm⁻³ of Na₂SO₄, and 250 dm³h⁻¹, taken from [54]

As it is already mentioned, it is important to note that an increase in current density does not necessarily enhance the oxidation efficiency or oxidation rate.

Hence, in the study of Rodrigo et al. [55], the trends obtained for the EO treatment of 4-chlorophenol (figure 3.4) were completely different. In this case, an increase of the current density resulted in a decrease of the effectiveness of the EO treatment. The negative influence of rising current density during the EO treatment of some organic pollutants has been attributed to the occurrence of the OER and/or mass transport limitations.

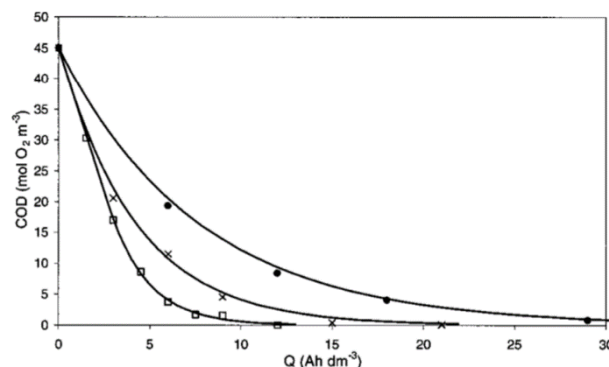


Figure 3.4 - Influence of current density on the trends of COD during the electrolysis of 7.8 mM 4-chlorophenol (4-CP) in 1 M H₂SO₄ with a BDD anode at 25 °C. i: (□) 15, (×) 30, and (●) 60 mA cm⁻², taken from [55]

The variation of current density therefore may affect the efficiency of the process. The action of other strong oxidants produced at the anode surface must not be ignored. The formation of such oxidants is regulated not only by the applied current but also by further operating

conditions (e.g., dissolved O_2 , pH, temperature, and inorganic ions) as well as by the anode material.

As suggested before, improper hydrodynamic conditions can cause mass transport limitations that affect the action of current density in EO. The stirring rate is one of the most important parameters in the case of batch cells, as well as the liquid flow rate in flow cells.

Proper stirring ensures homogeneous conditions minimizing the appearance of concentration gradients in the electrolytic cell. Moreover, it favors the movement of the generated ions, an increase in the pollutant removal efficiency, and the transport of the oxidants produced from the anode surface toward the bulk of the solution.

Likewise, liquid flow rate in flow cells must be regulated to obtain fast homogenization of treated solution, avoid deposition of solids and ensure proper mass transfer of pollutants toward electrodes. Ideally, the turbulent flow along the reactor should be guaranteed to provide a good mixing and avoid any sedimentation.

Fluid dynamics strongly influences EO efficiency and is completely related to cell or reactor design. However, as in the case of the increase of the current density, an increase in the turbulence does not automatically produces an increase in the oxidation efficiency or oxidation rate, as reported in several papers.

Hence, on one hand, Panizza et al. [56] showed the effect of the flow rate during the oxidation of the methylene blue with an electrochemical flow cell at 20 mA cm^{-2} with the BDD anode (figure #). The COD and dye removals are more effective at higher flow rates, thus the oxidation is mass transport controlled. The increase in the flow rate enhances the contact between organics and electrogenerated hydroxyl radicals near to the electrode surface, thereby minimizing their decomposition to O_2 .

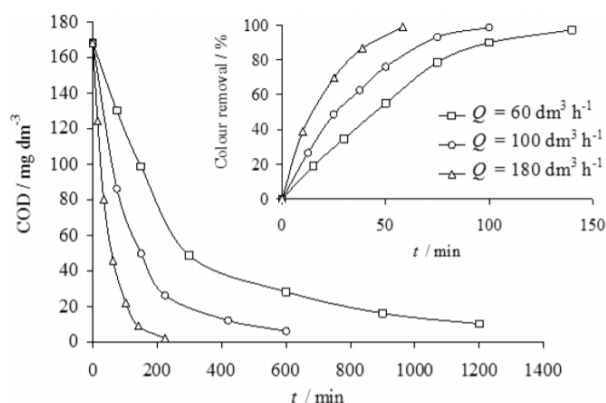


Figure 3.5 - Influence of the electrolyte flow rate on the COD evolution and color removal during the EO treatment of 80 mg dm^{-3} methylene blue in $0.5 \text{ M Na}_2\text{SO}_4$ at 20 mA cm^{-2} and $20 \text{ }^\circ\text{C}$. From [56]

On the other hand, the study of Peralta-Reyes et al. [57] on the electro-oxidation of 2-chlorophenol using BDD electrodes in a continuous flow electrochemical reactor showed different trends. The percentages of mineralization of 2-CP achieved the values of 90%, 96%, and 87% for a flow rate of 0.5 , 1.0 , and 1.5 L min^{-1} , respectively. Hence, the maximum percentage of 2-CP mineralization was 96%, obtained at 1.0 L min^{-1} . When the flow rate increases the turbulence increases and this enhance the radicals desorption which is inconvenient in this case as these radicals may disappear before encountering an organic

molecule to degrade. This is also due to the halflife time of the $\bullet\text{OH}$, 10^{-10} s, which is quite short, thus there is not enough time to provide the contact between radicals and molecules. Instead, when the electrochemical reactor operates at $Q=0.5 \text{ L min}^{-1}$, the 2-CP in the synthetic solution is less likely to encounter the produced $\bullet\text{OH}$, hence resulting in the lowest mineralization value reached.

In conclusion, the fluid dynamics is completely related to the reactor design, and highly affects the effectiveness of the EO. These engineering issues will be further discussed in the next chapter.

3.3.2 Effect of supporting electrolyte nature and concentration

Supporting electrolytes are used in EAOPs for the degradation of compounds to allow the flow of electrical current. Furthermore, the efficiency of EAOPs for the remediation of real effluents can be improved by the addition of ions, not only to make better electrical current flow but also to produce of strong oxidizing agents like active chlorine species.

The electrolyte in electrochemical water treatment could come from a drinking water source, could be wastewater, either raw or modified, or a synthetic aqueous solution with salts prepared to promote the production of oxidants and then to be added to the wastewater.

Typically, several lab-scale studies reported in the literature employ synthetic solutions of a given pollutant (pure or in a mixture) and high concentrations of salts, added as supporting electrolyte to increase the ionic conductivity.

The most used supporting electrolytes are sodium sulfate (Na_2SO_4), sodium chloride (NaCl), potassium chloride (KCl), sodium perchlorate (NaClO_4), sodium nitrate (NaNO_3) and sodium carbonate (Na_2CO_3).

The supporting electrolyte can affect the degradation kinetics as the presence of some ions in solution can promote the formation of strong oxidants such as active chlorine species produced by direct oxidation of chloride at the anode. However, the production of dangerous by-products like chloroderivatives can occur. Moreover, in the presence of sulfate and chloride the scavenging of $\bullet\text{OH}$ can take place. Furthermore, the unwanted consumption of potential oxidative species such as hydrogen peroxide H_2O_2 can occur in the presence of SO_4^- and HClO at pH between 3 and 8.

Most studies reported in literature employed concentrations of salts much higher than those found in real effluents and the studied concentrations of the pollutants also tended to be extremely high. The main drawback is that the study becomes unrealistic using these conditions, also considering the application for drinking water treatments.

In any case, this option is acceptable for a preliminary understanding of the process in terms of the study of reaction pathways, which is the main ambition of lab-scale studies. Moreover, by using high concentration of salts important operational difficulties such as the extreme E_{cell} values and high temperatures because of ohmic drops are avoided.

However, the treatment of actual water is much more difficult. Modifications of the composition of raw water should be carefully regulated. The addition of large concentrations of salts to an actual water source is not good practice either and should be avoided because it also produces of secondary pollution.

If the water conductivity is too low, three main alternatives can be suggested ^[19]:

- The electrochemical treatment must be rejected
- Special microfluidic reactors must be employed; these new reactors are used to perform the treatment in the absence of added supporting electrolytes under a continuous mode with very promising results ^{[58], [59]}
- The electrochemical process can be used as a post-treatment after a preconcentration step like membrane filtration; it helps to produce a concentrated water for which mass transfer inefficiencies are lower in the following electrolytic stage.

3.3.3 Effect of the nature and concentration of the organic pollutant

A key point to be addressed in all EAOPs is the effect of the nature and concentration of the pollutant to be degraded.

The influence of the type of pollutant is directly related to the nature of the anode material. In the case of nonactive anodes, the nature of the pollutants seems to exert only a small effect on the degradation rate and the effectiveness of the process. However, it depends on the reactive oxidizing species generated at the anode surface, which in turn is not only related to the anode material. Contrarily, at active anodes, different efficiencies can be expected when the nature of the organic pollutants change.

Nevertheless, it is important to underline that these effects are further made complex by the interaction with other operation factors such as pH, passivation or corrosion of the surface, temperature, stirring rate, and possible reactions of adsorption or desorption of the organic pollutant at the anode surface.

Regarding the effect of the starting concentration, it is intuitive that solutions with higher amount of organics need longer treatment times to reach a desired degradation degree. A larger initial organics concentration leads to lower percentages or efficiencies of pollutants removal.

Moreover, this aspect causes the removal of more amounts of pollutants per unit of time, thereby a higher pollutants removal rate. This can be ascribed to a faster oxidation of organics with $\bullet\text{OH}$, inhibiting parasitic reactions.

The initial concentration could also influence the reaction kinetics. It is theoretically expected that kinetic constants for pollutants removal are independent of the substrate content. However, it has been experimentally seen lower kinetic constants for increasing pollutants concentrations.

3.3.4 Effect of the pH

The pH solution is an important parameter in electrochemical processes because in most cases there is an optimum pH value for the pollutant removal efficiency. This behaviour is due to the chemical structure of the pollutant. However, the pH change can have contrasting effects on the degradation efficiency, thus the optimum pH value depends on the specific case for direct oxidation processes.

In contrast, pH changes mostly affect the IEO process, such as when Cl^- ion is present in the medium, or direct process in presence of chlorine in the solution to be treated.

Several studies have been conducted to evaluate the effect of pH in EO. For example, Ammar et al ^[60] investigated the effect of current and pH during the electrochemical oxidation an indigo carmine solution with Na_2SO_4 as supporting electrolyte in a cell with a Si/BDD anode and a stainless steel cathode. At pH 3.0, a faster TOC decrease can be observed in figure 3.6 (a) with the increase of the current from 100 to 300 mA due to the higher production of active

BDD(\bullet OH) that enhance the oxidation of organics. Contrarily, at 100 mA, the solution became colorless more rapidly at pH 10.0 (120 min) in comparison with pH 3.0 (270 min), as can be observed in fig. 3.6 (b), as the electroactive species in alkaline medium was more easily oxidized.

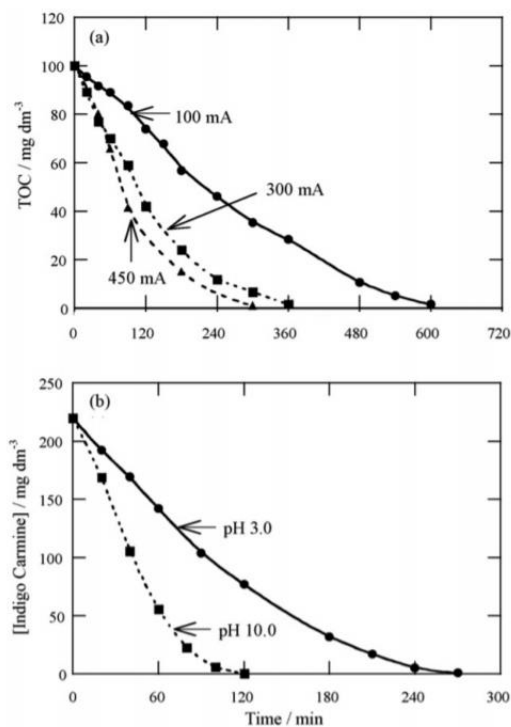


Figure 3.6 - (a) Influence of current on TOC removal vs electrolysis time for the EO treatment of 100 cm³ of 220 mg dm⁻³ indigo carmine solutions in 0.05 M Na₂SO₄ at pH 3.0 and 35 °C with a stirred undivided cell with a 3 cm² Si/BDD anode and a 3 cm² stainless steel cathode. (b) Indigo carmine concentration decay at pH 3.0 and 10.0 at 100 mA. From [60]

3.3.5 Effect of the temperature

In contrast to other parameters, the effect of temperature on the overall efficiency of the EO process has not been largely evaluated. Typically, a change in temperature has a slight influence on the EO under the action of hydroxyl radicals.

However, some authors have suggested that high temperatures lead to greater mass transport toward the anode due to the decreasing viscosity of the medium. An increase in temperature would also cause an increase in kinetic constants.

In some papers is reported that the positive effect of high temperatures may be caused to an enhanced anode activity; actually the efficiency in the pollutant removal is due to an increase of the indirect reaction of organics with electrogenerated oxidizing agents from electrolyte oxidation (especially when sulfates and chlorides are present in the medium). Moreover, at high temperatures, thermal decomposition of some oxidants could occur.

Articles reporting EO treatments at different temperatures involving only \bullet OH radicals show an improvement of the degradation process when nonactive anodes are used upon increase of temperature and flow rate.

Nevertheless, operation at ambient temperature is usually preferred as it provides electrochemical processes with lower energy costs. Hence, the lab-scale tests are carried out mostly at ambient temperature, although some findings suggest the need to optimize the temperature to achieve the highest oxidation ability. In the next chapter further information will be provided on the heat transfer effects on the decisions during the reactor design.

4. Reactor design for EAOP

In the context of electrochemical applications, it is possible to distinguish:

- Galvanic cell or voltaic cell or pile: electrochemical cell working spontaneously. It is a device able to transform chemical energy into electrical energy, thus providing electrical work.
- Electrolytic cell: electrochemical cell that causing reactions opposite to spontaneity. A power generator is used to supply direct current to the system. Electrical energy is transformed into chemical energy. The process is not spontaneous and requires electrical work.

In our case the focus is on electrolytic cells able to perform the removal of refractory matter from water.

An electrochemical reaction is a heterogeneous chemical process which involves the transfer of charge between electrodes, usually metals or semiconductors. Charge transfer can occur at the cathode, where a chemical species is reduced when it receives electrons from another electrode. Conversely, charge transfer can be an anodic process in which one species is oxidized due to the transfer of electrons to another electrode.

An anode and a cathode must be present in an electrochemical cell and, to ensure its correct working, the accumulation of net positive or negative charge must be avoided.

Electrons must pass from the anode to the cathode through an external electrical circuit that connects the two electrodes. There must also be a mechanism able to transport the charge between the electrodes into the cell. The maintenance of electroneutrality within the electrolytic solution is guaranteed by the movement of the ions through the solution and by the separators present inside the cell: anions and cations movements must maintain the charge balance.

In this chapter, after a brief introduction to the principles governing the design and the sizing of electrochemical flow reactors, some configurations of reactors used in water disinfection are presented.

4.1 Principles of electrochemical reactors design

Although each specific application has well-defined characteristics related to the optimization of the process of interest, the following are some basic principles for electrochemical reactor design ^[61]:

- Moderate capital and operating costs, thus the use of low-cost components, low cell potential difference and a low pressure drop across the entire cell is preferable.
- Convenience and reliability, adequacy in design and installation, presence of monitoring and maintenance procedures.
- Adequate engineering equipment for control and monitoring of concentration, potential, current density and an adequate mass transport regime.
- Simplicity and versatility are perhaps the least quantified and the most overlooked factors, but the most important for achieving an elegant and long-lasting design.

- Modular configuration to facilitate scale-up by adding unit cells or by increasing the size of each unit.

4.1.1 Cell potential difference

The ideal, thermodynamically available energy in an electrochemical reactor at equilibrium is related to the Gibbs free energy change for the cell reaction, ΔG_{cell} , which is directly linked to the cell potential difference at the equilibrium U_e , as reported in the following equation (4.1).

$$\Delta G_{cell} = zFU_e = zFE_{cell} \quad (4.1)$$

Where F is the Faraday constant, z is the electron stoichiometry and E_{cell} is the cell potential difference at the equilibrium.

When current flows in the system, the cell potential difference can be expressed in function of other parameters (equation 4.2).

$$U = U_e + \sum |\eta| + \sum |IR| \quad (4.2)$$

The cell potential difference to provide is higher than the equilibrium cell potential, as it can be seen in the figure 4.1 [62].

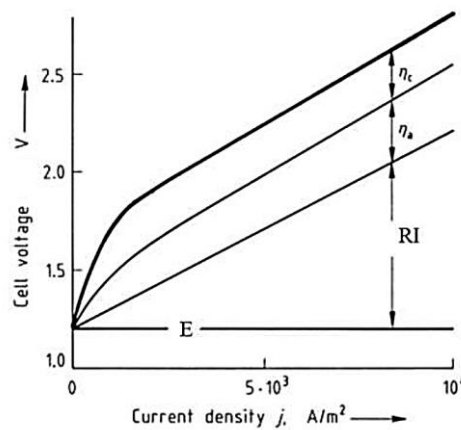


Figure 4.1 - Typical behaviour of the I-V relationship in an electrochemical reactor, from [62]

Equilibrium cell potential difference U_e depends on electrode reactions and thermodynamics, the second term is related to electrode kinetics and mass transport, and the third term to ohmic losses. The previous expression can be expanded as follows (equation 4.3).

$$U = U_e + |\eta_{c,act}| + |\eta_{a,act}| + |\eta_{c,conc}| + |\eta_{a,conc}| + \sum |IR| \quad (4.3)$$

$\eta_{c,act}$ and $\eta_{a,act}$ are the activation overpotentials at the cathode and at the anode respectively, and represent the kinetic limitations to the charge transfer which are dominant at low current densities. These overpotentials can be minimized by using catalysts appropriate for a particular reaction or by using higher temperatures.

Concentration overpotentials $\eta_{c,conc}$ and $\eta_{a,conc}$ are important at high current densities. They cause a drop in potential due to the limitations of mass transport of electroactive species. They can be minimized by employing high surface area electrodes, by improving mass transport or by using turbulence promoters.

The term IR is the sum of all the ohmic resistances across the reactor, electrodes and electronic connections. Minimizing these resistances reduces energy loss and can be achieved in different ways:

- Using a suitable catalyst to reduce the overpotentials of the reactions at the electrodes;
- Reducing the resistances through the cell, by acting on membrane (if present), electrolyte(s) and electrodes. For an electrolytic reactor the required cell potential difference is minimized by decreasing potential losses in the reactor.

The cell potential difference U can be evaluated as follows (equation 4.4).

$$U = -E_c + E_a + \sum |IR| \quad (4.4)$$

The summation term on the right side corresponds to the sum of all the potential drops due to the ionic resistances through the entire cell, but it does not include the overpotentials due to the reactions of the electrodes. These overpotentials are considered within the electrode potentials of the anodic reaction E_a and the cathodic reaction E_c , respectively (equations 4.5 and 4.6).

$$E_a = E_{e,a} + \sum \eta_a \quad (4.5)$$

$$E_c = E_{e,c} + \sum |\eta_c| \quad (4.6)$$

$E_{e,a}$ and $E_{e,c}$ are the potentials of the anodic and cathodic reactions at equilibrium, while η_a and η_c are respectively the anode and cathode overpotentials.

4.1.2 Rate control of an electrode process

The current density j at an electrode is an important parameter to evaluate the current I per unit electrode surface A (equation 4.7). It is very useful in comparing electrode performance.

$$j = \frac{I}{A} \quad (4.7)$$

It is important to underline the differences between the conditions that control the reaction rate. Depending on the nature of the reaction and the cell conditions and materials, a process can be under charge transfer control or under mass transport control, or in an intermediate situation.

Under pure charge transfer control, the movement of electrons dominates; the electrode should be selectively catalytic, its microscopic area should be large, and the velocity of the reaction is very sensitive to potential changes.

For example, in a charge transfer controlled anodic oxidation, the partial current I , for the desired reaction, varies exponentially with the overpotential η :

$$I = zFAk_a c \exp\left(\frac{\alpha_a F \eta}{RT}\right) \quad (4.8)$$

It is therefore necessary to use a high surface area A , together with an electrocatalyst which ensures a high rate constant k_a for the desired reaction. It is also important to have a sufficiently high concentration level c of the reagent.

Overpotential due to charge transfer may be obtained from the Butler-Volmer equation (4.9), which links current density and overpotentials.

$$j = j_0 \left[\exp\left(\frac{\alpha_A n F}{RT} \eta\right) - \exp\left(\frac{-\alpha_C n F}{RT} \eta\right) \right] \quad (4.9)$$

This relationship represents the fundamental equation of the electrode kinetics. The current density j depends on the exchange current density j_0 , the cell overpotential η , the charge-transfer coefficients α , the number n of electrons exchanged in the half-reaction, the universal constant of the gases R and the working temperature T .

The exchange current density is the current flowing in the circuit when there is a dynamic equilibrium on the electrode surface: oxidation and reduction have the same rate so that they do not lead to any change in the composition of the solution. It is a very useful parameter in the description of the kinetics of electrode reactions but it is mainly a measure of the electron transfer activity in the equilibrium situation. A high value indicates that oxidation and reduction are occurring to a high degree simultaneously and it is related to an intrinsic rate of the reaction. A small value of the exchange current density suggests that electron transfer occurs to a lesser extent at equilibrium potential and is related to a slow electrode reaction.

The anodic and cathodic charge-transfer coefficients for simple electrode reactions, in which only one electron is exchanged between the electrode and the electrolyte, are close to 0.5, but may be different for more complex reactions.

For small overpotentials, the Butler-Volmer equation slightly changes as follows (equation 4.10).

$$j = j_0 \left(\frac{nF\eta}{RT} \right) (\alpha_A + \alpha_C) \quad (4.10)$$

For high overpotentials, one of the two terms usually overcomes the other, and the relation is given by a single term describing either the anodic or the cathodic current density, as it can be seen in the following expressions (equations 4.11 and 4.12).

$$j = j_0 \left[\exp\left(\frac{\alpha_A n F}{RT} \eta\right) \right] \quad (4.11)$$

$$j = j_0 \left[\exp\left(\frac{-\alpha_C n F}{RT} \eta\right) \right] \quad (4.12)$$

Under these conditions the equation can be transformed into the Tafel equation (4.13).

$$\eta = a + b \ln|j| \quad (4.13)$$

With $a = (RT/nF\alpha)\ln(j_0)$ and $b = RT/nF\alpha$, where α can be α_A or α_C . Hence, the overpotential for a given anodic or cathodic current density j is related simultaneously to the exchange current density j_0 and the Tafel slope b , both experimentally evaluable.

Under mass transport control, the maximum current for a given reaction is called the limiting current I_L . The limiting current I_L , is directly influenced by the relative velocity v between the electrode and the electrolyte (equation 4.14).

$$I_L = zFcAk_m = K v^w \quad (4.14)$$

K and w depend on the geometry of the electrode, the composition of the electrolyte and the transport and temperature properties. The velocity is a characteristic velocity which is related to the geometry of the system.

Therefore, it is important to have a large electrode surface A and a high mass transport coefficient k_m , using a sufficiently high relative velocity between the electrode and the electrolyte.

4.2 Principles of reactor design in EAOP for water disinfection

After a brief introduction on the main principles to consider in the electrochemical reactor design, in this section a review of other more practical aspects of the reactor design is presented.

The main points to be evaluated in electrolytic cell design are electrodes, electrolyte, cell and electrode configurations, flow patterns, operation mode, heat transfer, and scale-up. Electrodes and electrolytes have been discussed in the previous chapter and so, in the next sections, the role and influence of the other elements on results are discussed.

However, given the great amount of lab-scale research and the scarcity of large scale studies, the attention will be focused mostly on the construction aspects related to the laboratory or pilot scale cell. Hence, several aspects related to larger scales will be neglected, due to the lack of information. Some examples of lab-scale tested reactors will be presented in the next sections.

4.2.1 Cell configurations: divided and undivided reactors

One of the first choices in reactor design concerns the use of an ion exchange membrane or a porous separator to divide the cathodic and anodic compartments, or the use of a single electrolytic compartment.

Where possible, an undivided reactor geometry with a single electrolyte compartment is preferable for the simplicity and the low costs. This arrangement also reduces potential drops and mass transport problems typically present in reactors with ion exchange membranes and microporous separators. Furthermore, the degradation of the membranes and their cost, also associated with the gaskets necessary to fix the separator, must be considered.

On the other hand, dividing the reactor into two compartments with two separate electrolytic circuits offers several advantages. The main advantage is due to the reduced loss of reagents or products on the electrodes; there are no unwanted side reactions to the opposite electrodes due to the mixing of anode and cathode electrolytes. Furthermore, ions migration is controlled, dangerous mixtures can be separated and the protection of the electrodes from corrosion caused by aggressive chemicals is ensured.

In this context, the selection of a divided or undivided reactor for EAOP in water treatment appears to be a major point. Generally, oxidation, direct or mediated, occurs in the anode compartment: in this case a divided reactor would be recommended. As previously reported, in some cases, a two-step degradation process is used: first the oxidants are produced in the reactor, and then they are added to the water to be treated. Hence, in a divided reactor, oxidation, direct or mediated, can be carried out at the anode compartment, where single species and mixtures of highly oxidizing species assure the effectiveness of the treatment.

Moreover, the management of hydrogen evolving at the cathode is one of the main concerns which would suggest the use of undivided cell, especially at a large scale. This is still an unresolved problem, since large amounts of this gas are expected to be formed during the

treatment of water. In undivided cells, hydrogen is mixed with oxygen and this mixture should be dangerous. The use of membranes in divided cells may reduce this problem, but it increases operation costs because of the higher cell potential.

However, in small-scale systems like those commonly reported in the literature for lab-scale studies, total amount of hydrogen formed is negligible and a good dissipation system prevents hazardous situations.

At small-scale, an example of the use of divided and undivided reactors, which led to small differences, was reported in a 5-fluorouracil (5-FU) degradation study ^[63]. By using a divided reactor, a degradation efficiency of 77% was achieved, while with an undivided reactor of 75%, using 50 mg l⁻¹ FU at 150 A m⁻², 13 l h⁻¹ and 6 h of electrolysis.

Thus, considering the slight differences between the two configurations at the small scales, as well as the negligible amount of hydrogen produced, the prevailing configuration present in most of the literature studies is the undivided one, because of the simplicity and the low costs.

4.2.2 Electrode configurations: monopolar or bipolar connections

The parallel plate cell, undivided or divided, is the classic geometry of industrial electrochemical cells. Such a parallel plate cells can constitute a single unit and operate in a monopolar mode.

However, several single electrochemical cells can be also put together to increase the area, thus the capability to handle larger volumes, and can be arranged with a monopolar connection as shown in figure 4.2 (a), where each electrode is positive or negative. This arrangement keeps constant the cell voltage of a single cell but it is capable of generating high currents. To increase the voltage, the connected monopolar cells can be arranged in series, as it can be seen in figure 4.2 (b).

Another strategy is to connect the cells in a bipolar configuration as is shown in figure 4.2 (c), which is commonly used in electro-synthesis cells, fuel cells and redox flow batteries. In the bipolar connection only the last electrodes are connected to a power source, and the current passes through the other electrodes, polarizing them. In this configuration the voltage depends on the number of cells. The electrodes acquire a different charge on each side, and at the same time the oxidation reaction takes place on one side, and the reduction on the other. The bipolar arrangements of the electrodes allow more compact cells than monopolar connections, given the absence of electrical cables to connect each electrode. Bipolar electrodes typically contain an electronic conductive flat plate in the center which is a barrier to positive and negative electrolytes and acts as an electronic connection to transfer electrons.

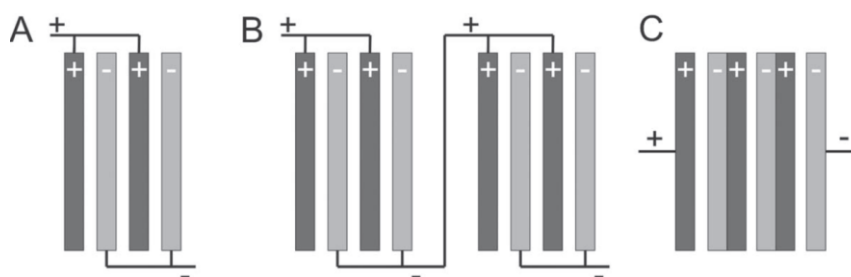


Figure 4.2 - (A) monopolar electrode connections, (B) monopolar cell stacks connected in electrical series, (C) bipolar electrodes, from [64]

The advantages and drawbacks of both types of configurations have been studied in many technologies of electrochemistry, but mainly in electrocoagulation. This is due to the lack of lab-scale studies on the stacking of several cells and the small numbers of EAOP pilot plants research found in literature.

However, generally bipolar electrodes have been proved to be most efficient, but the monopolar configuration implies lower operation costs because of the resulting lower cell potential. Moreover, the bipolar connection allows engineers to look for more interesting and compact mechanical designs of the cell. This can be seen in the figure 4.2, where it is showed the external aspect of two commercial cells, Diacell, with the same number of electrodes but with different types of electrode configurations.



Figure 4.3 - External aspect of Diacell stacks with monopolar (left) and bipolar electrodes (right), from [19]

4.2.3 Flow pattern: mixed-tank and flow cells

Flow pattern is a crucial aspect to consider in order to increase the efficiency of electrochemical processes. As previously presented, one of the main concerns of EAO reactors is that most relevant reactions take place on the electrode surfaces, and so mass transport of species from and toward the electrode is usually a drawback in the technology. In this context, the proper choice of flow pattern, determined by the cell design, may resolve this limitation.

The two main kinds of electrochemical cells used in the degradation of organic pollutants from water in the scientific literature are the mixed-tanks and the flow cells.

Mixed tank cells are the most classical example of electrochemical cell used at laboratory scale. They are employed because they are the simplest cells for measuring the effectiveness of EAOP technologies, due to the simplicity of mathematical interpretation of results. In lab-scale literature research, mixing is typically realized by magnetic stirring rods, mechanical stirrers, or recycling pumping. In contrast to what could be expected, no turbulence promoters are usually employed in studies carried out with tank cells so as to achieve the increase the

efficiency of the process. Consequently, the main drawback is the very low mass transport coefficient k_m obtained by using these configurations and thus the lower current efficiency compared with flow cells. With a view to the potential scale-up, k_m low value makes the process inefficient when the concentration of substances to remove becomes low. Hence, this flow pattern can only be recommended at full scale for a mild removal of pollution and only if mass transport is not limiting the kinetics of the process.

Therefore, flow cells are the most interesting alternative found in the literature to mixed-tank cells. This type of cell is typically associated with lab-scale studies to evaluate kinetic data and some additional information about process effectiveness, to assess the applicability of the technology on a larger scale. The main advantage of type of cell is its higher mass transport coefficient respect to mixed-tank, making it suitable for treating much lower concentrations than mixed cells.

In this context, an interesting comparison between mixed-tank and flow-pass cells for the treatment of actual petrochemical wastewater under similar conditions has recently been published [19]. In this confrontation pollutant removal was found to be more efficient when an electrochemical flow-pass cell was used because of the higher mass transport coefficient, despite the similar values for the other parameters.

Table 4.1 - Comparison between mixed and flow cell, from [19]

Mixed cell		
$k_m = 5.9 \times 10^{-6} \text{ m s}^{-1}$	%COD removal	
Current density and T	Anode	
	Ti/Pt	BDD
15 mA cm ⁻² (25°C)	33.8	50.3
30 mA cm ⁻² (25°C)	46.5	57.5
Flow cell		
$k_m = 2.0 \times 10^{-5} \text{ m s}^{-1}$	%COD removal	
	Anode	
	Ti/Pt	BDD
20 mA cm ⁻² (25°C)	64.5	76.2
40 mA cm ⁻² (25°C)	90.7	94.5

4.2.4 Continuous and discontinuous mode

The operation mode is a key point to consider in the reactor design. This is not only related to the productivity and the capacity to treat larger amount of water, but also to other aspects, like hydrogen handling and mass transport effectiveness.

In literature, most studies are carried out in discontinuous operation mode. In this mode, single-pass cells are connected to a reservoir tank through a recirculation pump in order to increase the number of times water passes through the cell and thus the flow rate (figure 4.4). The recycle helps to solve problems associated with gas evolution. The bubbles formed at the cathode are dragged out of the cell that otherwise would accumulate in it, causing the increase of the ohmic resistance of the electrolyte and thus the cell potential. Moreover, by using a high recirculation flow rate, mass transport is improved, leading to greater removal of organic pollutants. In this case, the system could be modeled from the macroscopic point of view as a mixed-tank reactor.

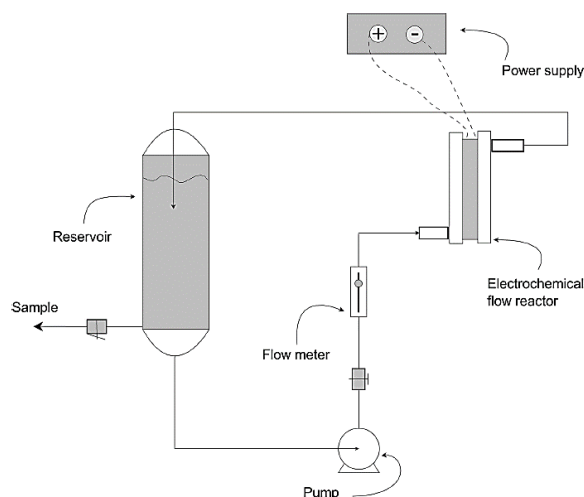


Figure 4.4 - - Typical system of flow-cells in discontinuous mode

The transformation of the discontinuous process into a continuous one could be done simply through the addition of an inlet of wastewater and an outlet of treated water. This configuration has the same advantages previously presented. Furthermore, the continuous mode leads to higher productivities.

In any case, very few research were found on the study of the continuous process. This is due to the complete set of data with less experimental effort achievable by using a discontinuous process. The continuous mode should only be employed in large applications, but the technology is not yet mature enough for such applications as frequently reported in the previous sections.

4.2.5 Interelectrode gap

Interelectrode distance is one of the main construction details. As is reported in literature, the space between two electrodes, known as gap, influences the total resistance of the cell and thus the ohmic losses. The electrolyte resistance depends almost linearly on this gap, therefore low distances between electrodes lead to lower the cell potential. Hence, it also affects the reactions taking place in the bulk. Moreover, the interelectrode gap also affects the gases to be dragged out, as well as the power required to pump the liquid into the cell.

Thus, an optimum distance between the electrodes is required for the effectiveness of water treatments. Most lab-scale works report the use of an interelectrode gap between 0.5 and 3.0 cm.

However, some recent studies ^{[58], [59], [65]} have reported the good performances of microfluidic reactors with a gap in the order of some tens of microns. However, recirculation flow rate becomes critical when extreme narrow gaps are employed because it determines the stripping of gas bubbles.

However, in the context of electrochemical processes, the development of microcells for applicative purposes is not yet mature, but the results are very promising. A further explanation of microfluidic reactor principles will be provided in the next section.

4.2.6 Heat transfer

Regarding the heat transfer occurring during the removal of organics, it is worth underline that this may become a key point because temperature affects oxidants electrochemically produced.

As reported in the previous chapter, high temperature enhances mediated electro-oxidation processes, and thus, it improves the decontamination effects. However, many aspects may affect the treatments. For example, from peroxocompounds, such as peroxodisulfate and peroxodiphosphate, less powerful H_2O_2 can be formed if temperatures overcome $50\text{ }^\circ\text{C}$ [67].

The increasing temperature due to the heat transfer either in wires or into the electrolyte is a problem in large-scale reactors because of the huge amount of energy and heat that must be dissipated. However, heat exchangers can help to reduce the problem, removing the overheating caused by ohmic drops. Using heat exchangers is especially important in the dissipation of heat from the stacks; a bad design could seriously harm the frame of the cells.

As the typical desired range of temperature is between room temperature and $60\text{ }^\circ\text{C}$, water can be used as a heat exchange fluid. Usually, an external heat exchanger within the recirculation circuit, located between the tank and the reactor is used for flow-cells. It is clearly shown in the figure 4.4, taken from the site of Diamond Abrasives Australia, [68] a company based in Melbourne, producer of commercial electrochemical cells. The effluent to be treated is held in a process tank and then pumped through the Diamox cell, a stack of cells arranged with electrode bipolar connection.

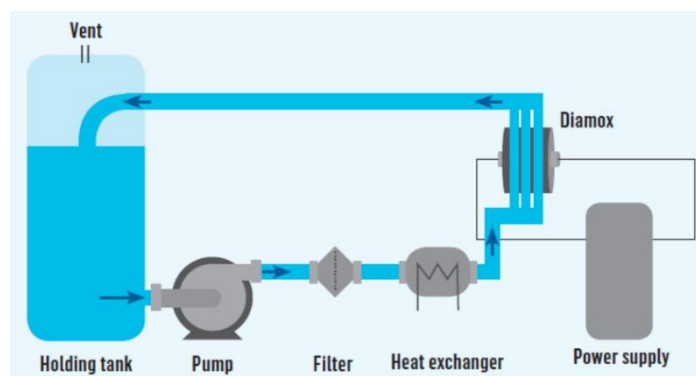


Figure 4.5 - Scheme of a Diamox cell arrangement with the heat exchanger, from [68]

Despite the presence of heat exchangers in several commercial cells, at the small scale of the tests reported in literature is not required much attention to their design.

4.2.7 Scale-up

Scale-up from the lab to the full scale is an issue of huge importance in electrochemical technology. There are two main aspects to be considered: increasing the electrode area for a single cell and stacking of cells.

Regarding the stacking of cells, no great difficulty is found, but very few studies report results on the treatment of organics at the pilot plant scale. Moreover, they are not focused on these potential problems because they are only preliminary approaches to the scale-up. An example of pilot plant composed by different stacks can be seen in figure 4.6.



Figure 4.6- Stacking of cells in a 1 m² pilot plant for the electrolysis of wastewater

As reported in the previous sections, the main problems regarding stacking are related to the handling of heat and hydrogen. These problems become extremely important when the scale increases. The recovery of hydrogen and its valorization in a fuel cell could be considered, but the realization is not simple and only small devices have been developed up to now. The use of divided cells may reduce hydrogen problem, but it increases cell potential. Regarding heat issues, heat exchangers can help to diminish the problem. Given the scarcity of studies carried out on these issues, much work needs to be done in the near future to overcome these limitations.

The size of the electrode in the cell affects the probability to have current and potential distribution patterns not uniform. Naturally, current and potential distribution also depends on many factors as for instance the flow patterns, the uniformity of the electrode surface or the existence of turbulence promoters. In contrast to other electrochemical technologies, such as electroplating, where obtaining a perfect layer is crucial, very little attention has been paid to the removal of organics via EAOP up to now.

However, this is very important because most EAOP operate under diffusion control and the role of mass transport is not negligible. The efficiency is limited by the velocity at which pollutants arrive to the electrode surface, and the highest efficiency is obtained when the electric charge transfer rate and the pollutant's mass transfer rate are balanced. Differently, side-processes could prevail, thus leading to less effective organic removal.

Hence, the larger the electrode, the more difficult it is to reach a uniform current and potential distribution on its surface. Conversely, a large electrode surface helps to minimize the number of cells that should be included in the stack to obtain the area required for a given process, and this reduces the investment cost of the cell.

In this context, the use of CFD simulation tools is becoming crucial in electrochemical engineering in the attempt to obtain the best configuration for high efficiency. CFD is useful in evaluating hydrodynamics, mass transport and current distribution within the reactor. Great attention is paid to hydrodynamics studies, but very little on the studies for the removal of organics. However, the most important references are focused on the removal of simple and single pollutants, thus simulating reactor effectiveness for unrealistic effluents. More information on CFD simulations for EAO reactors will be provided in the next chapter.

4.3 Examples of EAO reactor for water disinfection

4.3.1 The planar electrode in a flow cells: commercial alternatives

The planar electrode flow cell is the most used configuration in continuous electrochemical flow processes, providing a reproducible flow profile, with the same core design for laboratory and larger scale reactors. As previously mentioned, the rapid mass transport rates let the flow cells outperform stirred tank cells for their effectiveness in degradation processes.

Further improvements are achieved through turbulence promoters to increase solution mixing, incorporating porous electrodes to increase the electroactive area, or through combining multiple stacked cells in sequence or parallel configurations. This latter option is applied when a larger scale is desired respect to the classical single flow cell employed at lab-scale.

Generally, at the laboratory scale these types of reactors are assembled as a filter-press, and can constitute a single cell or, because of their modularity, they can be easily stacked. Some of the most commonly used reactors in scientific studies, as well as other commercially popular reactors, are listed below.

Among the variety of the different kinds of cells, the FM01-LC is one of the most diffused [71]. The FM01-LC reactor is a laboratory-scale, electrochemical filter-press cell with a projected electrode area of 64 cm² in its basic configuration (figure 4.7). It has a rectangular electrolyte flow channel, empty or equipped with a turbulence promoter. The channel of the FM01-LC was originally based on the larger FM21-SP electrolyser of 2100 cm² projected electrode area employed in the chlor-alkali industry. The needs required for a good electrochemical design are well met by controlled flow and plane parallel cells which can be easily assembled in a modular way. Moreover, FM01-LC can be extremely versatile in the choice of electrode form, material and surface morphology, which makes this reactor one of the most studied. A further explanation of the reaction environment in the FM01-LC will be done in the next chapters.

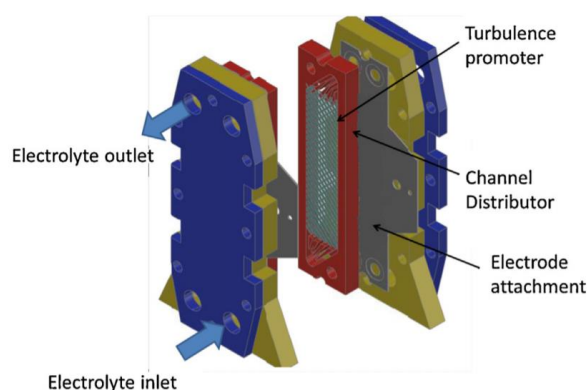


Figure 4.7 - The FM01-LC electrochemical reactor

Other examples of commercial reactors are provided by the ElectroCell, a swedish company which supplies high quality electrochemical cells. Reactors equipped with electrodes of greatly different scales are produced, starting with the ElectroMP cell (0.01–0.2 m² of electrode projected area, fig. 4.8) up to the ElectroProd cell (0.4– 16 m², fig. 4.8) [69], suitable for several purposes. These types of reactors provide very versatile design and the electrode areas, as well as other construction parameters, can vary over a wide range. However, unlike the FM01-LC reactor, no literature papers has been found regarding degradation studies by using these kind of cells.



Figure 4.8 - ElectroMP cell (left), ElectroProd cell (right), from [69]

Within the commercial market of electrochemical cells for water treatment the DiaCell (WaterDiam, France) is highly interesting because this reactor was specially designed for this purpose, in contrast with many other cells, like the FM01-LC or the ElectroCell, which are suitable for water treatment but not specifically constructed for this scope. Several studies have been found on the comparison of different configurations of DiaCell[®]. DiaCell[®] 101 (Fig. 4.9 a) is used for bench-scale studies, while the DiaCell[®] 1001 (Fig. 4.9 b) is a stack of cells employed as a pilot plant (Fig. 4.9 b), and either are equipped with circular electrodes. The DiaCell 401[®] type is instead a module which can be assembled with one, two, three and four compartments, each of them being fed with water by internal parallel inlets.

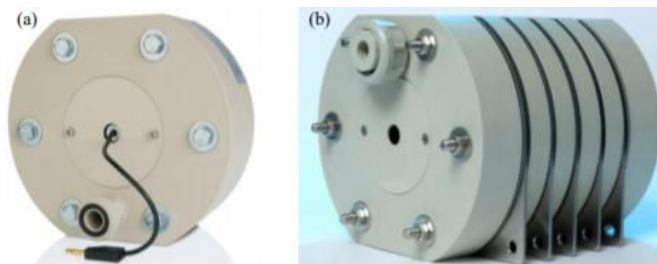


Figure 4.9 - (a) DiaCell[®] 101; (b) DiaCell[®] 1001

As already mentioned, stacking is the best way to obtain a high electrode surface typically required for full-scale processes. Testing in-house cells for this purpose will only give poor information about the changes in the performance and it should be recommended the use of commercial cells in these studies, as the DiaCell.

Hence, among the various works found, Martín de Vidales M. J. et al. [72] investigated the effect of the scale-up of electrochemical oxidation processes with diamond anodes for the degradation of organic pollutants treating urban wastewater. Results achieved with a single DiaCell[®] 101 were compared with those obtained with a single-stack DiaCell[®] 1001 and with a pilot plant made by five of these stacks. Results demonstrated that scale-up is very complex process: not only the electrode connection is important but also mass transfer conditions. As electrochemical disinfection is not a surface process, but mainly occurs in the bulk by the attack of electrogenerated radicals, it is more efficient at bench scale.

Other interesting observations were found in the work made by Cano A. et al. [73]. They studied the disinfection of a municipal wastewater using DiaCell® 401 and DiaCell® 1001 (figure 4.10) arranged with BDD electrodes, and with bipolar and monopolar connection respectively. They used very low current densities ($0.14\text{--}10\text{ A m}^{-2}$), in order to avoid the formation of chlorates and perchlorates during the electrolysis. In comparing the two systems, DiaCell® stacks containing bipolar connected electrodes resulted more efficient than those containing monopolar connection. The higher cell voltage applied in the bipolar stack resulted in an enhanced reduction of nitrates to ammonium. This increased the subsequent formation of chloramines as the main positive effect. On the other hand, the increase in the power consumed in bipolar connections was the primary negative consequence.

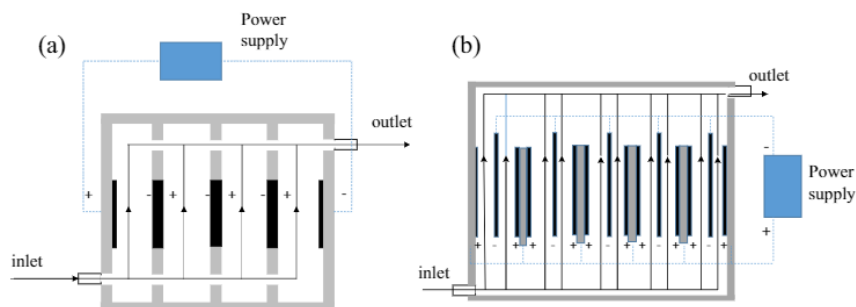


Figure 4.10 - (a) DiaCell 401® (bipolar connection) and (b) DiaCell® 1001 (monopolar connection), from [73]

4.3.2 Three-dimensional EAO cell

Three-dimensional (3D) electrode or bed electrode guarantees an excellent solution to the drawbacks which limit the application of two-dimensional (2D) electrode.

3D electrochemical technology is based on 2D electrochemical process with several analogies such as electrode materials and treatment processes. The only difference is the third electrode. It is also named *particle electrode* or *bed electrode*, and it is basically constituted by granular materials which are filled between two counter electrodes, as can be seen in the figure 4.11. When there is a conventional system but the electrodes are three-dimensional, they also can be regarded as a type of 3D reactor.

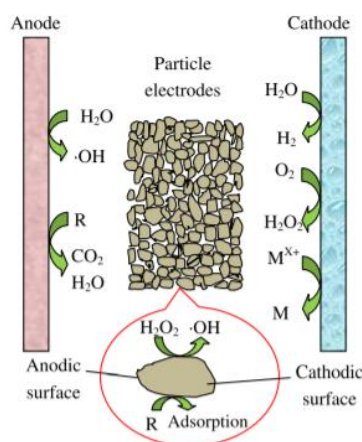


Figure 4.11 - Scheme of 3D electrode

The addition of granular activated carbon (GAC) or metal particles may also increase the conductivity and mass transport or the adsorption of pollutants if compared with the 2D process. Moreover, respect to the 2D electrode, the high specific surface areas of these particles can give more reactive sites for matter adsorption or even catalytic reactions, thus providing higher removal efficiency.

However, since the technology of 3D electrode is emerging in the recent years, its development is slower respect to that of 2D system. Its application in water treatment is extremely wide, from metal ions removal to different types of wastewater, like oil refinery wastewater or other water effluents including dyes, phenolic compounds and derivatives, hydrocarbons.

At a pertinent voltage, these particles can be polarized to form a charged microelectrodes. Thus, a surface of these particles can be considered as anode while the other as cathode. Thanks to the presence of particle electrodes, 3D electrochemical process demonstrates a better performance than conventional 2D electrochemical cell. In table 4.2 is reported a comparison between different results obtained by using 3D and 2D system under similar conditions for different pollutants degradation. COD removal effectiveness in 3D system is 10-50% higher than that in 2D system, showing the advantages of 3D system sufficiently.

Table 4.2 - Comparison of pollutants removal efficiency between 2D and 3D electrode system

Wastewaters	Reactor types	Particle electrodes	Removal efficiency (%)	Ref.
Heavy oil refinery wastewater	2D	-	30.8	[74]
	3D	GAC and PCP	45.6	
<i>p</i> -Nitrophenol	2D	-	37	[75]
	3D	AC	91.4	
Reactive brilliant red X-B	2D	-	20	[76]
	3D	CA	95	
Paper mill wastewater	2D	-	45.8	[39]
	3D	GAC	86.3	
Formic acid	2D	-	6	[77]
	3D	GAC	69	

The degradation mechanism of pollutants in 3D electrochemical process is complex. However, except for the role of particle electrode, the mechanism of electrochemical reactions on electrodes are identical with that in 2D reactors. The particles located between the electrodes can be compared to an adsorbent and they enhance the ionic charge distribution. The main reactions occur on the electrode surface.

As previously introduced, when an external electrostatic field is imposed to the particle electrode surface immersed in an aqueous electrolyte solution, two sides of the particle will acquire positive charges and negative charges, respectively. The charged ions shift to the opposite side of charged particle electrodes, resulting in the electrosorption. Thus, the combination of adsorption and electrosorption enhance the removal of organic pollutants. The particle electrodes used in 3D system include GAC, metal particles, carbon aerogel (CA) and modified kaolin. These materials often have large electrical conductivity and high surface area.

Three-dimensional (3D) electrochemical process has been recognized as an efficient method for wastewater treatment, but still need further studies to be applied to larger scales.

4.3.3 Microfluidic reactors

Among the various types of reactors, in the recent years microfluidic cells have been successfully employed for the treatment of wastewaters contaminated by organic pollutants. Microfluidic electrochemical cells exhibit very small distances between electrodes of tens or few hundreds of micrometers, and therefore they present several advantages for the wastewater treatment with respect to conventional flow or tank cells.

As previously reported, electrochemical conventional technologies have some drawbacks which can be solved by using these microfluidic cells. Firstly, it is difficult to guarantee sufficient cell voltages when the medium has not a large conductivity, thus supporting electrolytes are added to the system when using conventional treatments. This can be an obstacle for a wide application of conventional electrochemical. Indeed, chemicals addition may be the cause of the formation of secondary pollutants.

Moreover, low current efficiencies are usually reached in direct oxidation processes when a high degradation is required, mostly due to the mass transfer limitations when treating pollutants at low concentrations.

In this context, the use of microfluidic device appears to be a major challenge. The small distances between the electrodes produce a drastic reduction of the ohmic resistances, thus allowing the removal of organic pollutants with lower cell potentials even in solution with low conductivity. Moreover, this distance enhances the mass transport of the pollutants towards electrode surfaces, thus increasing the current efficiencies. Eventually, simpler scale-up procedure through easy parallelization of many small units can be realized.

However, the use of microdevices have some potential disadvantages such as an easier fouling and clogging, and the volume of the solution treated is still limited. Some examples of degradation studies using these devices are listed below.

Ma et al. [78] studied the treatment process of a real wastewater (initial TOC of 210 mg l⁻¹) characterized by low conductivity (1.4 mS cm⁻¹) by anodic oxidation at BDD comparing three different systems: (i) conventional cell with no supporting electrolyte; (ii) conventional cell with the addition of supporting electrolyte; (iii) microfluidic cell, not using a supporting electrolyte. Sodium sulfate was employed as supporting electrolyte, largely reducing the cell voltages and thus the energetic consumptions and the operating costs. However, under different operating conditions, the addition of Na₂SO₄ caused a lower removal of the TOC. Working with microfluidic cells without supporting electrolyte allowed very high TOC removals and low energy consumptions and operating costs, because of the small interelectrode distances that reduces the ohmic drops and intensifies the mass transport of the organics to the anode. Some results obtained in this study can be seen in Table 1.

Table 4.3 - Main results obtained by the study of [78]

System	Operative conditions	TOC removal (%)	Electric energy cost (€/m ³)
Macro cell without supporting electrolyte	I = 0.1 A t = 7 h	70	19.8
Macro cell with 0.05 M Na ₂ SO ₄	I = 0.06 A t = 7 h	80	2.4
Micro cell without supporting electrolyte	I = 0.1 A Flow rate 0.4 ml/min	79	1.0

Another study recently published by Perez et al. [66] made a comparison between two systems of microfluidic reactors: (i) flow-by and (ii) flowthrough (figure) for the degradation of a synthetic solution with very low conductivity (1 mS cm⁻¹), including 100 mg l⁻¹ of the clopyralid pesticide. The anode and the cathode employed were Nb/BDD and stainless steel, respectively, distanced 400 μm one from the other. The flowthrough configuration showed higher efficiency and lower energy consumption for mineralization of clopyralid as it only took 2.3 Ah dm⁻³ and 12.5 kWh m⁻³, in comparison with 11.4 Ah dm⁻³ and 75 kWh m⁻³ in the flow-by system. Furthermore, the specific energy consumption of the flow-through cell is six times smaller (12.5 vs. 75 kWh m⁻³) than the flow-by cell because of the faster degradation and the lower cell voltage.

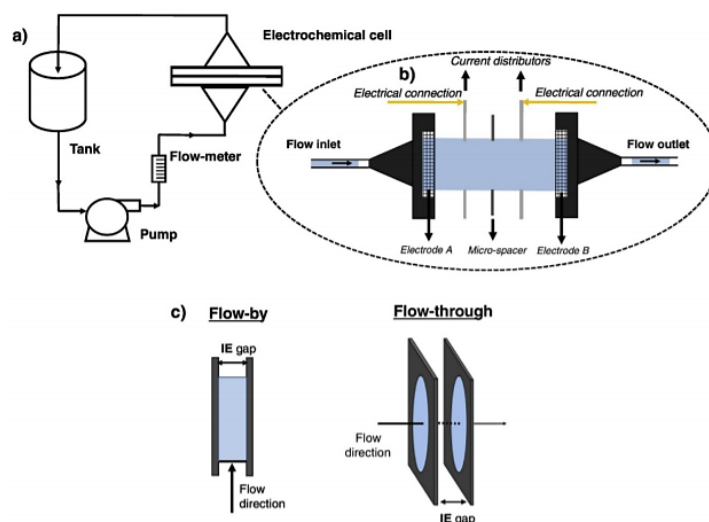


Figure 4.12 - Experimental setup used of the microfluidic cells. (a) Flow diagram, (b) electrochemical cell (c) comparison of flow-by and flow-through configurations [66]

The MF-FT represents a promising approach to the development of electrochemical reactors for water disinfection, but the number of studies regarding these kinds of device are still scarce.

5. Mathematical modelling of EAO reactors

Mathematical modelling and simulation of electrochemical reactors (ECRs) by computational fluid dynamics (CFD) techniques have been raising during the last fifteen years ^[79] due to the need to improve the performance of existing reactors or the development of new technologies.

Commercial and open-source CFD codes are very effective tools in studying these reactors. ECRs studied by CFD simulations are widely used in several applications, such as electrosynthesis of chemicals and drugs, chlor-alkali, fuel cells and electrochemical advanced oxidation processes.

In this context, mathematical modelling of the phenomena occurring during the EAOPs for water disinfection have not been widely studied in the recent years. Hence, there is a lack of paper regarding a complete characterization of the reaction environment during the abatement of organics in EAO reactors. However, a lot of studies focused on hydrodynamics and mass transport in electrochemical reactors have been published. Thus, a first step in modelling EAO processes can be made by referring to these research, as a lot of reactors employed in other fields, such as electrodeposition or electrocoagulation, are the same used for water disinfection.

Generally speaking, several ECRs performances have been enhanced through the characterization of the reaction environment, with some adjustments made inside the cells, such as the electrode configuration, the use of plastic meshes acting as turbulence promoters, the design of 3D printed electrodes, use of new manifolds at the inlet of the cells to distribute the fluid, and optimization of the operational parameters like flow rate, current density, species concentration and temperature.

In this chapter, after a general introduction to the mathematical modeling of the existing EAO reactors, a review of the tools involved in modeling the main three branches assessed in the simulations, hydrodynamics, mass transport and current distribution, will be provided.

5.1 *EAO reactors studied in CFD simulations*

As already discussed, several papers deal with the use of parallel plates as electrodes in reactors for characterizing diverse electrochemical processes, but several drawbacks are related to these kinds of configuration (Section 4.2.3). In this context, the use of well-engineered EAO reactor is fundamental for lab studies to test and characterize electrochemical processes, before the scaling up and the industrial development.

Among many possible reactor configurations and designs, the plane parallel electrode configuration, assembled as a filter press, is definitely the most common type of reactor studied in the papers regarding the mathematical modeling of EAO reactors.

As above presented, the commercially available reactor is the FM01-LC (Fig. 5.1 a), but also other in-house cells (Fig. 5.1 b) are widespread. As it is clear from the figure, the only aspects that change between the various configurations are the geometric dimensions, as well as the presence or not of flow distributors and turbulence promoters. However, the same mathematical models are usually employed to simulate these kinds of reactor.

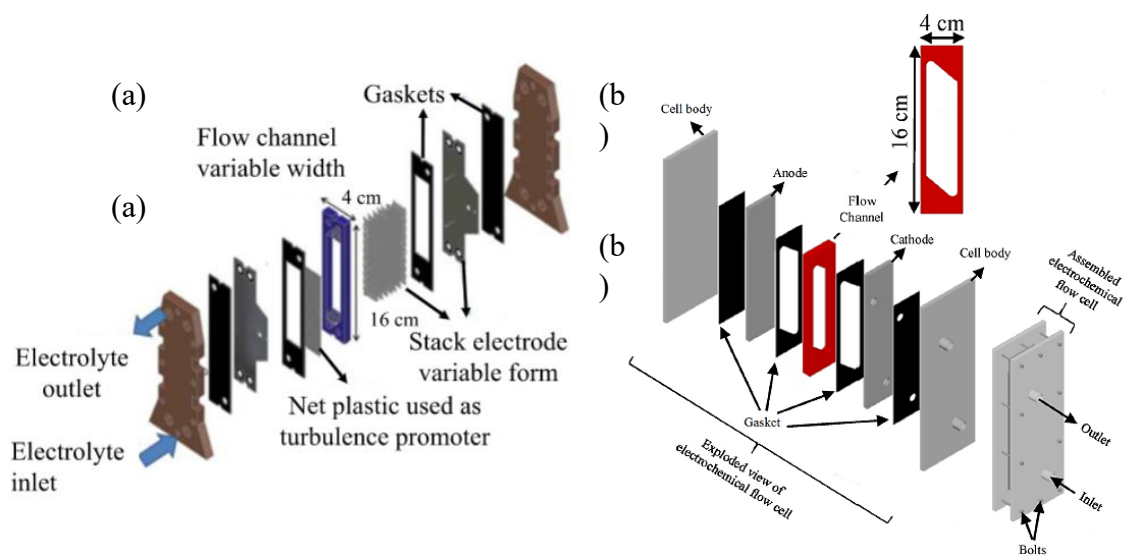


Figure 5.1 - (a) FM01-LC [71], (b) In-house filter-press cell [80]

A slightly different configuration has been also used, as can be seen in figure 5.2, the Filter-press type reactor in horizontal mode, in a serpentine array [81]. In the FM01-LC reactor, the electrolyte is fed in parallel to each of the cells in the multielectrode stack arrangement, contrary to what happens in the up-flow electro-chemical reactor in a serpentine array, which behaves like a cascade reactor. However, only a first characterization study is present in literature regarding this type of configuration.

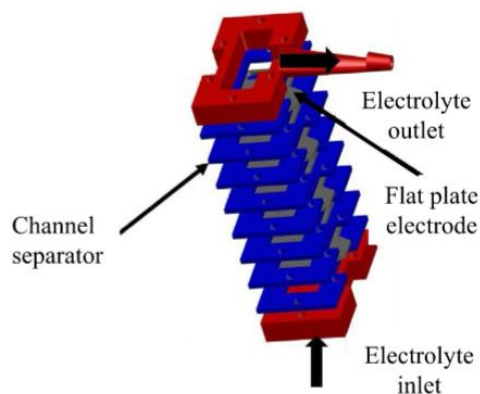


Figure 5.2 - Exploded view of the filter-press reactor in stack of eight channel in a serpentine array [81]

Another configuration studied in some papers [65] is the electrochemical cell known as Diacell (Fig. 5.3), which has a reaction volume of 117 cm^3 and includes two circular electrodes (10 cm diameter), with a surface area of 70 cm^2 and two spacers. Santos et al. [83] performed a characterization of fluid dynamics and mass-transfer in an EO cell by experimental and CFD studies, while Barrios et al. [82] studied a more complex two-phase hydrodynamic model and an experimental characterization of flow reactor treating an activated sludge. However, no more CFD studies using DiaCell were found in literature.

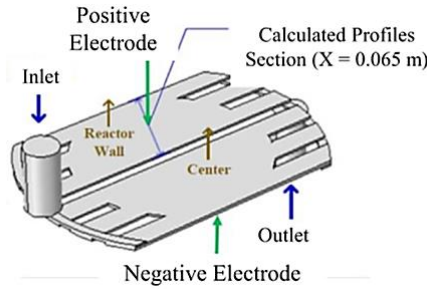


Figure 5.3 - Geometry of the electrochemical flow cell (DiaCell®) computational domain [83]

5.2 Mathematical modeling of EAO reactors

The characterization of the EAO reactors can be performed experimentally, but these experiments are too costly and long. In this context, the recent development of CFD techniques has promoted the design, characterization, and scale-up. Several researchers have used CFD techniques to model the hydrodynamics, mass transfer, potential and current distributions in many EAO reactors, but mostly for filter-press types.

The CFD technique allows to solve the fundamental transport equations within the electrochemical reactor in the 3D domain, using grid methods such as the finite-volume or finite-element methods. Both numerical procedures give similar results. In this work a multidisciplinary software for multiphysics simulation which use the Finite Element Method (FEM) has been used. A further explanation of this method will be provided in the next chapter.

In the following sections a review of the various models used in EAO reactors simulations will be given, regarding the three main physical aspects to evaluate: hydrodynamics, mass transport and current and potential distribution. The attention will be focused only on the filter-press type reactors, the commercial one and the manufactured one.

5.2.1 Hydrodynamics modeling

One of the most important issues in the mathematical modeling of EAO reactors is the analysis to understand and predict the single-phase flow pattern and magnitude. Computational fluid dynamics (CFD) tools are employed to numerically solve the governing equations that describe the local velocity distribution of the electrolyte within the flow channels.

Governing equations in laminar flow conditions for incompressible fluids, considering electrolytes as Newtonian fluids, are the well-known Navier-Stokes (NS) equations. They are a set of partial differential equations that include the fluid velocity equations for each coordinate. The transport equations are coupled with the continuity equation to describe the fluid mass balance. In a transient regime, a simple vector form of these equations can be expressed in the following way (Equations 5.1, 5.2).

$$\rho(\mathbf{u} \cdot \nabla)\mathbf{u} = \nabla \cdot [-PI + \mu(\nabla \cdot \mathbf{u})] \quad (5.1)$$

$$\nabla \cdot (\rho \mathbf{u}) = 0 \quad (5.2)$$

Where ρ is the fluid density, \mathbf{u} is the velocity vector of the fluid, μ is the dynamic viscosity and P is the pressure.

If we are in turbulent conditions, a great amount of velocity fluctuations is present and the flow is no more under laminar conditions, at which the fluid tends to flow without lateral mixing, and adjacent layers slide past one another. Thus, motion and continuity equations must be corrected to study such fluctuations.

The modeling of turbulence is still a major challenge since the turbulence phenomena should be described at different space and time scales. Hence, several approaches exist to correlate the velocity and pressure fluctuations in turbulent conditions.

The most diffused mathematical approach to represent the turbulent equations is the time average of velocity and pressure variables. According to this approach, the NS equations become Reynolds Average Navier-Stokes (RANS) equations. The RANS and continuity equations are represented as follows (Equations 5.3 and 5.4).

$$\rho(\mathbf{u} \cdot \nabla) \mathbf{u} = -\nabla P + \nabla \cdot ((\mu + \mu_T)(\nabla \cdot \mathbf{u} + (\nabla \cdot \mathbf{u})^T)) \quad (5.3)$$

$$\nabla \cdot (\rho \mathbf{u}) = 0 \quad (5.4)$$

Where the so-called Reynolds stresses can be stated in terms of a turbulent viscosity μ_T . Several models describing μ_T have been investigated, but the most common one is the k- ε turbulent model due to its wide range of applicability, accuracy in the description of fluid motion (if confronted with experimental data) and simplicity. This sophisticated model describes the appearance and disappearance of turbulence. According with the k- ε model, μ_T can be described as follows (Equations 5.5, 5.6, 5.7).

$$\mu_T = \rho C_\mu \frac{k}{\varepsilon} \quad (5.5)$$

$$\rho(\mathbf{u} \cdot \nabla) k = \nabla \cdot \left[\left(\mu + \frac{\mu_T}{\sigma_k} \right) \nabla k \right] + P_k - \rho \varepsilon \quad (5.6)$$

$$\rho(\mathbf{u} \cdot \nabla) \varepsilon = \nabla \cdot \left[\left(\mu + \frac{\mu_T}{\sigma_\varepsilon} \right) \nabla \varepsilon \right] + C_{\varepsilon 1} \frac{\varepsilon}{k} P_k - C_{\varepsilon 2} \rho \frac{\varepsilon^2}{k} \quad (5.7)$$

Where k , ε and P_k are the turbulent kinetic energy, turbulent energy dissipation rate and the energy production term, respectively, and C_μ , σ_k , σ_ε , $C_{\varepsilon 1}$ and $C_{\varepsilon 2}$ are constant values (dimensionless) that are obtained by data fitting for a wide range of turbulent flows.

It is important to note that these sophisticated models describe the appearance and disappearance of turbulence in regions in which the flow is turbulent. For the classical two-equation models (k- ε and k- ω), the use of wall function as boundary condition is essential.

The complex solving of velocity equations in the boundary layer zone will require a very finer mesh resolution near the wall. These functions are built up using the logarithmic wall law that relates the velocity and shear stress at the damping zone.

The region attached to the wall is called laminar sub-layer (Fig. 5.4), and here the viscosity controls the normal momentum, and the non dimensional velocity U_n^+ follows Eq. 5.8. At larger distance from the wall, there is a so-called logarithm region where turbulence controls the normal transport of momentum, and U_n^+ follows Eq. 5.9. The use of wall functions allows to evaluate the step changes between the two regimes without any additional mesh refinements.

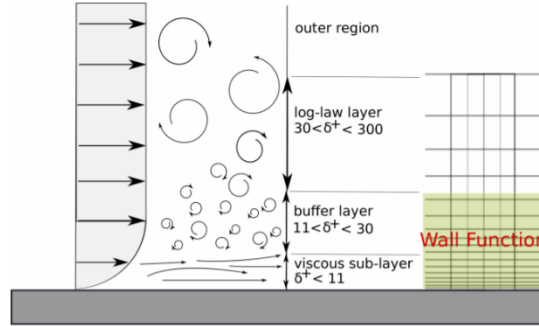


Figure 5.4 - k-ε model: near-wall treatment

$$U_n^+ = u_\tau \frac{\delta}{\nu} \quad (5.8)$$

$$U_n^+ = \frac{1}{K} \ln(\delta^+) + B \quad (5.9)$$

Where u_τ is the friction velocity, δ the distance perpendicular to the wall, and $\delta^+ (= \delta u_\tau / \nu)$ the non dimensional distance, $K = 0.41$ is a constant, as well as $B = 5.2$. The model k-ε is widely employed thanks to its easy convergence and its robustness, specially in the bulk region.

All the equations reported above, under laminar or turbulent flow regime, generally, do not have an analytical solution. Then, the application of numerical methods is needed to solve such equations. In this work COMSOL Multiphysics has been the tool used for solving the governing equations, based on the finite element method, but also other software has been employed in different papers, as Ansys Fluent or OpenFOAM.

Below are some examples concerning the hydrodynamic modeling of different filter-press cells, the most studied in the field of EAO reactors.

One of the first studies was performed by Vazquez et al. ^[84] to analyze the hydrodynamics of FM01-LC reactor operating with characteristic linear flow velocities between 0.024 and 0.192 m s⁻¹ (150 < Re < 550). The study had the only aim to evaluate the evolution of the flow pattern within the cell and was a preliminary theoretical test before a further validation using comparison to flow visualization techniques. Electrolyte flow through the reactor channel was numerically evaluated using a finite volume approach to solve the Navier–Stokes equations with a RNG k-ε model for turbulent flow. The flow predictions show that the flow development is highly affected by the manifold causing strong vortex structures at the entrance and exit of the channel. The flow disturbances are flow rate dependent but gradually disappear downstream along the channel length. However, fully developed flow is not reached.

Nevertheless, CFD analysis showed that the inlet manifolds break the electrolyte volume at the entrance and guarantee a correct distribution of the fluid along the channel and avoiding recirculation at the exit. The FM01-LC develops better hydrodynamics performance than many electrochemical in-house filter press cells, in absence of manifolds ^[85].

In the case of the FM01-LC, the particular shapes of the entrance and exit manifolds create flow inhomogeneities with different velocities that slide on top of each other, thus forming eddies increasing in size. Moreover, as already mentioned, the fluid flow in the FM01-LC usually does not reach a fully developed flow before leaving the reactor, leading to inlet and outlet effects. Hence a high turbulence level is present regardless the range of the Re number studied. These observations seem to be valid also for other in-house cells reported in literature, despite the absence of flow distributors. Indeed, turbulent model were successfully applied to simulate flows, even at low Re numbers.

It is worth mentioning that Re number is evaluated considering the mean liner flow velocity, which is given by the ratio between the flow rate and the cross section of the cell, and the equivalent diameter (Eq. 5.10, 5.11).

$$Re = \frac{vd_e}{\nu} \quad (5.10)$$

$$d_e = \frac{2BS}{(B + S)} \quad (5.11)$$

Where v is the linear flow velocity, d_e the equivalent diameter, μ the viscosity, B the flowchannel width and S the flowchannel thickness.

Following there is a table (Table 5.1) resuming some of the paper which studied the hydrodynamics in filter-press reactors with the same model.

Table 5.1 - Different reactors using RANS equations; k-ε model

Reactor	Re	Hydrodynamics model	Ref.
In-house filter press reactor	227-386	RANS equations; k-ε model	[80]
FM01-LC reactor	187-1407	RANS equations; k-ε model	[86]
FM01-LC with turbulence promoter	413-2454	RANS equations; k-ε model	[87]
Up-flow reactor	193-966	RANS equations; k-ε model	[81]

As it can be seen from the table, in the paper studied, Re ranges between values which are characteristic flows of a laminar regime. However, as already mentioned, due to the changes in geometry and flow direction, acceleration of the flow is possible, which can cause high velocity streams that can provoke 3D flow instabilities; therefore, RANS equations appear to be the best for the simulation of hydrodynamics.

Finally, there are different experimental methods to validate the results of the hydrodynamics simulations. The RTD method, one of the most employed, provides retention time distribution curves. These curves, experimentally obtained, are then compared with RTD simulation results. By using hydrodynamics results, a model for the mass transport (using velocity from hydrodynamics simulation) is implemented to evaluate the transport of a tracer in the reactor.

The classical Gaussian pulse function is used as the boundary condition of the general diffusion-convection equation (Eq. 5.12).

$$\frac{\partial c}{\partial t} = D\nabla^2 c - \mathbf{u}\nabla c \quad (5.12)$$

Here c is the tracer concentration and D its diffusion coefficient, respectively, and its numerical value should be used to construct the corresponding RTD curves.

A further validation method is constituted by the particle image velocimetry (PIV), which allows to obtain velocity profiles in high cross-sectional and electrode areas. Moreover, for small electrochemical cells, the laser Doppler velocimetry (LDV) technique could be used since the measurement of large electrochemical systems is affected by the surrounding light sources.

Simulation of single-phase flow allows to have a comprehensive outlook of the phenomenological behavior of the most common reactor used. Nevertheless, the rigorous study of an electrochemical reactor should comprise the strong coupling of several phenomena.

5.2.2 Mass transport modeling

Another important aspect to be assessed in EAO reactors is mass transport because of the well-known heterogeneous nature of the electrochemical reactions. Mass transport is linked to the concentration field of ionic species from the bulk to the electrode surface in the presence of an electric field.

The radicals formed at the electrode travel from the interface to the bulk and then they react with the pollutants. In this context, an analysis of the concentration evolution through mathematical simulation is a powerful tool to evaluate the treatments effectiveness.

Governing equations describing the mass transport within the cells are mass balance (Eq. 5.13) and the Nernst-Planck equation (Eq. 5.14).

$$\frac{\partial c_i}{\partial t} = -\nabla N_i \pm R_i \quad (5.13)$$

$$N_i = -z_i u_i F c_i \nabla \phi - D_i \nabla c_i + c_i \mathbf{u} \quad (5.14)$$

Where N_i , c_i , z_i , u_i are the molar flux, the concentration, the ionic charge, the ionic mobility of the i species, respectively. ϕ is the potential, D_i the diffusion coefficient, \mathbf{u} is the local velocity vector and R_i accounts for all the homogeneous reactions.

The first term in Eq. 5.14 represents the migration of ionic species in an electric field, the second is the diffusion term, while the last describes the convection.

These equations require a multi-coupled resolution, as it involves different variables, such as \mathbf{u} and ϕ , coming from different governing equations. However, in most of the studies found in literature, some assumptions have been done to simplify the analysis.

Hence, several mass transport studies have been carried out by assuming the migration term of Eq. (5.14) negligible. This assumption is valid in the case of presence of supporting electrolyte and if the desired electroactive species are present in dilute form, conditions commonly employed in several lab-scale degradation studies. Moreover, stationary regime is often considered and the absence of the homogeneous reactions in bulk is assumed, due to an instantaneous abatement of the pollutant on the electrode surface, thus setting a zero

concentration of the species on the electrode. In this way, only the resolution of the hydrodynamic field and the convection-diffusion equation for all the species must be solved.

Moreover, another important aspect should be considered during the mass transfer calculation under turbulent flow regime. In this case, an additional term must be evaluated in the Nerst-Plank equation, as follows ^[86] (Eq. 5.15).

$$\mathbf{N}_i = -z_i u_i F c_i \nabla \phi - (D_i + D_{i,t}) \nabla c_i + c_i \mathbf{u} \quad (5.15)$$

The term $D_{i,t}$ represents the turbulent diffusivity, which can be obtained by the turbulent Schmidt number as follows, in the equation 5.16.

$$D_{i,t} = \frac{\nu_t}{Sc_t} \quad (5.16)$$

However, the number of works on mass transport calculation in EAO reactors by using CFD is scarce.

In a very interesting paper by Rivero et al. ^[86] is reported a new model to evaluate the mass transport coefficient, k_m , the main scope of mass transport calculation. Nevertheless, they did not consider any degradation, but the study was conducted on the potassium ferro-ferricyanide electrochemical system with sodium sulfate as supporting electrolyte. This kind of solution is widely used as test system to assess the mass transport in the cells employed in these technologies. They used standard k - ϵ turbulence model, where the average velocity field and the turbulent viscosity from RANS equations were employed to evaluate the convection, the turbulent diffusivity and the concentration wall function. Indeed, the model involving the simplified eq. 5.15 (no migration term) and 5.16 has to be solved in the same fluid region where RANS equations are valid. However, due to the use of wall functions, in the near-wall zone, turbulent viscosity and average velocity field are unknown, thus they used a concentration wall function to evaluate the concentration profile near the wall. Then, k_m was calculated by using the diffusive flux at the electrode surface calculated by CFD as follows (5.17).

$$k_m = \frac{\int_{A_e} (N_i \cdot \mathbf{n}) dA_e}{c_{i,0}} \quad (5.17)$$

N_i is the local mass transfer flux over the electrode surface, $c_{i,0}$ is the inlet concentration of the i species, A_e is the electrode area and \mathbf{n} is the normal vector. For a more detailed explanation of the model, refer to the cited paper.

Following this route, the only work found on the evaluation of the k_m by CFD in a degradation study was that of Gharibian et al. ^[80]. They studied Methylene blue (MB) removal by using of an in-house filter press electrochemical flowcell operating in recycle mode with graphite electrodes.

Finally, another interesting and more complex work was conducted Rivero et al. ^[88]. They developed a 3D mass transfer model in filter-press reactor to simulate active chlorine generation in a filterpress electrolyzer to degrade an organic pollutant in recirculation operating mode. They used the same model employed in a previous paper to model the near-wall concentration ^[86], adding the effect of the migration term, assessed by studying the current distribution within the cell. This study is outside the scope of this work, which is not focused on the use of active chlorine, that could also lead to secondary pollution. However, this is the only model found in

literature, regarding a degradation study, comprising the coupling of the three main branches of ECRs modeling: hydrodynamics, mass transport and current and density distribution.

In this context, due to the lack of works, an alternative route to evaluate the mass transport within the cell is the use of empirical correlations.

Vazquez et al. ^[84] found mass transport profiles at FM01-LC channels assuming that the mass transport coefficients can be obtained by using an empirical power law expression (eq. 5.18).

$$k_m = av^b \quad (5.18)$$

Where a and b are empirical constant, while v is the mean linear flow velocity previously defined. They determined local k_m , using this global correlation as an approximation to calculate local mass transport coefficients, leading to results having good fit with experimental data.

Other correlations which can be used derive from calculation of the limiting current. Indeed, experimental mass transport characterization represents a starting way to evaluate the performance of electrochemical reactors since it provides empirical equations linking limit current density and mass transport coefficient.

Several papers have shown the experimental determination of k_m under mass transport control, in the limiting current region plateau, when the current can be directly linked to the global mass transport coefficient k_m as follows (Eq. 5.19).

$$k_m = \frac{I_L}{AzFc_0} \quad (5.19)$$

I_L is the limiting current density, experimentally determined, A is the effective area of the working electrode, z is the ionic charge, F is the Faraday constant and c_0 is the starting concentration.

In practice, the mass transport is usually characterized by experimentally assessing the limiting current over a range of different mean linear velocities. The convective-diffusion mass transport dependency relative to convection is expressed by a dimensionless group correlation, as follows (Eq. 5.20).

$$Sh = a Re^b Sc^{0.33} \quad (5.20)$$

Where a and b are empirical constant, related to flow channel shape, cell dimensions and electrolyte hydrodynamics. The Reynolds number (Re) is defined as in the equation 5.10. The Sherwood number (Sh) is given by the following equation (5.21).

$$Sh = \frac{k_m d_e}{D} \quad (5.21)$$

D is the diffusion coefficient of the electroactive species, while the Schmidt number is linked to the fluid transport properties, as shown in equation 5.22.

$$Sc = \frac{\nu}{D} \quad (5.22)$$

The exact form of the mass transport correlation is obtained through a fit of the experimental data and will depend on the electrode and flow channel geometries as well as the type of fluid and the electroactive species flow in the channel.

Table 4 summarises the mass transport correlation found for several electrochemical systems using different kind of filter-press cell. The test system used in the different works is always the reduction of ferrocyanide. The constant a is characteristic of the design geometry, whereas b reflects the fluid flow influence. The addition of the turbulence promoters provides not only an increase of the coefficient a but also a lower coefficient b , reflecting the decrease of the fluid flow influence in the mass transport and a higher relevance of inlet/outlet configuration.

Table 5.2 – Empirical correlations for different types of reactors

Channel configuration	Re range	a	b	Electrode material	Ref.
<i>Filter-press type reactors</i>					
FM01-LC					
Empty channel	200<Re<1000	0.22	0.71	Stainless steel	[71]
Channel with turbulence promoter	200<Re<1000	0.74	0.62	Stainless steel	[71]
<i>DIACELL</i>					
Empty channel	25<Re<100	0.69	0.36	BDD	[83]
Empty channel	100<Re<2500	0.14	0.45	BDD	[83]

5.2.3 Current and potential distribution modeling

The current and potential distribution within the cell and the electrodes are among the main engineering and design aspects. The non-uniformity of current and potential may cause scarce performance in terms of current efficiency due to the occurrence of parasitic reactions.

This is associated with electrode shape and material, cell geometry, electrochemical reaction steps and mass transport aspects. To evaluate the potential and current distributions in 2D electrodes, it may be taken into account that the current density, \mathbf{j} at any point inside the cell can be determined from the local potential gradient $\nabla\phi$, according to Ohm's law (Eq. 5.23).

$$\mathbf{j} = -k\nabla\phi \quad (5.23)$$

Where k is the electrolyte conductivity, determined by the mobility of species.

At steady state, the electric potential can be described by the Laplace equation, as reported in equation 5.24.

$$\nabla \cdot \mathbf{j} = -k\nabla^2\phi = 0 \quad (5.24)$$

In the electrolyte, which is an ion conductor, the net current density can be used as the sum of the fluxes of all ions, as expressed in equation 5.25.

$$\mathbf{j} = F \sum_{i=1}^n z_i \mathbf{N}_i = F \sum_{i=1}^n z_i (-z_i u_i F c_i \nabla\phi - D_i \nabla c_i + c_i \mathbf{u}) \quad (5.25)$$

\mathbf{N}_i can be obtained by equation 5.14, neglecting or not, the migration term. However, the last equation, in its complete form, must be solved only in the case of a tertiary current distribution.

Hence, three different cases of potential and current distribution can occur in electrochemical cells.

The primary current distribution considers only the losses due to the resistance of the solution, neglecting the electrodes kinetic effects and the effects depending on the concentration. Charge transfer in the electrolyte obeys to Ohm's law. Consequently, the first hypothesis is that the electrolyte is electroneutral, which cancels the convective contribution to the current density in equation (5.25), and the second hypothesis is that the concentration gradient in the electrolyte is negligible, which cancels the diffusive contribution to the current density in equation (5.25) and allows us to treat the ionic strength as a constant. Hence, the remaining term of equation (5.25) results in Ohm's law for the current density of the electrolyte.

At the electrode-electrolyte interface we assume that the electrolysis reaction is so fast that we can neglect the influence of the electrode kinetics, and therefore the potential difference at the electrode-electrolyte interface deviates negligibly from its equilibrium value. Thus, there is no activation potential and an arbitrary current density can occur through electrolysis. Therefore, the primary current distribution depends only on the geometry of the anode and cathode.

The secondary current distribution takes into account electrode kinetics, as well as the resistance of the solution. The assumptions about the composition and behavior of the electrolyte are the same as for the primary current distribution, resulting in Ohm's law for the electrolyte current. The only difference between the primary and secondary current distributions is in the description of the electrochemical reaction at the interface between the electrolyte and the electrode.

The influence of electrode kinetics is included here; the potential difference may differ from its equilibrium value due to the presence of an overpotential, which is the difference between the actual potential difference and the equilibrium potential difference.

The tertiary current distribution considers the effect of changes in electrolyte composition and ionic strength, as well as the resistance of the solution and the kinetics of the electrodes. To do this, the equation (5.25) must be explicitly solved for each chemical species to describe its mass transport through diffusion, migration, and convection. Furthermore, the concentrations of the species are subject to the approximation of electroneutrality. Kinetic expressions for electrochemical reactions depend both on activation and concentration overpotential, thus the reactions can be limited by transport from reagent depletion at the electrode-electrolyte interface. In this model all ions and all electroactive species in the electrolyte must be included in the model.

Finally, the three distributions differ in the boundary conditions. The primary current distribution needs a Dirichlet or constant potential boundary condition. For secondary and tertiary potential and current distribution, a relationship between current density and electrode potential is needed, for instance a Butler-Volmer expression. A zero flux condition is set at the insulating walls of the cell. All these conditions are reported in the following table (5.3), where the overpotential is related to the magnitude of the local current density through the Tafel approximation.

Table 5.3 - Boundary conditions for different current distribution

Type of current distribution	Boundary conditions
Primary	$\phi = \phi_i$ (5.26)
Secondary	$-k \frac{\partial \phi}{\partial \xi} = j_0 \exp\left(\frac{\eta}{b}\right)$ (5.27)
Tertiary	$-k \frac{\partial \phi}{\partial \xi} = \frac{c}{c_0} j_0 \exp\left(\frac{\eta}{b}\right)$ (5.28)
Insulating walls	$-k \frac{\partial \phi}{\partial \xi} = 0$ (5.29)

ξ represents the normal to the electrode surface, whereas b can be either the anodic or cathodic Tafel slope.

Although the number of works reported for other electrochemical applications, like fuel cells and batteries, is large, the references that employ CFD to evaluate current and potential distribution in electrolyzers are limited.

In this context, only a single study regarding the analysis of current and potential distribution in reactors for water disinfection was found. Perez T. et al ^[90] studied the primary and secondary current distributions along a BDD anode of a filter-press-type FM01-LC reactor. The analysis was performed on water discharge for hydroxyl radicals formation. This work will be explained in the next chapter, as it constitutes the reference for current distribution analysis in the case study analyzed.

6. Design of an electrochemical advanced oxidation reactor

Looking at the previous chapters, the scientific literature is plenty of experimental studies proving the effectiveness of electrochemical advanced oxidation treatments for water disinfection, whereas there are few CFD studies on reactor modeling.

Furthermore, most of the works are focused on the study of pollutants present in wastewaters, while very few studies on water intended for purification are present. However, as reported in the section 2.2.2, in some contexts, also wastewaters may be used as drinking water sources.

In this context, the aim of this work is to study the reaction environment of a filter press reactor using CFD.

For this purpose, a study by Gharibian et al. [80] was taken as a starting point for a first characterization. They studied hydrodynamics and mass transfer inside an in-house filter press reactor, using the degradation of methylene blue as test system. Methylene blue is a refractory organic molecule used as dye and largely employed as a stain in bacteriology, as indicator in oxidation reactions and as an antidote to cyanide. MB produces intense blue color in aqueous solutions and causes negative effects on humans and environment.

In this chapter, after a brief description of the software used for the modeling, the methods used for CFD analysis, the mathematical model, as well as the boundary conditions are explained.

6.1 COMSOL Multiphysics

COMSOL Multiphysics® is a multidisciplinary software for multiphysics simulation which use the Finite Element Method (FEM) and is widely used in the context of EAO reactors mathematical modeling.

The finite element method (FEM) is a method for numerically solving differential equations present in engineering and mathematical modeling. The FEM is a general numerical method able to solve partial differential equations in two or three space variables. In order to solve a problem, the FEM subdivides a big system into smaller parts, called finite elements. This can be done by discretize the object of study in the space dimensions, achieved through the construction of a mesh, which represents the numerical domain for the solution. Eventually, the finite element method formulation produces a system of algebraic equations. The simple equations modeling these finite elements are then set up into a larger system of equations that models the entire problem.

In this context, COMSOL Multiphysics® is a user-friendly software which is able to simulate, thanks to the coupling of one or more physics, a huge variety of phenomena occurring in electromagnetism, structural mechanics, acoustics, fluid dynamics, heat transfer and chemistry.

In this thesis, Comsol Multiphysics® has been used because it allows to reproduce the geometry of the electrochemical reactor and the considered physics, in this case the single-phase fluid flow used to understand the hydrodynamics of the reactor, which is linked to the mass transport, and the electrochemistry module, to investigate the current and potential distribution within the cell.

The software allows to choose the dimension of the problem according to different commands. In this case, due to the complexity of the geometry and the asymmetries, the choose is 3 Dimension (3-D).

After the choice of the dimension, physics have to be added. After the simulation of the flow through the single-phase flow interface, using the k- ϵ model, the electrochemistry module has been implementend; primary and secondary current distribution have been studied.

The last step is to choose the type of study, which can be stationary or time dependent. In this case all the phenomena have been studied in stationary.

Following these passages is then to create the geometry of the object, using or not the COMSOL geometry tools, then to choose the materials involved in the simulation and to impose the boundary conditions. Further descriptions of the steps will be provided in the next sections.

6.2 Case study

The case study, as reported in the introduction of the chapter, is a filter press reactor used for the direct oxidation of methylene blue, using graphite electrodes.

The configuration and constituting parts of electrochemical flowcell used in the study of Gharibian et al. ^[80] are shown in figure 6.1. The classical system with the recycle has been used to increase the decay of MB concentration. The reactor used, very similar to the FM01-LC, did not have spacer, manifold, and flow distributors.

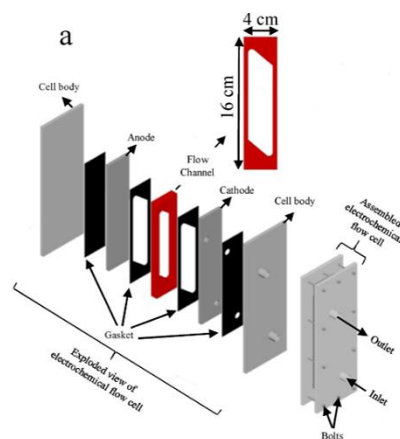


Figure 6.1 - Exploded view of the electrochemical flow cell

In their study, Gharibian et al. ^[80] characterized the reactor by studying hydrodynamics and mass transport. The hydrodynamic results were validated through the Residence Time Distribution curves (see section 5.2.1), while the k_m values were validated through experimental electrochemical degradation of MB.

In this study, the hydrodynamic part is simulated using the same model of the case study. Due to the lack of studies in this context, rather than directly calculating the global mass trasport

coefficient, a characterization of the cell is carried out to study the local mass transport coefficient profiles, taken as a reference a work by Vázquez et al. [89].

They derived local mass transport coefficient profiles in a FM01-LC reactor and demonstrated correspondence with experimental data, starting from a global correlation (equation 5.20), which links the hydrodynamics in the reactor to the mass transport coefficient. Local velocity profiles were calculated using CFD simulations, dividing the reactor into several volumes and sections. Then they used global correlations to derive local mass transport coefficients, obtaining results in agreement with the experimental data.

This type of approach, where global correlations are used as an approximation to calculate local mass transport coefficients, was then then applied by several works on the same types of reactors [84], [85].

Similarly, after the validation of the hydrodynamic results, the same procedure is applied in this work to have a first characterization of the mass transport inside the reactor.

The reactor was divided into three sections and each section was subdivided into 20 lines in order to obtain local average velocity profiles. For each average velocity, a local Reynolds number, as well as a local Sherwood number were calculated, using the correlation deriving from the case study and two other correlations valid for other types of reactors, to provide a direct comparison between the different reactors.

6.3 Mathematical model and simulation

In order to simulate electrolyte flow inside channel and determine local mass transport coefficient, simulations were carried out in 3D due to axial and transversal velocity variations and effects of inlet/outlet. The maximum volumetric flow rate of the work was studied, corresponding to a mean linear velocity of 0.0231 m s^{-1} and $Re = 386$ (table 6.1). The flow pattern was simulated by solving Reynolds Averaged Navier-Stokes (RANS) equations and a standard k- ϵ model was employed for the turbulence. Mass transport characterization was performed by cutting the reactor in different sections, building up 20 lines for each section in order to evaluate locally the velocity magnitude. Then, the correlation obtained from the study of Gharibian et al. was used to calculate the local mass transport coefficient.

Table 6.1 - Operating conditions

Operating conditions	
Q	0.53 L min^{-1}
$v = Q/A_t$	0.0231 m s^{-1}
$Re = vd_h\rho/\mu$	386

In the first part of this section the reactor geometry and the tools used to design the domain are described. Successively, the equations of the hydrodynamic model are listed, as well as the boundary conditions. Regarding the mass transport, the methodology for calculating local mass transport coefficients is explained.

6.3.1 Geometry

The geometric domain object of the simulation is constituted by the empty area inside the spacer (figure 6.2) which divides the two electrodes and represents the space in which the fluid flows, therefore the body of the reactor.



Figure 6.2 - Spacer inside the cell

The geometric measurements of the reactor are listed in the following table (6.2).

Table 6.2 - Geometric measurements of the reactor

Reactor length, L	16 cm
Reactor width, B	3 cm
Reactor thickness, S	1.1 cm
Inlet/Outlet area, A_{inlet}	0.00006338 m ²
Channel transversal area, A_t	0.000385 m ²

For ease of drawing, AutoCAD was used as a tool for plane geometry design. In COMSOL is possible to use a “work plane” to first draw the plane geometry and then modify it through the several features present in the software. Thus, 2D geometry was drawn in AutoCAD and successively, thanks to COMSOL features, it was possible to import the geometry as .dxf format, as shown in figure 6.3.

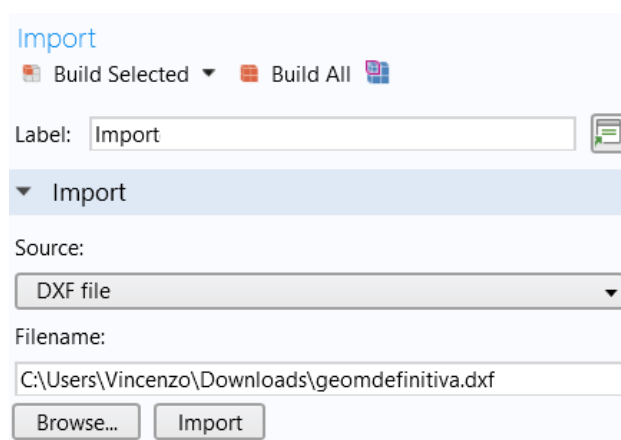


Figure 6.3 - – “Import” command in geometry settings

In this way the plane geometry was imported into the work plane (figure 6.4).



Figure 6.4 - 2D geometry in the “work plane”

Successively, it was possible to transform the geometry from 2D to 3D thanks to the "extrude" command (Figure 6.5) and obtain the domain in the figure 6.6. The distance from the plane, set at 1.1 cm, represent the thickness of the reactor.

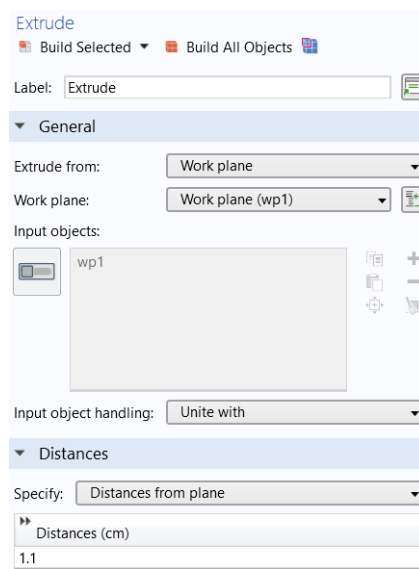


Figure 6.5 - “Extrude” command in geometry settings

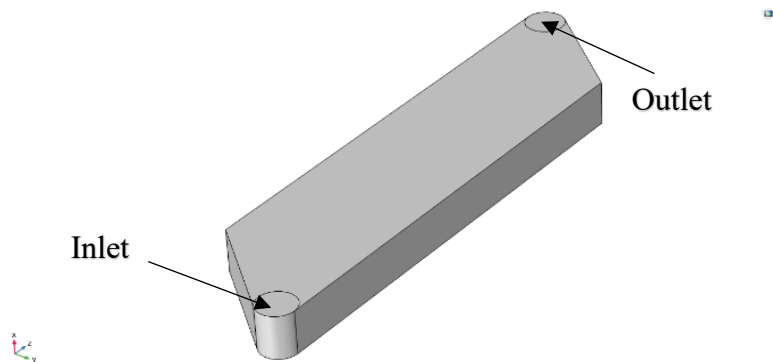


Figure 6.6 - Final 3D computational domain considered inside electrochemical flowcell

6.3.2 Simulation

Governing equations for momentum equations coupled with turbulence model equations were solved numerically by finite element method, using COMSOL Multiphysics® 5.5. Several mesh configurations were assessed in order to achieve the best compromise between computational cost and results accuracy, eventually obtaining negligible local velocity magnitude variations with change of mesh cell size. The final mesh used for the simulations was the default coarse mesh provided by the options in the software, because it satisfied the requirements discussed.

Final mesh for computational domain (Fig. 6.7) consisted of 409269 elements, of which 276266 tetrahedral mesh elements. Default solver options of software were used. The material used for the simulation is liquid water, chosen from the material library. The temperature was set at 298 k.



Figure 6.7 - Mesh generated for simulation of hydrodynamics inside electrochemical flowcell

6.3.3 Hydrodynamic

As reported in the previous chapter, the use of turbulence models coupled to Reynolds-averaged Navier–Stokes equations, RANS, is an efficient and practical tool for this type of problems. One complication when using this procedure is the presence of solid walls, because standard turbulence models are valid only in regions far enough from the wall so as to consider isotropic flow and high-Reynolds-number conditions. Wall functions were employed to solve this problem, assuming the flow in the near-wall region based on a universal velocity distribution, thus avoiding the resolution of transport equations in this region.

Turbulence and RANS models with wall functions seem to be appropriate for evaluating most of the main flow characteristics and have proven to be useful also in predicting flow at low Re numbers, as discussed in section 5.2.1.

Assuming negligible variation of viscosity, density, and electrolyte temperature, continuity and RANS equations for flow of an incompressible Newtonian fluid under turbulent conditions at steady state were used. The expression used are the same presented in the previous chapter (Eq. 5.3 - 5.7).

The values of the dimensionless constant C_μ , σ_k , σ_ε , $C_{\varepsilon 1}$ and $C_{\varepsilon 2}$ are listed in the following table (6.3).

Table 6.3 - Constant values of the k- ε model

C_μ	$C_{\varepsilon 1}$	$C_{\varepsilon 2}$	σ_k	σ_ε
0.09	1.44	1.92	1	1.3

According to logarithmic law of universal velocity distribution for turbulent region, the following expression was used at the walls (Eq. 6.1).

$$u^+ = 5.5 + \frac{1}{\kappa} \ln y^+ \quad (6.1)$$

Where u^+ is dimensionless velocity, κ is Karman constant (=0.41) and y^+ is dimensionless distance to the wall ($y^+ = \rho u_T / \mu$), u_T is the friction velocity ($u_T = C_\mu^{1/4} \sqrt{k}$), and y is distance from the wall.

Boundary conditions for solving Eqs. 6.2-6.5 are:

- At the inlet, normal uniform inflow velocity was considered through equation 6.2:

$$\mathbf{u} = U_0 \cdot \mathbf{n} \quad (6.2)$$

Where, $U_0 (= Q/A_{inlet})$ is the starting average velocity calculated using cross section area of the inlet and \mathbf{n} is the normal vector. Values of k_0 and ε_0 were evaluated from turbulent intensity I_T (0.05) and turbulent length scale L_T (0.035) according to Eqs 6.3, 6.4.

$$k_0 = \frac{3}{2} (U_0 L_T)^2 \quad (6.3)$$

$$\varepsilon_0 = C_\mu^{\frac{3}{4}} \frac{k^{\frac{3}{2}}}{L_T} \quad (6.4)$$

Value of L_T in pipes is calculated according to Eq. 6.5, where r is the radius of connecting tubes.

$$L_T = 0.07r \quad (6.5)$$

- At the outlet of the reactor, no gradient forces are presents and normal stress is equal to the pressure at the outlet (Eq. 6.6-6.8). In this work pressure at the outlet is considered zero ($P_0 = 0$).

$$[-P + (\mu + \mu_T)(\nabla \mathbf{u} + \nabla \mathbf{u}^T)] \cdot \mathbf{n} = 0 \quad (6.6)$$

$$\nabla k \cdot \mathbf{n} = 0 \quad (6.7)$$

$$\nabla \varepsilon \cdot \mathbf{n} = 0 \quad (6.8)$$

- Logarithmic wall function (Eq. 6.1) for all the walls.

Accuracy of the turbulence mesh size was evaluated through the attainment of an indistinguishable difference of local velocity magnitude between the different meshes. y^+ value of approximately 11 was obtained, value at which the logarithmic layer meets the viscous sublayer and wall function treatment is valid.

6.3.4 Mass transport

As already discussed, due to the lack of studies in this context, rather than directly calculating the global mass transport coefficient, a characterization of the cell was carried out to evaluate the local mass transport coefficient profiles, taken as a reference a work by Vázquez et al. [89].

Dimensionless flux, expressed by Sh , is a function of the dimensionless fluid velocity (Re) multiplied by the dimensionless fluid properties (Sc). In forced convection reactors, this correlation is reported in form of equation 5.20, from the previous chapter.

If a realistic flow pattern is provided from numerical simulation and an appropriated mass transport correlation is selected for a given electrochemical reactor, then the mass transport coefficient (k_m) can be evaluated by using Sh number definition, as given by Eq. 5.20.

The correlations employed in this work are reported in the following table (6.4). The first one was obtained from the linear fitting of the k_m resulting from the work of Gharibian et al., whereas the other two were used to have a direct comparison with the more widespread FM01-LC, taking as references works with different spacing S between the electrodes (both valid in the Re range observed).

Table 6.4 - Value of constant a and b for $Sh = a Re^b Sc^{0.33}$ correlation

Reactor	a	b	Re range	Ref.
In-house filter press cell	0.39	0.79	227-386	[80]
FM01-LC ($S = 0.55$ cm)	0.22	0.71	200-1000	[71]
FM01-LC ($S = 1.95$ cm)	0.49	0.62	187-1407	[86]

The correlations chosen were coupled with the flow field obtained. It was then possible to estimate the dimensionless groups Re , Sh and k_m at different positions in the flowcell channel by considering a fundamental assumption.

The hydrodynamic behaviour within the flowcell influences the mass transport coefficient and the electrode current when the process is mass transport controlled, thus the mass transport controls the rate of the reaction. This was also confirmed by the study of Gharibian et al., as the experimental MB concentration decay over time was found to fit a first order kinetics (from a mass balance over whole electrochemical system), which is characteristic of a mass transfer controlled electrochemical reaction. In this case, the reaction kinetics at the electrode is considered instantaneous.

Local mass transport coefficients were evaluated considering three different sections, at $z = 5$ cm; $z = 8$ cm; $z = 11$ cm. At each value of z selected, 20 different parallel lines starting from one extremity of the channel until reaching the opposite one were drawn, as it is shown in figure 6.8 for $z = 5$ cm.

For each line, a theoretical velocity profile was obtained with 20 local average flow velocities along the channel width (y dimension). Each average velocity profile was obtained by using the command “Line Average” and it was considered to be the local mean flow velocity (v) representative of the line. A local mean Re was computed, for each corresponding local mean flow velocity (v), according to equation 5.10.

For a given mass transport correlation (see Table 6.4), a local mean Sh was calculated, through equation 5.20, for each corresponding local mean flow velocity (v) and local mean Re. For each corresponding local mean Sh obtained, an average k_m value was evaluated from Eq. (6.9) and was considered as the averaged k_m for each line.

$$k_m = D \left(\frac{Sh}{d_e} \right) \quad (6.9)$$

D is the coefficient of diffusion of the electroactive species, in this case $6.74E-10 \text{ m}^2 \text{ s}^{-1}$.

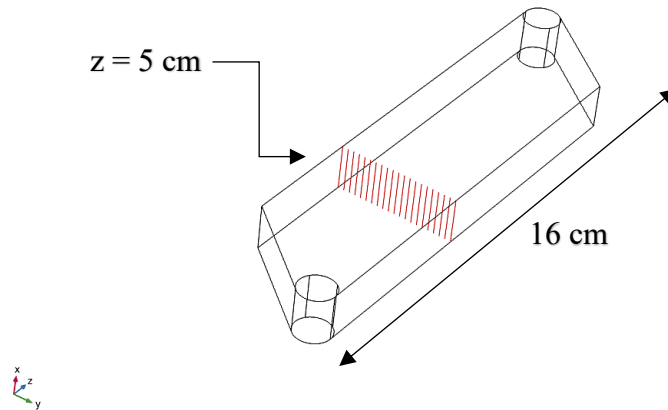


Figure 6.8 - The flow channel, showing the positions of the lines at $z = 5 \text{ cm}$

6.3.5 Current and potential distribution

For the study of the current and potential distribution, the work of Perez et al. ^[90] was taken as a reference. At first, their model was validated, taking as object of study only the central part of the channel of a FM01-LC. In the case of their work, the channel had a spacing between the electrodes of 0.55 cm, while in the case study analyzed is 1.1 cm (Table 6.5). Hence a new domain was used, considering only the central part of the channel, which is the place where the radicals are generated during water discharge. The domain is show in figure 6.9.

Table 6.5 - Geometrical characteristics of the channel

Electrode length, L	16 cm
Electrode height, B	4 cm
Electrode spacing, S	0.55 cm
Electrode area, A	64 cm^2

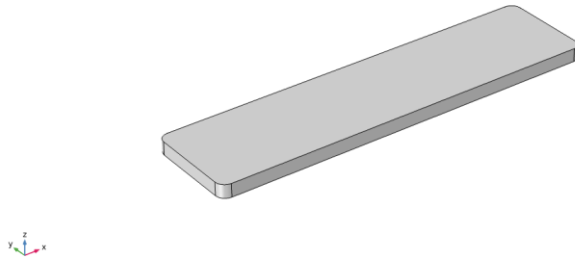


Figure 6.9 - 3D domain of the channel

Primary and secondary current distributions were calculated. Primary current distribution is determined by the cell geometry, whereas secondary current distribution is used to describe the effects of charge transfer during hydroxyl radical formation. Oxidation of water from an acidic sulfate electrolyte was used as a test system.

Inputs for the simulations were taken from the microelectrolysis studies of water oxidation performed by the same authors (Table 6.6).

Table 6.6 - Parameters used in the numerical simulation at 298 K

Electrolytic conductivity, k	35 S m ⁻¹
Anode open circuit potential, ϕ_a	0.6 V
Cathode open circuit potential, ϕ_c	0.0 V
Working electrode	
Tafel slope, b_a	0.25 V
Exchange current density, j_0	3 x 10 ⁻⁷ mA cm ⁻²
Counter electrode	
Tafel slope, b_c	-0.12 V
Exchange current density, j_0	3 mA cm ⁻²

It was assumed that the potential drop along the BDD was negligible. Hence, the boron-doped diamond film on Ti has been considered by several authors as a highly conductive electrode. However, the thickness of the film, in this case 2 μm , probably plays a role in the electrode potential drop. In this work, doing the same assumption of the paper, the electrode potential has been considered constant at such thickness.

Current density at any point inside the channel was determined from the gradient of local potential, by using equation 5.23. Potential distribution in the electrolyte was described by the Laplace equation (5.24).

Depending on the characteristics of boundary conditions on the working electrode, three types of current distribution models can be studied. For a primary current distribution, the following boundary conditions along the anode and cathode were considered (6.10, 6.11).

$$\phi = \phi_a \quad (6.10)$$

$$\phi = \phi_c \quad (6.11)$$

For the insulating walls the equation 5.29 was employed.

ϕ_a and ϕ_c are anode and cathode surface potential, which were set equal to the potential of the solution adjacent to each electrode. Practically, the potential of the solution adjacent to each electrode corresponds to the open circuit potential. Electrochemical reaction on the working electrode was considered reversible and primary current distribution is exclusively dependent on the geometry of the cell.

A secondary current distribution can be obtained when the electrochemical reaction is dependent on the charge transfer, whereas the concentration gradient is considered negligible. Under these conditions, local current density on the electrodes can be related to the local overpotential. The overpotential is related to the local current density through the Tafel approximation:

$$j = j_0 \exp\left(\frac{\eta}{b}\right) \quad (6.12)$$

Where j_0 is the current density exchange and b is the Tafel slope, cathodic or anodic, from Table 6.6. η is the overpotential.

For the secondary current distribution model, boundary conditions are expressed as follows.

- No current flow at all insulating surfaces, Eq. (5.29).
- If Tafel kinetics is applied at the working electrode under charge transfer controlled conditions, Eq. (5.27).
- At the counter electrode, Eq (5.27).

The kinetics applied to the counter electrode was chosen among various kinetics for the hydrogen evolution reaction, in order to validate the model and have a similar I-E curve with respect to the considered work.

Once the model was validated, the trend of the I-E curves was evaluated with respect to the variation of the electrical conductivity and the spacing between the electrodes. In this way the specific energy consumption was calculated and a comparison was made between waters having high conductivity and waters intended for potabilization, therefore with low conductivity.

However, in this work the electrochemical process corresponds to the oxidation of water, thus tertiary current distribution is not studied. It is important to mention that during electrochemical degradation of organics, tertiary current distribution should be considered. This analysis should be useful to have starting point in which tertiary current distribution may be added.

7. Results and discussion

In this chapter, the results of the physics studied, as well as the improvements done to the reactor configurations and the comparison between different operational parameters, are presented.

7.1 Hydrodynamics and mass transport results

Simulated slices of velocity magnitude field inside flowcell are presented in Fig. 7.1 for a flow rate of 0.53 L min^{-1} , equivalent to a mean linear flow velocity of 0.0231 m s^{-1} . In the figure 7.1a is presented the cross sectional view of velocity distribution computed by Gharibian et al. ^[80] (validated by RTD curves), whereas in figure 7.1b are shown the slices of section velocity fields calculated in this work. It is clearly visible the similarity between the two results.

Inlet and outlet effects at the entrance and outflow is due to formation of higher velocity streams, named preferential flow zones.

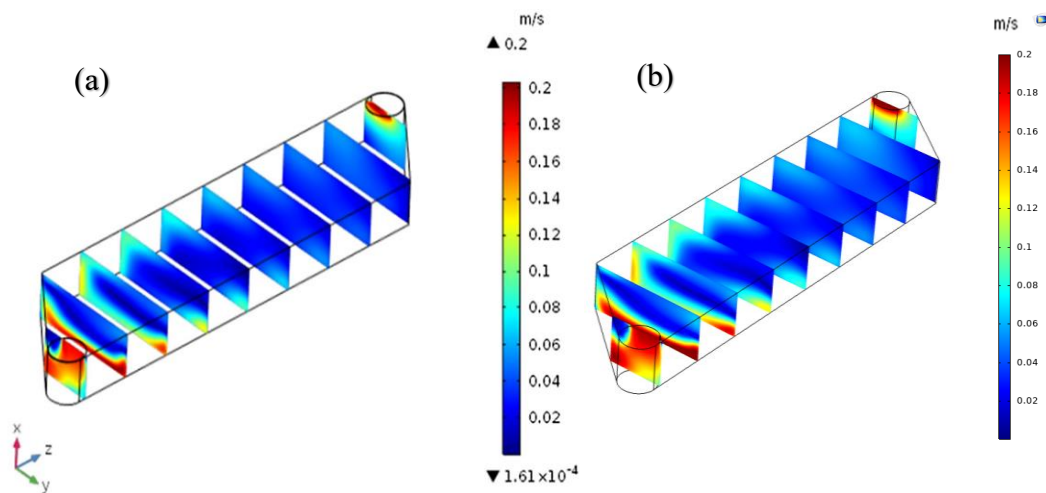


Figure 7.1 - (a) Cross sectional view of velocity distribution inside simulation domain for flowrate of 0.53 L min^{-1} of the study of Gharibian et al. ^[80]; (b) Computed cross sectional view of velocity distribution

To have a more precise comparison between the obtained results, the cell was divided into three different sections, in order to evaluate velocity profiles at different values of the coordinate z and compare the computed results with that from the case study. Velocity profiles along the cell length at the distance of $z=5, 8,$ and 11 cm from the entrance and $x = 0.55 \text{ cm}$ are presented in figures 7.2, 7.3, 7.4.

As can be seen from the figures, it is evident the correspondence between the profiles. Some slight discrepancy may be due to the different meshes employed in the two works.

However, inlet jet streams and almost developed flow near the outlet is clearly visible. In addition, velocity is almost uniform in the profile at $z = 8 \text{ cm}$, whereas at $z = 11 \text{ cm}$, the fluid is influenced by the outlet. This suggests that in the $6 < z < 9 \text{ cm}$ zone the velocity is almost uniform. Pérez et al. ^[85] studied the turbulent flow within a flowcell having a similar

configuration to this work. Complex hydrodynamic behavior found inside the cell is related to its geometry, since it presents an increment of transversal area at the entrance, followed by a constant transversal area and then a reduction of transversal area at the outlet.

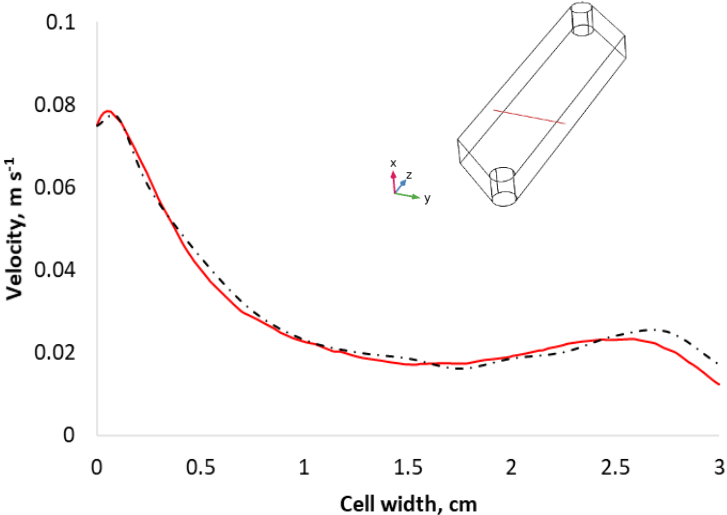


Figure 7.2 - Simulated velocity profiles at the distance of 0.55 cm from electrodes and 5 cm from flowcell inlet for flow rate of 0.53 L min^{-1} ; Dotted line: work of Gharibian et al. [80]; Red line: present work

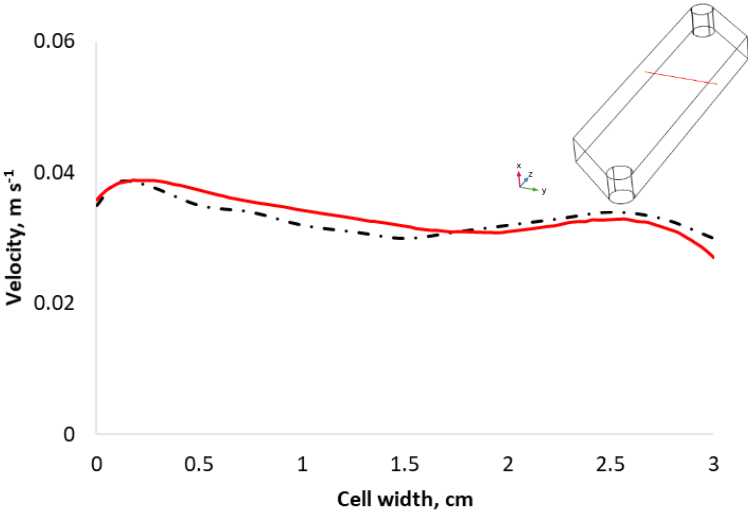


Figure 7.3 - Simulated velocity profiles at the distance of 0.55 cm from electrodes and 8 cm from flowcell inlet for flow rate of 0.53 L min^{-1} ; Dotted line: work of Gharibian et al. [80]; Red line: present work

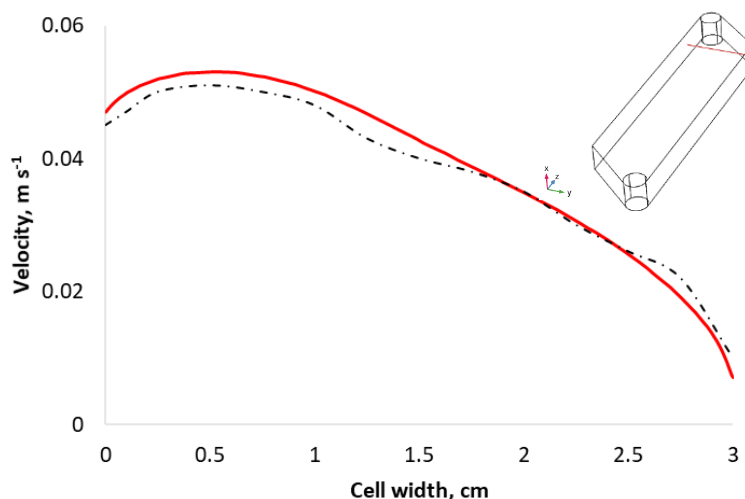


Figure 7.4 - Simulated velocity profiles at the distance of 0.55 cm from electrodes and 11 cm from flowcell inlet for flow rate of 0.53 L min^{-1} ; Dotted line: work of Gharibian et al. ^[80]; Red line: present work

Regarding the mass transport, the numerical simulation of a realistic flow pattern provides a very useful tool for predicting k_m in a reactor channel when an appropriate mass transport correlation is selected.

In the figures 7.5-7.7 are shown the trend of the local mass transport coefficients, calculated using the correlations indicated in table 6.4. As can be observed, the correlation obtained from the case study was the one providing the highest local mass transport coefficients.

Firstly, correlations are variable with the geometry, thus the experimental correlation obtained for the reactor studied is the one predicting the local mass transport coefficients at best. However, comparison between the different correlations may be useful to better understand the results obtained.

Much higher values of local k_m are probably due to the lower width (3 cm) and length (16 cm) of the flowcell considered respect to the FM01-LC reactors as can be clearly seen in table 7.1, and therefore the higher velocities achieved on average. In the case of a reaction controlled by mass transport, these velocities lead to larger local k_m . This could suggest that this type of cell, without inlet and outlet distributors, may have better performance than a FM01-LC reactor. Nevertheless, it must be considered that a stricter and shorter channel determines a smaller electrode area and therefore a lower surface available for degradation.

However, it is interesting to observe the local mass transport profiles obtained at the various z coordinates considered, which can be observed in the figures.

The results obtained are similar to the study of Vázquez et al. ^[89], which found an analogue behaviour through hydrodynamic CFD simulation of a FM01-LC reactor.

Hence, at the beginning (Fig. 7.5) an effect of the inlet can be seen, leading to local increase in k_m coefficients, while as z coordinate increases, more uniform profiles (Fig. 7.6) are found.

Moreover, in the central area, a decrease in k_m is also observed (Fig. 7.6), due to the velocity reduction, as previously seen in figure 7.3.

Instead, at the end of the channel (Fig. 7.7), an increase in k_m is evident due to the vortices caused by the outlet effects.

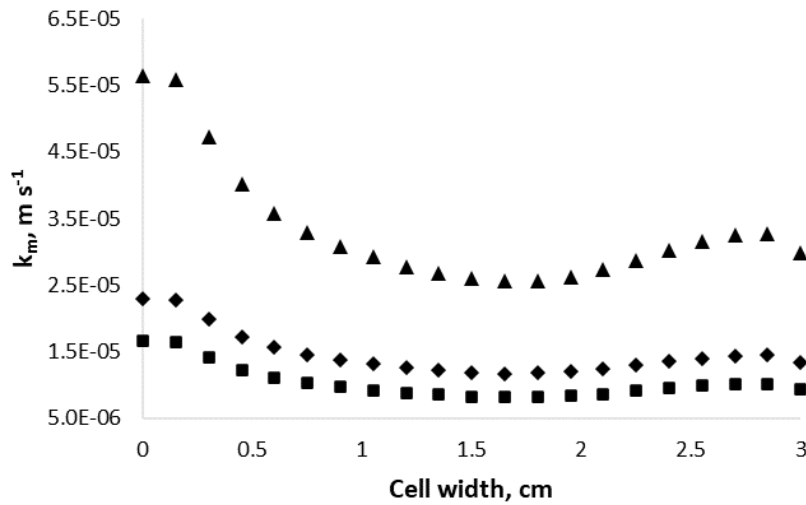


Figure 7.5 - Computed local k_m values for a mean linear flow velocity of $0.0231 m s^{-1}$, at 5 cm from the channel entrance; Triangle: correlation from [80]; Diamond: correlation from [86]; Square: correlation from [71]

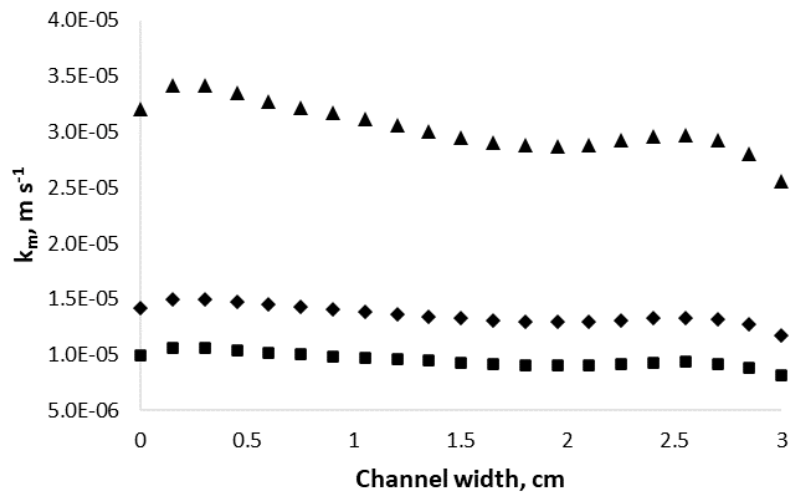


Figure 7.6 - Computed local k_m values for a mean linear flow velocity of $0.0231 m s^{-1}$, at 8 cm from the channel entrance; Triangle: correlation from [80]; Diamond: correlation from [86]; Square: correlation from [71]

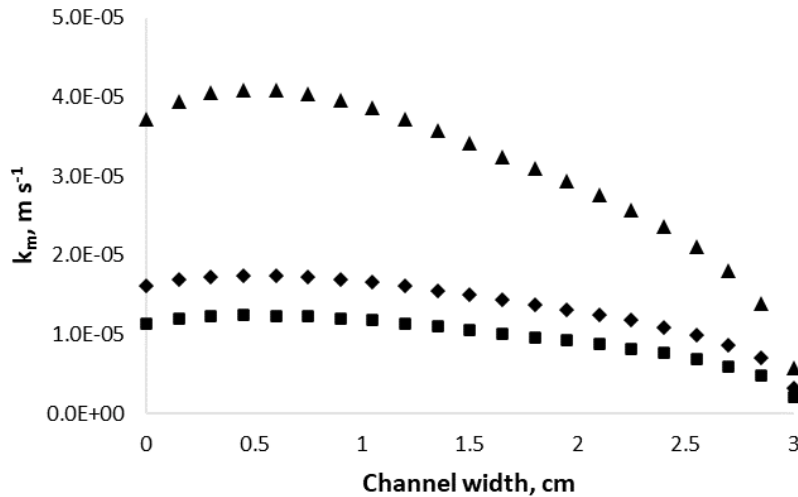


Figure 7.7 - Computed local k_m values for a mean linear flow velocity of 0.0231 m s^{-1} , at 11 cm from the channel entrance; Triangle: correlation from [80]; Diamond: correlation from [86]; Square: correlation from [71]

To better understand the hydrodynamic behavior of this reactor, which is atypical in CFD studies reported in the literature, it is worth making a comparison with the much more used reactor, the FM01-LC.

The mass transfer correlations for the reactor employed in this work, as well as other correlation for different types of reactors are shown in Figure 7.8. The differences are associated with the exact dimensions of the channels and the different configuration of the inlet and outlet. As already discussed, higher values of Sh at the same Re for the reactor used in this work are probably due to higher average velocities achieved because of the stricter and shorter channel.

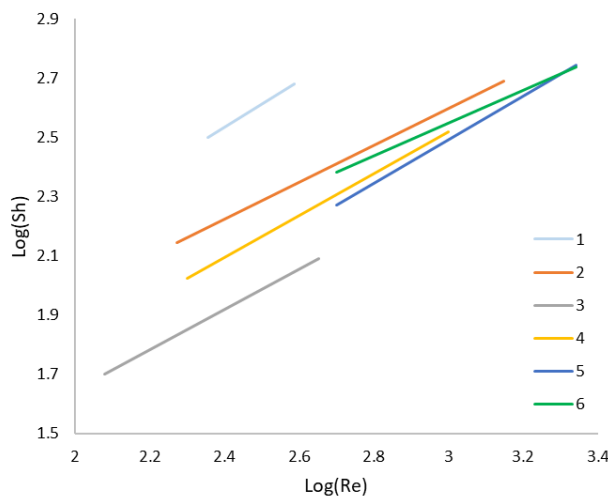


Figure 7.8 - Comparison of Sh calculated from the reactor of this work and other reactors (Reactors details in table 7.1)

As previously reported, the constant a is characteristic of the design geometry, whereas b reflects the fluid flow influence. The addition of the turbulence promoters provides an increase

of the coefficient and a decrease of coefficient b , reflecting the decrease of the fluid flow influence in the mass transport and a higher relevance of inlet/outlet configuration. These observations can be seen in the table 7.1.

Table 7.1 - Value of constant a and b for $Sh = a Re^b Sc^{0.33}$ correlation and geometrical characteristics for different type of reactors

Reactor	#	S [cm]	L cell [cm]	L electrodes [cm]	a	b	Re range	Ref.
In-house filter press cell	1	1.1	16	16	0.39	0.79	227-386	[80]
FM01-LC	2	1.95	22	16	0.49	0.62	187-1407	[86]
FM01-LC	3	0.55	22	16	0.17	0.68	120-450	[92]
FM01-LC	4	0.55	22	16	0.22	0.71	200-1000	[71]
FM01-LC	5	0.55	22	16	0.18	0.73	500-2200	[91]
FM01-LC with mesh turbulence promoter	6	0.55	22	16	0.71	0.55	500-2200	[91]

Moreover, Rivero et al ^[86] associated to the larger gap (1.95 cm) the different values of b for the reactor 2, if compared with the other type of FM01-LC correlations. They stated that a lower value of b corresponds to higher flow instabilities, due to the larger available area allowing for more flow fluctuations originating instability.

Similarly, a higher value of b for the reactor 1 employed in this work suggests that the flow is stabler respect to the FM01-LC, probably due to the absence of inlet/outlet distributors.

However, correlations for Sh obtained for a particular cell cannot be valid for another cell with different interelectrode gap or length, or different manifold configurations ^[86].

Nevertheless, in the case of a reaction controlled by mass transport the local velocity profile certainly affects the effectiveness of the process. Velocity profiles are influenced by the geometric dimension of the channel, as well as the presence of inlet and outlet distributors.

Rivero et al. already demonstrated that velocity profiles are deeply affected by inlet and outlet manifolds. They compared the classical FM01-LC with manifolds with another one having only the body of the FM01-LC. In the ideal case (no manifolds), the maximum velocity differences between the profiles at 0.04 and 0.12 m from the entrance were scarce, thus leading to constant mass transfer flux throughout the entire channel.

This means that jet streams generated by the fluid manifold at the inlet have a significant effect on mass transfer velocity, not only in the reactor at the entrance and the outlet of the cell, but also within the entire reactor volume. The presence of manifolds is typical of FM01-LC reactors.

Moreover, in the table 7.2 is shown the higher k_m coefficient achieved in the case of FM01-LC reactor, if compared with other filter-press reactor.

Table 7.2 - Comparison of mass transport coefficient for different filter-press type flow reactors at a mean linear flow velocity of 5 cm s^{-1} for ferricyanide ion reduction with an electrolyte kinematic viscosity, $\nu=0.1\text{ cm}^2\text{ s}^{-1}$ and an approximate diffusion coefficient, $D=6\text{ E}10^{-6}\text{ cm}^2\text{ s}^{-1}$

Reactor	Mass transfer coefficient, $k_m/10^{-5} \text{ m s}^{-1}$	Ref
FM01-LC	4.3	[86]
Diacell	2	[83]
ElectroSyn	3.1	[93]

The reactor used in this work, as already mentioned, is among the few without the inlet distributors, differently from the more used FM01-LC. Due to these reasons, it was decided to optimize the configuration of the reactor by adding inlet and outlet fluid distributors.

Hence, the distributors used were very similar to those employed in the FM01-LC reactors. They consist of 5 rectangular ducts, placed immediately after the reactor entrance. The geometric characteristics of the ducts are shown in the table 7.3. To have a direct comparison between the two configurations, it was decided to maintain the same electrode area and width of the channel, therefore reaching the characteristics of the reactor listed in the table 7.3.

Table 7.3 – Geometrical characteristics of the reactor with manifolds

Channel length, L	16.4 cm
Channel width, B	3 cm
Electrode spacing, S	1.1 cm
Electrode length, L	11.3 cm
A_{inlet}	0.975 cm^2
Cross section of manifold ducts	
Wide of ducts, p	0.28 cm
Height of ducts, r	0.9 cm

The manifolds were designed according to the study of Rivero et al. [86]. However, in this case, since the channel width, as well as the spacing between the electrodes were lower, the manifolds measures were also slightly remodulated. The distributors were designed in order to obtain 5 rectangular ducts, having the same spacing between them, as can be seen in the figure 7.9.

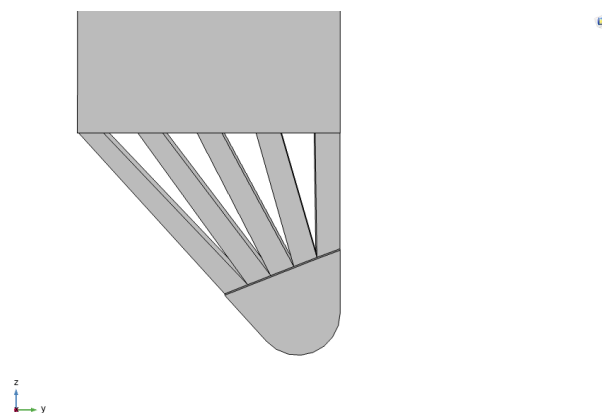


Figure 7.9 – View of the inlet distributor

The domain obtained is shown in the figure. As in the previous case, several meshes were evaluated in order to obtain the one being the best compromise between reliability of the results and computational cost. In this case the mesh was made of 386341 of elements. the computation time was 46.1 min.

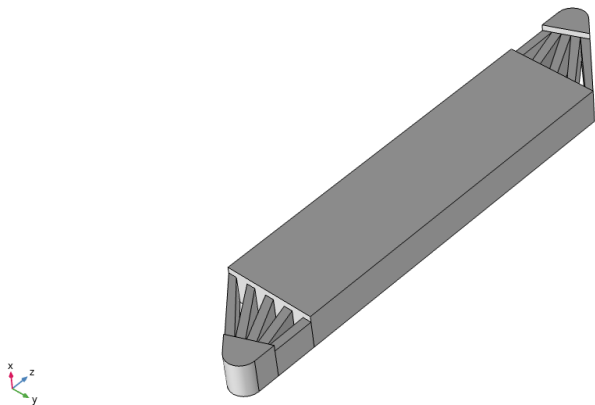


Figure 7.10 - Final 3D computational domain considered inside electrochemical flowcell with manifolds

The velocity profiles were studied at the same lines studied for the reactor without distributors (Figures 7.11-7.13). The results are very similar to the study by Rivero et al. [86]. Nevertheless, probably due to a different geometric configuration of the inlet area, the flow is slightly asymmetrical. However, in general it is possible to observe an average velocity profile which is higher than that obtained without the presence of manifolds. At no point along the channel width there are velocity values lower than the profiles obtained without distributors.

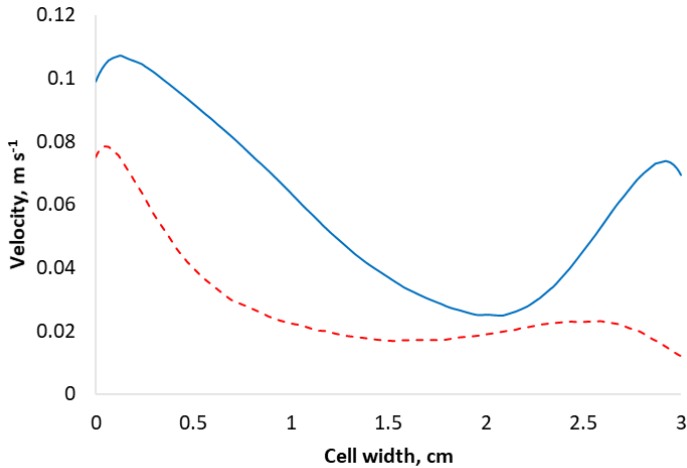


Figure 7.11 - Simulated velocity profiles at the distance of 0.55 cm from electrodes and 5 cm from flowcell inlet for flow rate of 0.53 L min⁻¹; Dotted red line: reactor without distributors; Blue line: reactor with distributors

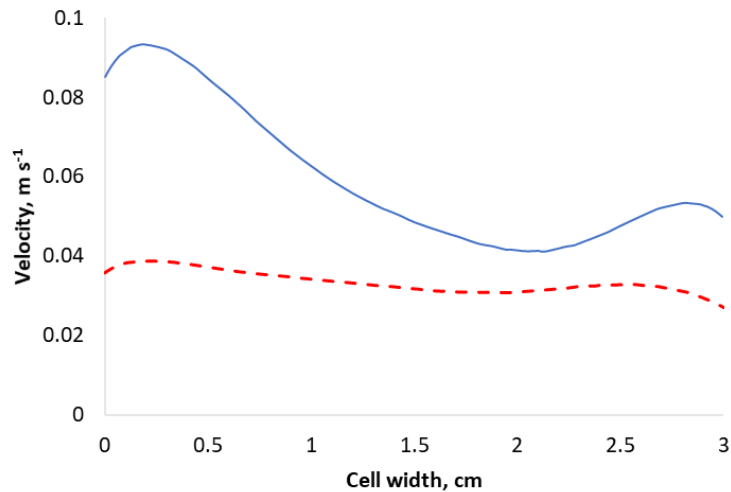


Figure 7.12 - Simulated velocity profiles at the distance of 0.55 cm from electrodes and 8 cm from flowcell inlet for flow rate of 0.53 L min^{-1} ; Dotted red line: reactor without distributors; Blue line: reactor with distributors

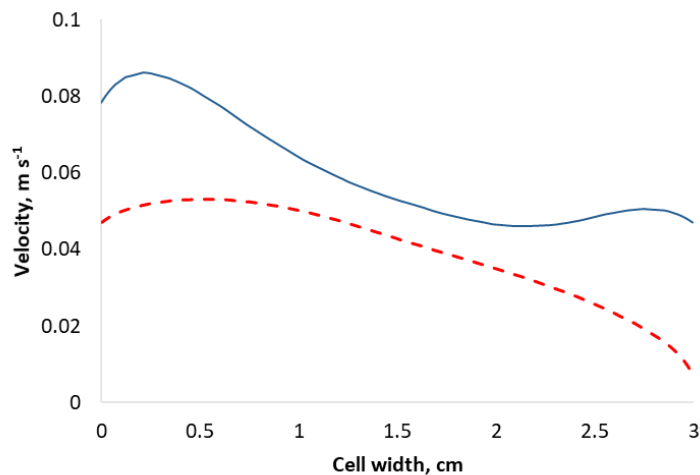


Figure 7.13 - Simulated velocity profiles at the distance of 0.55 cm from electrodes and 11 cm from flowcell inlet for flow rate of 0.53 L min^{-1} ; Dotted red line: reactor without distributors; Blue line: reactor with distributors

As expected, at the same inlet velocity, the velocity profiles are on average higher when using distributors. This definitely affects the mass transport in the reactor, as already reported in the comparison of Rivero et al., and in k_m literature data, as seen in Table 7.2.

However, due to the lack of works and the absence of experimental data from this new configuration, unfortunately it was not possible to quantify the changes in k_m values.

7.2 Current and potential distribution results

Regarding the current and potential distribution, the figure 7.14 shows a cross-sectional graph of the primary potential distribution inside the cell, perfectly coincident with the potential distribution in the work of Perez et al. [90]. From the analysis of this figure, it can be seen that the potential distribution within the cell is in accordance with the boundary conditions employed (Eq. 6.10-6.11). The primary current density along the BDD surface (at $z = 0$) was determined from the gradient of local potential, following Ohm's Law, Eq. (5.3), with the corresponding electrolytic conductivity.

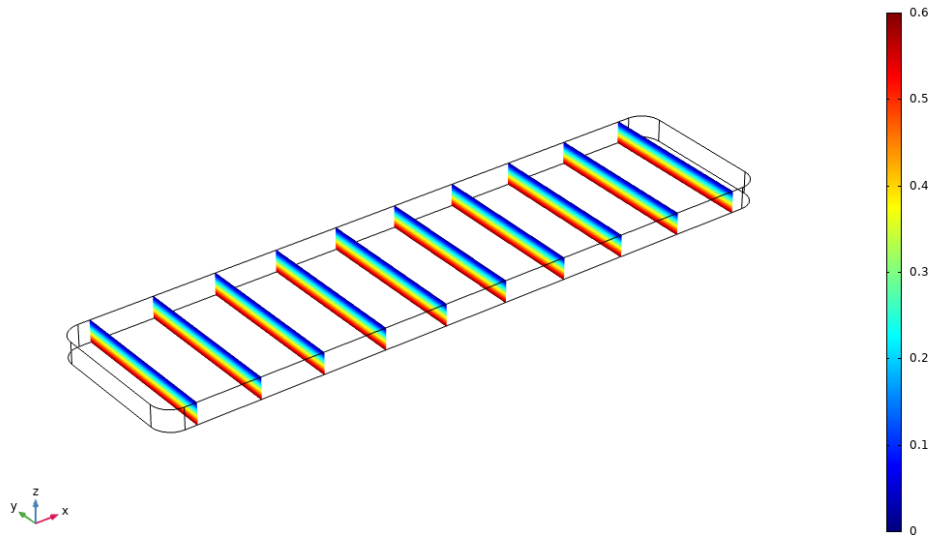


Figure 7.14 - Cross-sectional graph of the primary potential distribution inside the channel

Primary current analysis demonstrated that dimensionless current distribution j_x/j_{ave} is influenced from the curved corners, as can be seen in figure 7.15. The minimum value of j_x/j_{ave} obtained from the simulations differed from the value obtained in the reference work; however, the behaviour observed was the same. In this work, this value stands at 0.98, thus at maximum current values deviate of 0.2 % from j_{ave} , and this occurs only at the corners. Thus, primary current distribution at BDD anode (at $z = 0$) in the channel can be considered uniform, since border effects originated by the curved corners can be neglected.

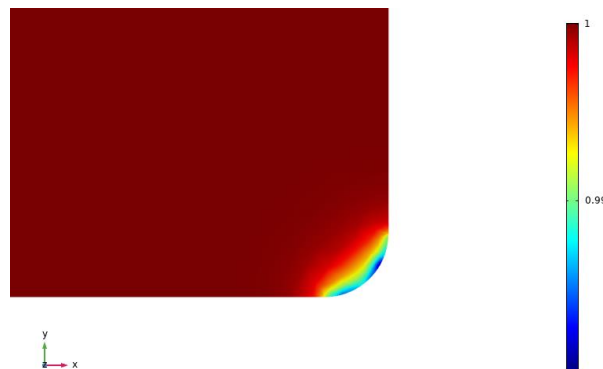


Figure 7.15 - Detail of dimensionless current distribution at the working electrode

The simulation of the secondary current distribution was performed at different cell potential, from 0.6 V to 3 V in order to reach potential interval including $2.3 < E < 2.75$ V, where the hydroxyl radical formation occurs. The normalized current density distributions were studied at two different heights, as shown in figure 7.16.

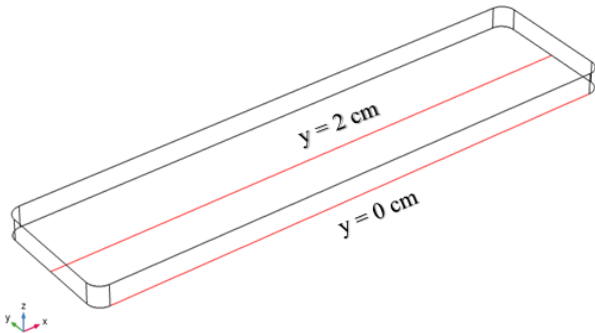


Figure 7.16 Scheme in the domain of the working electrode (BDD); The heights to establish the current distribution profiles are represented by the red lines

Secondary current distribution is shown in Fig. 7.17 and 7.18 at overpotential value of 1.7 V.

It is important to mention that the curves in Fig. 7.17 are located at the curved corners of the working electrode at $y = 0$ cm, where the length is smaller than the rest of the electrode (16 cm). Therefore, these curves do not encounter the borders of $x/L = 0$ and $x/L = 1$. Contrarily the curves depicted on figure 7.18 are located at $y = 2$ cm, considering the complete normalized electrode length.

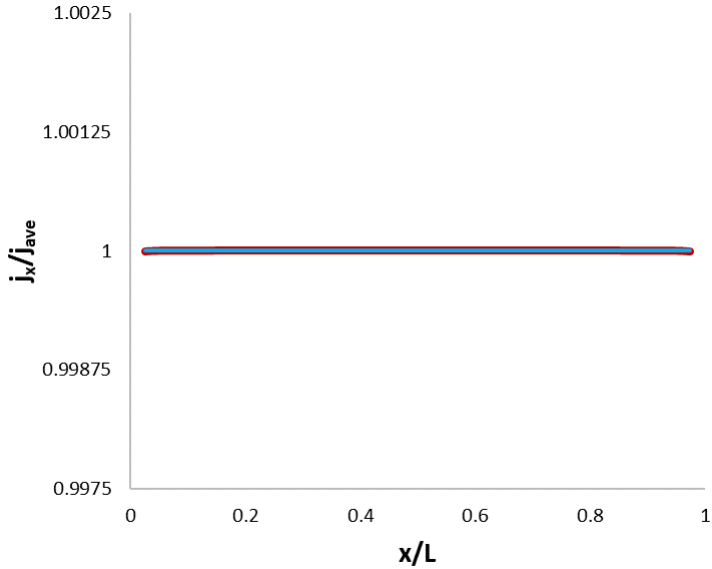


Figure 7.17 - Normalized secondary current distribution profiles along the BDD working electrode at $\eta = 1.7$ V at $y = 0$ cm; Blue line: work of Perez et al. [90]; Red line: Present work

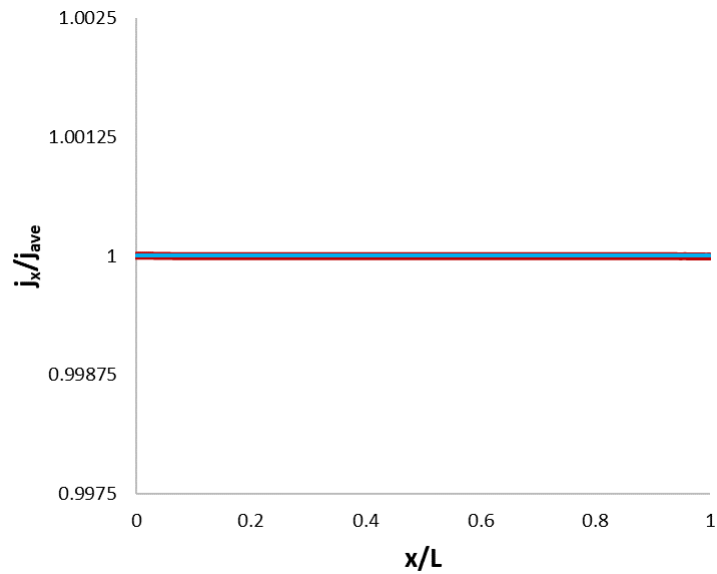


Figure 7.18 - Normalized secondary current distribution profiles along the BDD working electrode at $\eta = 1.7$ V at $y = 2$ cm; Blue line: work of Perez et al. [90]; Red line: Present work

The results obtained were in complete accordance with that of the paper of Perez et al. [90]. Moreover, it is clearly observed that at every height current distribution does not present border effects at the corners, contrarily to primary current distribution.

After verifying the uniformity of the current distribution, the relationship between voltage and current was studied, in the potentials range applied during the microelectrolysis test by the work of Perez et al. and considering the same electric conductivity of 35 S m^{-1} . The similarity between the I-E curves was ascertained, as can be seen from the figure 7.19.

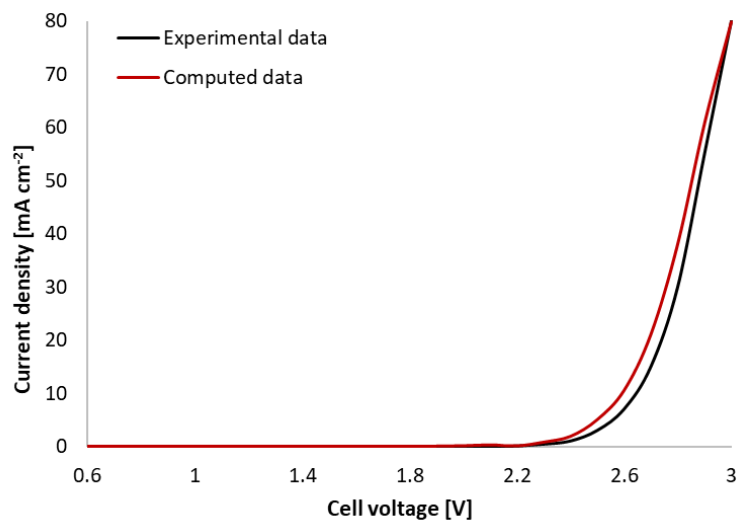


Figure 7.19 - Polarization plot - Comparison between experimental data from Perez et al [90] and computed results, $k = 35 \text{ S m}^{-1}$

Subsequently, several simulations were carried out in the reactor of the case study. Only the channel (not including the distributors) was simulated, as can be seen in figure 7.20.

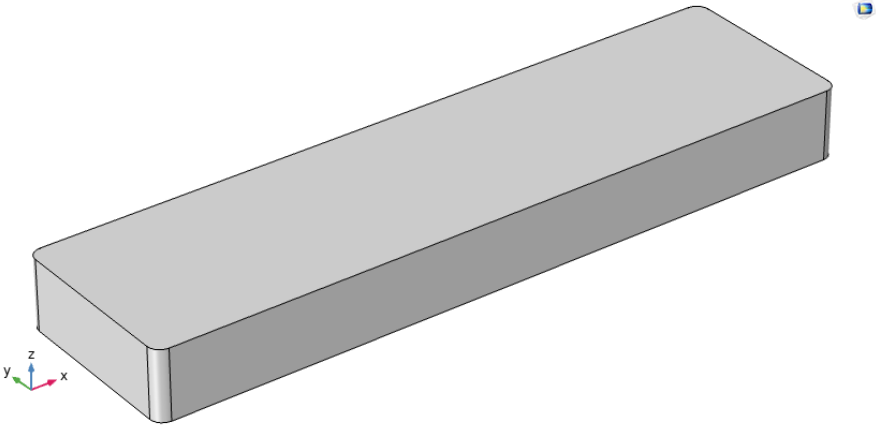


Figure 7.20 - Domain considered for simulations

The geometrical characteristics of the channel are listed in the table below (7.4).

Table 7.4 – Geometrical measures of the reactor

Electrode length, L	11.3 cm
Electrode width, B	3 cm
Electrode spacing, S	1.1 cm

At first a study was performed on the variation of the cell potential. The result is visible in the figure 7.21.

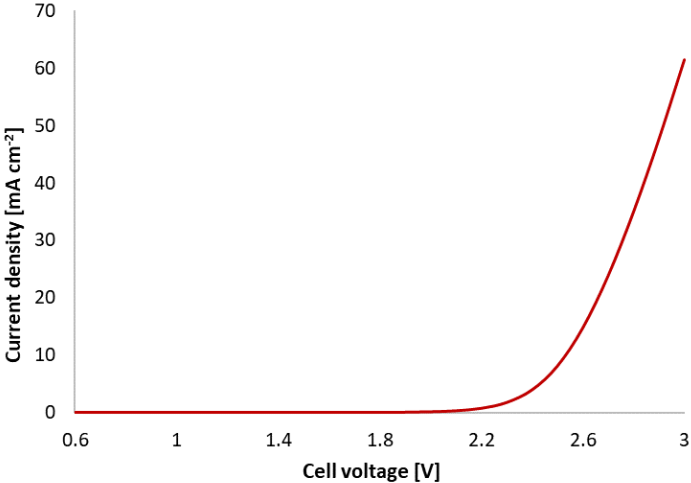


Figure 7.21 - Polarization plot - Computed results, $k = 35 \text{ S m}^{-1}$

The range at which various studies in the literature have operated for the FM01-LC reactor corresponds to current density range between 5 and 20 mA cm⁻² [94]. At that conditions, potential between 2.3 and 2.75 V were reached. At these potential values, the formation of hydroxyl radicals takes place, whereas at higher voltages, oxygen evolution reaction occurs. Considering the reactor studied, it can be seen (Fig. 7.22) that at the same conductivity of the work of Perez et al. ($k = 35 \text{ S m}^{-1}$), the potentials reached are in that range, which indicates that the reactor is effective in the formation of radicals to those current density.

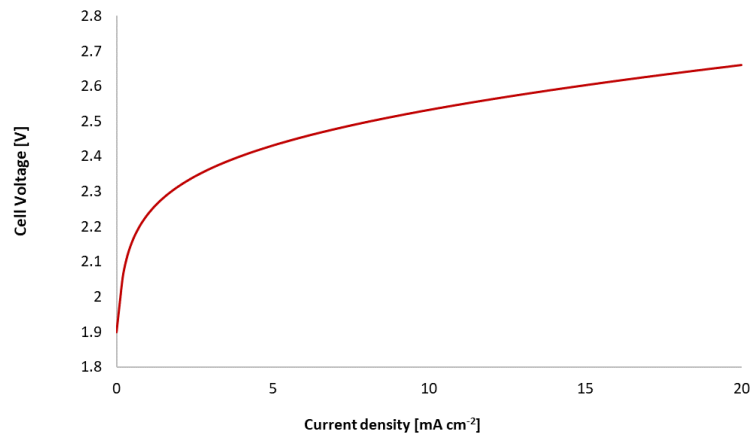


Figure 7.22 – Polarization plot at $k = 35 \text{ S m}^{-1}$

However, the purpose of this work is the study of the drinking water disinfection, therefore lower conductivities was studied.

At first, the trend of the I-E curve was studied for decreasing conductivities. The conductivity values used were 10, 20 and 35 S m⁻¹. The results are visible in the following figure (7.23).

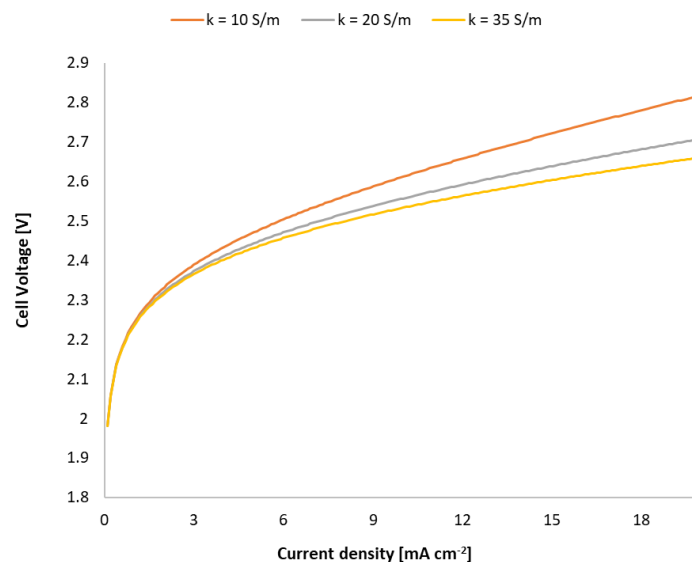


Figure 7.23 – Comparison of polarization plot at different conductivity values

As the conductivity decreases, ohmic losses in the solution increase, leading to potential increases that could lead to oxygen evolution. Furthermore, this would add further costs.

To solve these problems the spacing between the electrodes may be reduced to decrease the ohmic losses. Three different configurations were therefore considered. The spacing between the electrodes of the reactor considered so far is 1.1 cm. Two further configurations were added, $S = 0.55$ cm and $S = 0.4$ cm, (Table 7.5) in agreement with the values found in the literature for this type of cells.

Table 7.5 – Configurations of the reactor used for simulations at $k = 0.1$ S m⁻¹

Reactor	Electrode spacing, S
1	1.1 cm
2	0.55 cm
3	0.4 cm

At this point, the trend of the I-E relationship with the maximum permissible conductivity in the case of drinking water treatments was studied, considering the specifications of the companies that would like to build these plants. The maximum conductivity allowed, $S = 0.1$ S m⁻¹, corresponds to a much lower value than those found in the literature for wastewater treatments. It was studied the trend of the voltage to vary the current. The results are visible in the figure 7.24.

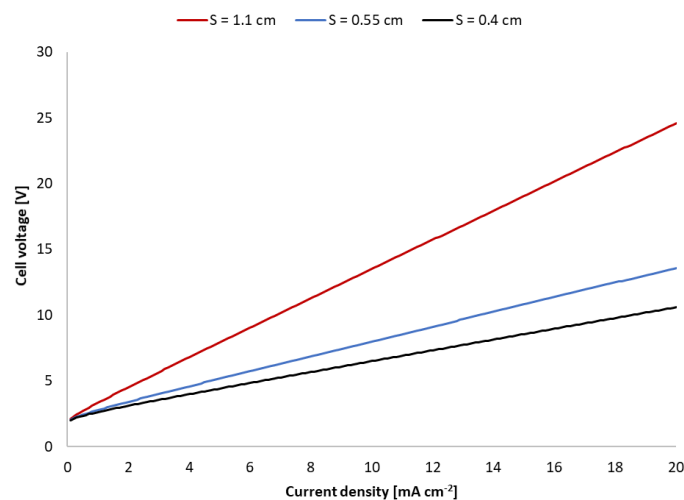


Figure 7.24 – Comparison of polarization plot for different electrode spacing, $k = 0.1$ S m⁻¹

As expected, in this case the potential values are much higher than the previously considered values in the presence of supporting electrolyte. The potential values reached are beyond the oxygen evolution potentials. Moreover, the higher amount of ohmic losses due to the low conductivity would increase the energetic consumption.

In order to have a direct measure of the differences between the cases, the specific energy consumption related to the treatment of 0.5 L of water in 6 h was considered, by referring to the case study initially considered. At first the study was carried out on the basic configuration ($S = 1.1$ cm and $k = 35$ S m⁻¹), then other configurations were studied.

Three different types of reactors with decreasing spacing between electrodes were considered (Table 7.5). The minimum spacing required for this type of cells was chosen in accordance to literature values. For values lower than 0.4 cm the pumping costs would be too large. Different conductivities values were evaluated for each configuration. The first three values, $k = 35$ S m⁻¹, $k = 20$ S m⁻¹, $k = 10$ S m⁻¹, are compatible with the values found in the literature for wastewaters treatment. These values are obtained by adding a support electrolyte, which in the case of wastewater treatment, if chosen appropriately, can be used. The conductivity value of 0.1 S m⁻¹ was then considered, the maximum permissible conductivity value in the water to be treated, indicated by the companies involved in the design of these plants. A single current density value, 10 mA cm⁻², was considered in accordance with scientific papers in which BDD electrodes were used. At this current value, the formation of the hydroxyl radicals involved in the degradation processes should take place. For each case, the corresponding voltage and finally the energy consumption were evaluated. The results are listed in the table 7.6.

Table 7.6 - Comparison of energy consumption of the 3 reactor configurations at different conductivity values, at 10 mA cm⁻²

Electrode spacing [cm]	Conductivity [S m ⁻¹]	Cell voltage [V]	Energy consumption [kWh m ⁻³]
1.1	35	2.53	8.61
	20	2.56	8.69
	10	2.61	8.88
	0.1	13.50	45.91
0.55	35	2.52	8.56
	20	2.53	8.60
	10	2.56	8.69
	0.1	8.00	27.21
0.4	35	2.51	8.54
	20	2.52	8.57
	10	2.54	8.64
	0.1	6.50	22.11

For high conductivity values, when the spacing decreases, there are slight variations in energy consumption. Voltage decrease occurs, leading to lower consumptions, but the variations are scarce. This suggests that, when using supporting electrolytes, the spacing between the electrodes does not have a great influence in the process. In the case at $k = 0.1$ S m⁻¹ and $S = 1.1$ cm, the energy consumption is more than quadruple of the cases with higher conductivities. By decreasing the spacing there is a considerable decrease, however the consumption remains at values much higher than twice respect to the ideal case. The percentage changes in energy consumption are resumed in the following table (7.7), when passing from 1.1 cm to 0.4 cm. It can be seen that the higher the conductivity, the lower energy consumption is affected by the decrease in electrode spacing.

Table 7.7 - Comparison of % change in energy consumption at different conductivity values, 10 mA cm⁻², from S = 1.1 cm to S = 0.4 cm

Conductivity [S m ⁻¹]	Energy consumption [kWh m ⁻³]		% Change
	S = 1.1 cm	S = 0.4 cm	
35	8.61	8.54	0.81
20	8.69	8.57	1.38
10	8.88	8.64	2.7
0.1	45.91	22.11	51.8

Although the larger percentage decrease (51.8 %), it is clear that energy consumption at $k = 0.1$ S m⁻¹ remains too high, if compared with the cases in which supporting electrolytes are used.

Since in the case of flowcells the spacing cannot be further reduced, alternatives should be found to reduce the too high costs that the use of these technologies would require when using water having very low conductivities.

8. Conclusions and future developments

The main objective of this work was to provide a first approach to the design of an electrochemical reactor for water disinfection by using CFD techniques.

The various reactor configurations used in this context were shown. The flowcell configuration was found to be the most employed, because of the better mass transport respect to the classical mixed tanks. Other innovative designs were presented, which may contribute in the future to solve the problems related to these technologies. One of the major drawbacks in this technology is the use of supporting electrolytes, which leads to lower energy consumption but could produce secondary pollution in water intended for potabilization.

Most of the works found in literature used lab-scale reactors, due to the fact that this technology is still relatively immature. Consequently, it was decided to study the physical aspects of a single cell at lab-scale, which could provide a basis for a future scale-up.

The different CFD models found in literature were described. In this context it is evident the lack of studies regarding the modeling of electrochemical reactors designed for water disinfection. However, a first characterization of a reactor was carried out.

The hydrodynamics studied by means of the RANS equations, coupled to the $k-\varepsilon$ turbulence models, gave results in agreement with the data obtained in the literature. If the process is controlled by mass transfer, improvements in hydrodynamics can lead to higher average velocity profiles within the single cell and therefore better mass transport. Hence, inlet and outlet distributors were found to be useful in providing a better hydrodynamic profile and mass transport.

Regarding the electrochemical aspects, a numerical simulation of primary and secondary current distribution was performed along the working electrode. Primary current distribution analysis demonstrated that current distribution is more uniform away from the curved corners originated by the spacer between electrodes; however, j_x/j_{ave} value was 0.98 at the corners, thus at maximum current values deviated of 0.2 % from j_{ave} . Therefore, the primary current distribution at the anode in the reactor studied can be considered uniform, since border effects at the curved corners of the cell can be neglected. Secondary current distribution at different overpotential values did not show border effects anywhere, hence confirming the convenience of using the cell due to its uniform current distribution at the anode surface, avoiding paraxite reactions.

However, it is important to mention that during electrochemical incineration of organics, when limiting current density is determined by the concentration of organics, tertiary current distribution should be studied. The present analysis should be useful as a starting point in which tertiary current distribution may be incorporated in the future.

From the trend of the I-E curves evaluated at different electrical conductivities and electrode spacings, energy consumption was calculated. For high conductivity values, when the spacing decreases from $S = 1.1$ cm to $S = 0.4$ cm, limited variations in energy consumption were observed, thus the spacing between the electrodes did not largely affect the process (at maximum 2.7% at $k = 10$ S m^{-1}). In the case at $k = 0.1$ S m^{-1} and $S = 1.1$ cm, thus considering the maximum conductivity allowed in the treatment of water intended for potabilization, the energy consumption is more than quadruple respect to all the cases with higher conductivities.

By decreasing the spacing there is a considerable decrease, however the consumption remains at values much higher than twice respect to the ideal case. Since in the case of flowcells the spacing cannot be further reduced, alternatives should be found to reduce too high costs that the use of these technologies would require when using water having very low conductivities.

Therefore, the use of these reactors seems to be very effective in wastewaters disinfection, since there is the possibility of using adequate support electrolytes and drastically lower energy costs, if compared to treatments of water intended for potabilization. Further technologies could be studied more deeply, such as the use of microfluidic reactors, which allow to operate without supporting electrolytes, avoiding secondary pollution. However, this technology is still immature.

In conclusion, this work is the starting point for the practical construction of an electrochemical reactor for water disinfection, as it included the main physics involved in the modeling of such reactors. Models for mass transport coefficient calculation, as well as tertiary current distribution modules, which also take into account concentration changes related to the degradation of organics, are other aspects to be added in the modeling, in order to provide more precise predictions.

9. Bibliography

- [1] WWAP, United Nations World Water Assessment Programme, 2009, The United Nations World Water Development Report 3: Water in a Changing World, Paris: UNESCO and London: Earthscan. Last access: 24/07/2017. Available online at <http://unesdoc.unesco.org/images/0018/001819/181993e.pdf>.
- [2] A/RES/64/292. The Human Right to Water and Sanitation, 2010, Resolution 64/292 adopted by the General Assembly on 28 July 2010. Last access 09/05/2017. Available online at <http://www.un.org/es/comun/docs/?symbol=A/RES/64/292&lang=E>.
- [3] WHO/UNICEF, 2017, Progress on Drinking Water, Sanitation and Hygiene: Update and SDB Baselines. Joint Monitoring Program, [ISBN 978-92-4-151289-3].
- [4] Gazzetta ufficiale della Repubblica italiana, Decreto legislativo 2/02/2001, n.31, available online at <https://www.gazzettaufficiale.it/eli/id/2001/03/03/001G0074/sg>.
- [5] Ministero della salute, Trattamenti e potabilizzazione delle risorse idriche, available online at http://www.salute.gov.it/portale/temi/p26.jsp?lingua=italiano&id=4235=acque_potabili&menu=acque.
- [6] EUR-lex, Directive (EU) 2020/2184 of the European Parliament and of the Council of 16 December 2020 on the quality of water intended for human consumption, available online at <https://eur-lex.europa.eu/eli/dir/2020/2184/oj>.
- [7] Ministero della salute, Utilizzo delle risorse pubbliche per uso potabile, available online at http://www.salute.gov.it/portale/temi/p2_6.jsp?lingua=italiano&id=4235&area=acque_potabili&menu=acque.
- [8] Ministero della salute, Qualità delle risorse idriche per uso potabile, available online at http://www.salute.gov.it/portale/temi/p2_6.jsp?lingua=italiano&id=4263&area=acque_potabili&menu=acque.
- [9] Falkenmark M., Berntell A., Jagerskog A., Lundqvist J., Matz M., Tropp H., 2007, On the Verge of a New Water Scarcity: A Call for Good Governance and Human Ingenuity, SIWI Policy Brief, SIWI, Sundbyberg, Sweden.
- [10] Palmas S., Mascia M., Vacca A., Mais L., Corgiolu S., Petrucci, E., 2018, Practical Aspects on Electrochemical Disinfection of Urban and Domestic Wastewater, in “Electrochemical Water and Wastewater Treatment”, (E. Carlos Alberto Martínez-Huitle, Manuel Andrés Rodrigo, Onofrio Scialdone, Butterworth-Heinemann), Chap. 16, pp 421-447. [ISBN 9780128131602].
- [11] Rodriguez C., Van Buynder P., Lugg R., Blair P., Devine B., Cook A., Weinstein, P., 2009, Indirect Potable Reuse: A Sustainable Water Supply Alternative, *International Journal of Environmental Research and Public Health*, **6**(3), 1174–1203.
- [12] Asano T., Burton F.L., Leverenz H.L., Tsuchihashi R., Tchobanoglous G., 2007, *Water Reuse– Issues, Technologies and Applications*, McGraw-Hill, New York, USA.
- [13] Gerba C. P., Pepper I. L., 2019, *Drinking Water Treatment. Environmental and Pollution Science*, 435–454.
- [14] Craun G.F., 1993, *Safety of water disinfection: balancing chemical and microbial risks*, International Life Sciences Inst., Washington, DC (USA).
- [15] Miklos D. B., Remy C., Jekel M., Linden K. G., Drewes, J. E., Hübner U., 2018, Evaluation of advanced oxidation processes for water and wastewater treatment – A critical review. *Water Research*, **139**, 118–131.

- [16] Alexander Kraft, 2008, Electrochemical Water Disinfection: A Short Review *Platinum Metals Rev.*, **52**, (3), 177
- [17] Ganiyu S. O., Martínez-Huitle C. A., Rodrigo M. A., 2020, Renewable energies driven electrochemical wastewater/soil decontamination technologies: A critical review of fundamental concepts and applications. *Applied Catalysis B: Environmental*, **270**, 118857.
- [18] Ganiyu S. O., Martínez-Huitle C. A., 2020, The use of renewable energies driving electrochemical technologies for environmental applications, *Current Opinion in Electrochemistry*, **22**, 211-220.
- [19] Martínez-Huitle C. A., Rodrigo M. A., Sirés I., Scialdone O., 2015, Single and Coupled Electrochemical Processes and Reactors for the Abatement of Organic Water Pollutants: A Critical Review. *Chemical Reviews*, **115**(24), 13362–13407.
- [20] Anglada A., Urtiaga A., Ortiz I., 2009, Contributions of electrochemical oxidation to waste-water treatment: fundamentals and review of applications, *Journal of Chemical Technology & Biotechnology*, **84**(12), 1747–1755.
- [21] Marselli B., Garcia-Gomez J., Michaud P.-A., Rodrigo M. A., Comninellis C., 2003, Electrogeneration of Hydroxyl Radicals on Boron-Doped Diamond Electrodes, *Journal of The Electrochemical Society*, **150**(3), D79.
- [22] Martínez-Huitle C. A., Andrade L. S., 2011, Electrocatalysis in Wastewater Treatment: Recent Mechanism Advances, *Quim. Nova*, **34**, 850–858.
- [23] Comninellis C., 1994, Electrocatalysis in the Electrochemical Conversion/Combustion of Organic Pollutants for Waste Water Treatment, *Electrochim. Acta*, **39**, 1857–1862.
- [24] Pletcher D., Walsh F. C., 1982, *Industrial Electrochemistry*, Chapman and Hall: London.
- [25] Martínez-Huitle C. A., Panizza M., 2011, Chapter 5 in “*Applied Electrochemistry*”, Singh V. G., Ed.; Nova Sci, New York.
- [26] Li X., Pletcher D., Walsh F. C., 2011, Electrodeposited Lead Dioxide Coatings, *Chemical Societ Reviews*, **40**, 3879–3894.
- [27] Yu X., Zhou M, Hu Y, Groenen-Serrano K., Yu F., 2014, Recent Updates on Electrochemical Degradation of Bio-Refractory Organic Pollutants Using BDD Anode: a Mini Review, *Environ. Sci. Pollut. Res.*, **21**, 8417–8431.
- [28] Alfaro M. A. Q., Ferro S., Martínez-Huitle C. A., Vong Y. M., 2006, Boron Doped Diamond Electrode for the Wastewater Treatment, *Journal of the Brazilian Chemical Society*, **17**, 227–236.
- [29] Panizza, M., Cerisola G., 2005, Application of Diamond Electrodes to Electrochemical Processes, *Electrochimica Acta*, **51**, 191–199.
- [30] Martínez-Huitle C. A., Quiroz, M. A., Comninellis C., Ferro S., De Battisti A., 2004, Electrochemical Incineration of Chloranilic Acid Using Ti/IrO₂, Pb/PbO₂ and Si/BDD Electrodes, *Electrochimica Acta*, **50**, 949–956.
- [31] Gherardini L., Michaud P. A., Panizza M., Comninellis C., Vatisas N., 2001, Electrochemical Oxidation of 4-Chlorophenol for Wastewater Treatment: Definition of Normalized Current Efficiency, *Journal of the Electrochemical Society*, **148**, D78–D82.
- [32] Panizza M., Cerisola G., 2004, Influence of Anode Material on the Electrochemical Oxidation of 2-Naphthol: Part 2. Bulk Electrolysis Experiments. *Electrochimica Acta*, **49**, 3221–3226.

- [33] Cañizares P., Díaz M., Domínguez J. A., Lobato J., Rodrigo M. A., 2005, Electrochemical Treatment of Diluted Cyanide Aqueous Wastes, *Journal of Chemical Technology & Biotechnology*, **80**, 565–573.
- [34] Weiss E., Groenen-Serrano K., Savall A., 2006, Electrochemical Degradation of Sodium Dodecylbenzene Sulfonate on Boron Doped Diamond and Lead Dioxide Anodes, *Journal of New Materials for Electrochemical Systems*, **9**, 249–256.
- [35] Stucki S., Kotz R., Carcer, B., Suter W., 1991, Electrochemical waste water treatment using high overvoltage anodes Part II: Anode performance and applications, *Journal of Applied Electrochemistry*, **21**(2), 99–104.
- [36] Pulgarin C., 1994, Electrochemical detoxification of a 1,4-benzoquinone solution in wastewater treatment, *Water Research*, **28**(4), 887–893.
- [37] Chen X., Gao F., Chen G., 2005, Comparison of Ti/BDD and Ti/SnO₂-Sb₂O₅ electrodes for pollutant oxidation, *Journal of Applied Electrochemistry*, **35**(2), 185–191.
- [38] Tanaka S., Nakata Y., Kimura T., Kawasaki M., Kuramitz H., 2002, Electrochemical decomposition of bisphenol A using Pt/Ti and SnO₂/Ti anodes, *Journal of Applied Electrochemistry*, **32**(2), 197–201.
- [39] Wang B., Kong W., Ma H., 2007, Electrochemical treatment of paper mill wastewater using three-dimensional electrodes with Ti/Co/SnO₂-Sb₂O₅ anode, *Journal of Hazardous Materials*, **146**(1-2), 295–301.
- [40] Hu Z., Cai J., Song G., Tian Y., Zhou M., 2020, Anodic oxidation of organic pollutants: anode fabrication, process hybrid and environmental applications, *Current Opinion in Electrochemistry*, 100659.
- [41] Shao C., Yu J., Li X., Wang X., Zhu K., 2017, Influence of the Pt nanoscale interlayer on stability and electrical property of Ti/Pt/Sb-SnO₂ electrode: A synergetic experimental and computational study, *Journal of Electroanalytical Chemistry*, **804**, 140-147. 426 39.
- [42] Li X., Yan J., Zhu K., 2020, Effects of IrO₂ interlayer on the electrochemical performance of Ti/Sb-SnO₂ electrodes, *Journal of Electroanalytical Chemistry*, **878**, 114471.
- [43] Bejan D., Malcolm J. D., Morrison L., Bunce N. J., 2009, Mechanistic investigation of the conductive ceramic Ebonex® as an anode material, *Electrochimica Acta*, **54**(23), 5548–5556.
- [44] Bejan D., Guinea E., Bunce, N. J., 2012, On the nature of the hydroxyl radicals produced at boron-doped diamond and Ebonex® anodes, *Electrochimica Acta*, **69**, 275–281.
- [45] Zaky A. M., Chaplin B. P., 2013, Porous Substoichiometric TiO₂ Anodes as Reactive Electrochemical Membranes for Water Treatment, *Environmental Science & Technology*, **47**(12), 6554–6563.
- [46] Tennakoon C. L. K., Bhardwaji R. C., Bockris J. O., 1996, Electrochemical treatment of human wastes in a packed bed reactor, *Journal of Applied Electrochemistry*, **26**(1), 18–29.
- [47] Walsh F. C., Wills R. G. A., 2010, The continuing development of Magnéli phase titanium sub-oxides and Ebonex® electrodes, *Electrochimica Acta*, **55**(22), 6342–6351.
- [48] El-Sherif, S., Bejan, D., & Bunce, N. J., 2010, Electrochemical oxidation of sulfide ion in synthetic sour brines using periodic polarity reversal at Ebonex® electrodes, *Canadian Journal of Chemistry*, **88**(9), 928–936.

- [49] Cai J., Zhou M., Xu X., Du X., 2020, Stable boron and cobalt co-doped TiO₂ nanotubes anode for efficient degradation of organic pollutants, *Journal of Hazardous Materials*, 122723.
- [50] Panizza M., Cerisola G., 2009, Direct And Mediated Anodic Oxidation of Organic Pollutants, *Chemical Reviews*, **109**(12), 6541–6569.
- [51] Chaplin B. P., Wyle I., Zeng H., Carlisle J. A., Farrell J., 2011, Characterization of the performance and failure mechanisms of boron-doped ultrananocrystalline diamond electrodes, *Journal of Applied Electrochemistry*, **41**(11), 1329–1340.
- [52] Chaplin B. P., Hubler D. K., Farrell J., 2013, Understanding anodic wear at boron doped diamond film electrodes, *Electrochimica Acta*, **89**, 122–131.
- [53] Chaplin B. P., 2014, Critical review of electrochemical advanced oxidation processes for water treatment applications, *Environ. Sci.: Processes Impacts*, **16**(6), 1182–1203.
- [54] Martínez-Huitle C. A., dos Santos E. V., de Araújo D. M., Panizza M., 2012, Applicability of diamond electrode/anode to the electrochemical treatment of a real textile effluent, *Journal of Electroanalytical Chemistry*, **674**, 103–107.
- [55] Rodrigo M. A., Michaud P. A., Duo I., Panizza M., Cerisola G., Comninellis C., 2001, Oxidation of 4-Chlorophenol at Boron-Doped Diamond Electrode for Wastewater Treatment, *Journal of The Electrochemical Society*, **148**(5), D60.
- [56] Panizza M., Barbucci A., Ricotti R., Cerisola G., 2007, Electrochemical degradation of methylene blue, *Separation and Purification Technology*, **54**(3), 382–387.
- [57] Peralta-Reyes E., Natividad R., Castellanos M., 2020, Electro-oxidation of 2-chlorophenol with BDD electrodes in a continuous flow electrochemical reactor. *Journal of Flow Chemistry*, **10**, 437–447.
- [58] Scialdone O., Guarisco G., Galia A., 2011, Oxidation of Organics in Water in Microfluidic Electrochemical Reactors: Theoretical Model and Experiments, *Electrochimica Acta*, **58**, 463–473. (253).
- [59] Scialdone O., Guarisco G., Galia A., Filardo G., Silvestri G., Amatore C., Sella C., Thouin L., 2010, Anodic Abatement of Organic Pollutants in Water in Micro Reactors, *Journal of Electroanalytical Chemistry*, **638**, 293–296.
- [60] Ammar S., Abdelhedi R., Flox C., Arias C., Brillas E., 2006, Electrochemical Degradation of the Dye Indigo Carmine at Boron Doped Diamond Anode for Wastewaters Remediation., *Environmental Chemistry Letters*, **4**, 229–233.
- [61] Walsh F. C., 2001, Electrochemical technology for environmental treatment and clean energy conversion, *Pure and Applied Chemistry*, **73**(12), 1819–1837.
- [62] Appunti Prof.ssa Stefania Specchia, 2019, Corso di Reattori Chimici ed Elettrochimici, Politecnico di Torino.
- [63] Ochoa-Chavez A. S., Pieczyńska A., Fiszka Borzyszkowska A., Espinoza-Montero P. J., Siedlecka E. M., 2018, Electrochemical degradation of 5-FU using a flow reactor with BDD electrode: Comparison of two electrochemical systems. *Chemosphere*, **201**, 816–825.
- [64] Perry S., Ponce de León C., Walsh F.C., 2020, Review—The Design, Performance and Continuing Development of Electrochemical Reactors for Clean Electrosynthesis, *The Electrochemical Society*, **167**(15).
- [65] Dos Santos E. V., Sena S. F. M., da Silva D. R., Ferro S., De Battisti A., Martínez-Huitle C. A., 2014, Scale-up of electrochemical oxidation system for treatment of produced water generated by Brazilian petrochemical industry, *Environmental Science and Pollution Research*, **21**(14), 8466–8475.

- [66] Pérez J.F., Llanos J., Sáez C., López C., Cañizares P., Rodrigo M.A., 2018, Development of an innovative approach for low-impact wastewater treatment: A microfluidic flow-through electrochemical reactor, *Chemical Engineering Journal*, **351**, 766-772.
- [67] Cañizares P., Larrondo F., Lobato J., Rodrigo M., Saez C., 2005, Electrochemical Synthesis of Peroxodiphosphate Using Boron-Doped Diamond Anodes, *Journal of the Electrochemical Society*, **152**, D191–D196.
- [68] Diamond Abrasives Australia, available online at <https://diamondabrasivesaustralia.com.au/index.php/waste-water-solutions/>
- [69] ElectroCell, Sweden, available online at <https://www.electrocell.com/>.
- [70] Martín de Vidales M. J., Cotillas S., Perez-Serrano J. F., Llanos J., Sáez C., Cañizares P., Rodrigo M. A., 2016, Scale-up of electrolytic and photoelectrolytic processes for water reclaiming: a preliminary study, *Environmental Science and Pollution Research*, **23**(19), 19713–19722.
- [71] Rivera F. F., Ponce de León C., Walsh F. C., Nava J.L., 2015, The reaction environment in a filter-press laboratory reactor: the FM01-LC flow cell, *Electrochimica Acta*, **161**, 436-452.
- [72] Martín de Vidales M. J., Cotillas S., Perez-Serrano J. F., Llanos J., Sáez C., Cañizares P., Rodrigo M. A., 2016, Scale-up of electrolytic and photoelectrolytic processes for water reclaiming: a preliminary study, *Environmental Science and Pollution Research*, **23**(19), 19713–19722.
- [73] Cano A., Barrera C., Cotillas S., Llanos J., Cañizares P., Rodrigo M. A., 2016, Use of DiaCell modules for the electro-disinfection of secondary-treated wastewater with diamond anodes, *Chemical Engineering Journal*, **306**, 433-440.
- [74] Wei L., Guo S., Yan G., Chen C., Jiang X., 2010, Electrochemical pretreatment of heavy oil refinery wastewater using a three-dimensional electrode reactor, *Electrochimica Acta*, **55**(28), 8615–8620.
- [75] Zhou M., Lei L., 2006, The role of activated carbon on the removal of p-nitrophenol in an integrated three-phase electrochemical reactor, *Chemosphere*, **65**(7), 1197–1203.
- [76] Wu X., Yang X., Wu D., Fu R., 2008, Feasibility study of using carbon aerogel as particle electrodes for decoloration of RBRX dye solution in a three-dimensional electrode reactor, *Chemical Engineering Journal*, **138**(1-3), 47–54.
- [77] Xiong Y., He C., An T., Zhu X., Karlsson H. T., 2003, Water, Air, and Soil Pollution, **144**(1/4), 67–79.
- [78] Ma P., Ma H., Sabatino S., Galia A., Scialdon O., 2018, Electrochemical treatment of real wastewater. Part 1: Effluents with low conductivity, *Chemical Engineering Journal*, **336**, 133–140.
- [79] Rivera F. F., Pérez T., Locksley F., Castañeda, Nava J. L., 2021, Mathematical modeling and simulation of electrochemical reactors: A critical review, *Chemical Engineering Science*, **239**, 116622.
- [80] Gharibian S., Hazrati H., Rostamizadeh M., 2020, Continuous electrooxidation of Methylene Blue in filter press electrochemical flowcell: CFD simulation and RTD validation, *Chemical Engineering and Processing - Process Intensification*, **150**, 107880.
- [81] Locksley F., Castañeda, Nava J. L., 2019, Simulations of single-phase flow in an up-flow electrochemical reactor with parallel plate electrodes in a serpentine array, *Journal of Electroanalytical Chemistry*, **832**, 31-39.

- [82] Barrios J.A., Solís-Caballero F.E., Cano A., Durán U., Orozco G., Rivera F.F., 2019, Two-phase hydrodynamic modelling and experimental characterization in an activated sludge electrooxidation flow reactor, *Chemical Engineering Research and Design*, **141**, 339-349.
- [83] Santos J.L.C., Geraldés V., Velizarov S., Crespo J.G., 2010, Characterization of fluid dynamics and mass-transfer in an electrochemical oxidation cell by experimental and CFD studies, *Chemical Engineering Journal*, **157**, 379-392.
- [84] Vázquez L., Alvarez-Gallegos A., Sierra F.Z., Ponce de León C., Walsh F.C., 2010, Simulation of velocity profiles in a laboratory electrolyser using computational fluid dynamics, *Electrochimica Acta*, **55**, 3437-3445.
- [85] Pérez T., Ponce de León C., Walsh F.C., Nava J.L., 2015, Simulation of current distribution along a planar electrode under turbulent flow conditions in a laboratory filter-press flow cell, *Electrochimica Acta*, **154**, 352-360.
- [86] Rivero E.P., Rivera F.F., Cruz-Díaz M.R., Mayen E., González M. R., 2012, Numerical simulation of mass transport in a filter press type electrochemical reactor FM01-LC: Comparison of predicted and experimental mass transfer coefficient, *Chemical Engineering Research and Design*, **90**, 1969-1978.
- [87] Lira-Teco J.E., Rivera F., Farías-Moguel O., Torres-González J., Reyes Y., Antaño-López R., Orozco G., Castañeda-Zaldivar F., 2016, Comparison of experimental and CFD mass transfer coefficient of three commercial turbulence promoters, *Fuel*, **167** 337-346.
- [88] Rivero E. P., Rodríguez F. A., Cruz-Díaz M. R., González I., 2018, Reactive diffusion migration layer and mass transfer wall function to model active chlorine generation in a filter press type electrochemical reactor for organic pollutant degradation, *Chemical Engineering Research and Design*, **138**, 533-545.
- [89] Vázquez L., Alvarez-Gallegos A., Sierra F. Z., Ponce de León C., Walsh F. C., 2013, CFD evaluation of internal manifold effects on mass transport distribution in a laboratory filter-press flow cell, *Journal of Applied Electrochemistry*, **43**, 453–465.
- [90] Pérez T, León M.I., Nava J.L., 2013, Numerical simulation of current distribution along the boron-doped diamond anode of a filter-press-type FM01-LC reactor during the oxidation of water, *Journal of Electroanalytical Chemistry*, **707**.
- [91] Griffiths M., de León C. P., Walsh, F. C., 2005, Mass transport in the rectangular channel of a filter-press electrolyzer (the FM01-LC reactor), *AIChE Journal*, **51**(2).
- [92] Hammond J.K., Robinson D., Walsh F.C., Kreysa G., 1991, Mass transport studies in Filterpress Monopolar (FM-type) electrolyzers (Ed.), *Electrochemical Cell Design and Optimisation Procedures*, *Dechema Monograph*, **123**, VCH, Weinheim, 279.
- [93] Montillet A., Comiti J., Legrand J., 1994, Application of metallic foams in electrochemical reactors of the filter-press type: Part II Mass transfer performance, *Journal of Applied Electrochemistry*, **24**(5).
- [94] Nava J.L., Núñez F., González I., 2007, Electrochemical incineration of p-cresol and o-cresol in the filter-press-type FM01-LC electrochemical cell using BDD electrodes in sulfate media at pH 0, *Electrochimica Acta*, **52**(9), 3229-3235.

10. Appendix

10.1 Grid independence analysis for hydrodynamics simulations

To obtain a result which is independent from the mesh employed, a grid independence analysis was performed within the domain of the hydrodynamics simulations. Three meshes were chosen in order to evaluate the variation of the velocity magnitude profile at three different sections, $z = 5$ cm, $z = 8$ cm, $z = 11$ cm. All the mesh parameters, as well as the computation time, are listed in the following table (10.1).

Table 10.1 - Settings and computation time for the 3 meshes employed

Mesh parameters	Mesh 1	Mesh 2	Mesh 3
Number of elements	226569	409269	1112048
Element size parameters			
Maximum element size [cm]	0.242	0.186	0.125
Minimum element size	0.0745	0.0559	0.0373
Maximum element growth rate	1.25	1.2	1.15
Curvature factor	0.8	0.7	0.6
Resolution of narrow regions	0.5	0.6	0.7
Computation time	23.41 min	48.11 min	2.13 h

All the simulations were performed by using the equations listed in the section 6.3.3. An inlet velocity of 0.13 m s^{-1} were employed to account for the solution change when adopting different mesh configurations. The three different velocity profiles in the sections studied are visible in the following figures (10.1, 10.2, 10.3).

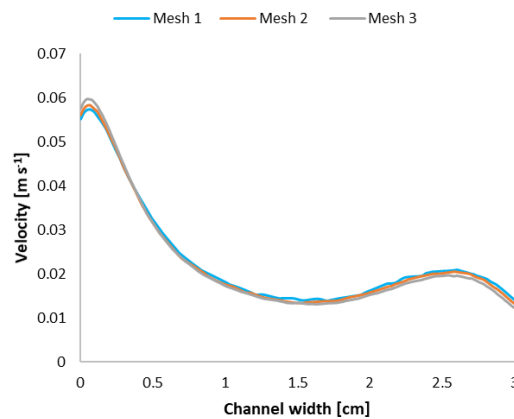


Figure 10.1 - Simulated velocity profiles at the distance of 0.55 cm from electrodes and 5 cm from flowcell inlet for inlet velocity of 0.13 m s^{-1}

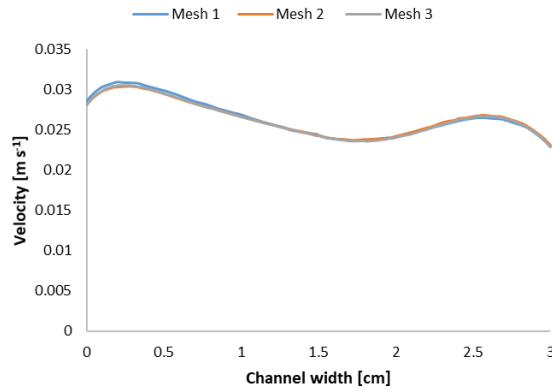


Figure 10.2 - Simulated velocity profiles at the distance of 0.55 cm from electrodes and 8 cm from flowcell inlet for inlet velocity of 0.13 m s^{-1}

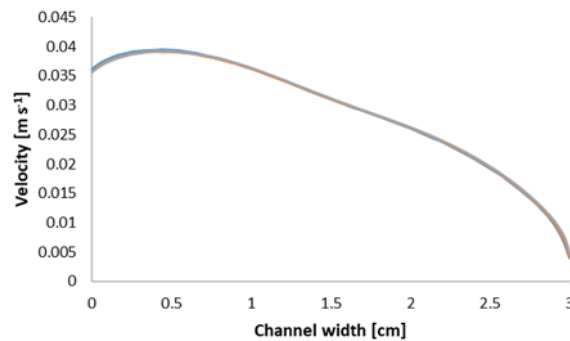


Figure 10.3 - Simulated velocity profiles at the distance of 0.55 cm from electrodes and 11 cm from flowcell inlet for inlet velocity of 0.13 m s^{-1}

As can be seen from the velocity profile graphs, the deviations between the solutions are minimal and therefore negligible. For this reason it was chosen to use mesh 2, an intermediate solution between the other choices.

Regarding the simulations using the other configurations with the distributors, the same analysis was performed, but at a inlet velocity of 0.11 m s^{-1} . The characteristics of the meshes employed are listed in the following table (Table 10.2).

Table 10.2

Mesh parameters	Mesh 1	Mesh 2	Mesh 3
Number of elements	156964	386341	679857
Element size parameters			
Maximum element size [cm]	0.403	0.262	0.202
Minimum element size	0.0101	0.0806	0.0605
Maximum element growth rate	1.3	1.25	1.3
Curvature factor	0.9	0.8	0.7
Resolution of narrow regions	0.4	0.5	0.6
Computation time	19.54 min	46.1 min	1.51 h

Velocity profiles are shown in the following figures, at three different position of the coordinate z , $z = 5 \text{ cm}$, $z = 8 \text{ cm}$, $z = 10 \text{ cm}$.

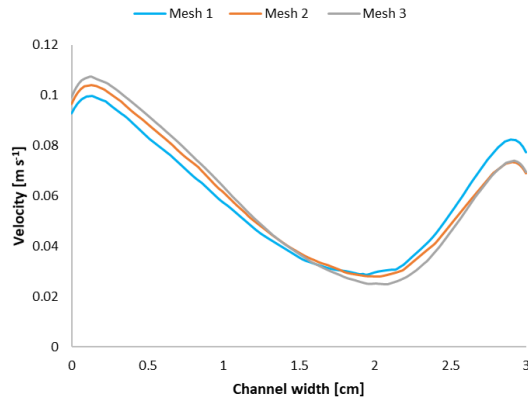


Figure 10.4 - Simulated velocity profiles at the distance of 0.55 cm from electrodes and 5 cm from flowcell inlet for inlet velocity of 0.11 m s^{-1}

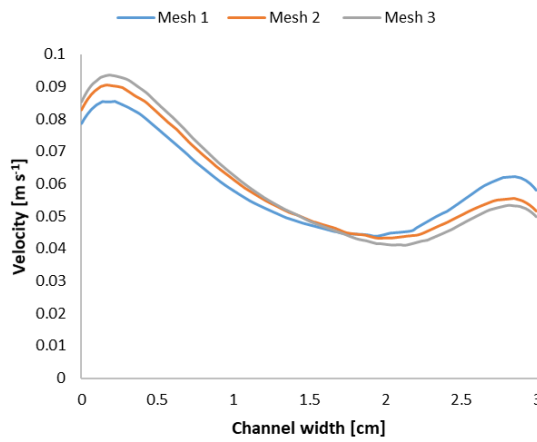


Figure 10.5 - Simulated velocity profiles at the distance of 0.55 cm from electrodes and 8 cm from flowcell inlet for inlet velocity of 0.11 m s^{-1}

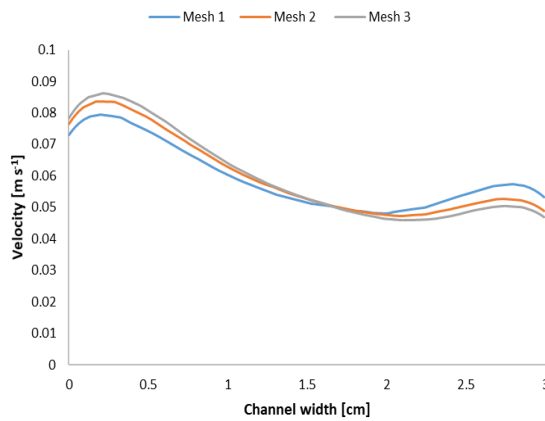


Figure 10.6 - Simulated velocity profiles at the distance of 0.55 cm from electrodes and 10 cm from flowcell inlet for inlet velocity of 0.11 m s^{-1}

Also here there is not a large difference between the profiles. However, the profiles obtained by using mesh 2 are intermediate between the two choices, so it was decided to carry out the simulations with mesh 2, the best compromise between computational cost and reliability of the results

10.2 Grid independence analysis for current distribution simulations

Three meshes were chosen in order to evaluate the variation of the normalized current density profile at $y = 0$. All the mesh parameters, as well as the computation time, are listed in the following table (10.1).

Mesh parameters	Mesh 1	Mesh 2	Mesh 3
Number of elements	172548	488963	909174
Element size parameters			
Maximum element size [cm]	0.174	0.117	0.0923
Minimum element size	0.0522	0.0348	0.0174
Maximum element growth rate	1.2	1.15	1.13
Curvature factor	0.7	0.6	0.5
Resolution of narrow regions	0.6	0.7	0.8
Computation time	1.1 min	2.03 min	2.56 min

All the simulations were performed by using the equations listed in the section 6.3.5 for the primary current distribution. The three different profiles are visible in the following figure (10.7).

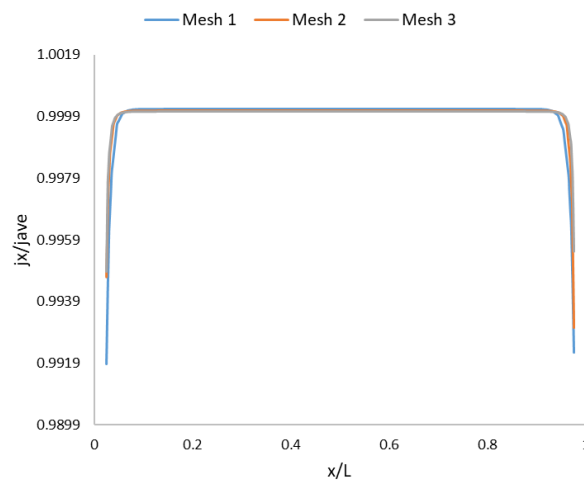


Figure 10.7 - Normalized current density for different Mesh configurations

As it is clearly visible, no appreciable variations were observed when using different configurations. The mesh 2 was used to solve the problem.

